1-1-2013

Striatal Dopamine Dynamics Upon Manganese Accumulation

Madiha Khalid
Wayne State University,

STRIATAL DOPAMINE DYNAMICS UPON MANGANESE ACCUMULATION

by

MADIHA KHALID

DISSERTATION

Submitted to the Graduate School

of Wayne State University,

Detroit, Michigan

in partial fulfillment of the requirements

for the degree of

DOCTOR OF PHILOSOPHY

2013

MAJOR: CHEMISTRY (Analytical)

Approved by:

_____

Advisor Date

_____

_____

_____

_____

DEDICATION

A lot of people have gone further than they thought they could because someone else thought they could. – Zig Ziglar

This work is dedicated to my mentors in chemistry,

who believed I was capable of this long before I did:

Dr. Colleen O'Keefe, Dr. Krisanu Bandyopadhyay, Dr. Tiffany Mathews

ACKNOWLEDGEMENTS

The past five years could not have been possible without the input and support of many people, whom I would like to thank and acknowledge here. First and foremost, my advisor Dr. Tiffany Mathews, thank you for the unlimited support and mentorship you have provided over the years. Thank you also to my graduate committee members, Dr. Claudio Verani, Dr. Sarah Trimpin, Dr. Brandon Aragona, and Dr. Parastoo Hashemi for their guidance, suggestions, and time throughout this process. Additionally, the informal conversation and advice of Dr. Tamara Hendrickson, Dr. Mary Rodgers, and Dr. Kelly Bosse has been invaluable and extremely appreciated. Dr. Krisanu Bandyopadhyay, without your efforts I never would have made it to graduate school; thank you most of all for your continued interest and support for my education and career.

I would not have made it past the first year had it not been for the guidance and companionship of my lab members, both past and present. They made this lab a place I looked forward to come to every single day, therefore I most gratefully acknowledge Dr. Francis Maina, Dr. Rabab Aoun, Stella Wisidamage, Johnna Birbeck, Brooke Newman, and Aaron Apawu. They, like all the other amazing friends I have made here at Wayne State, have really made graduate school a memorable and fulfilling experience in my life.

Most importantly, I would like to thank my family: my mom, my dad, Najia, Fareeha, Nida, and Ali, for supporting me through the stressful times and celebrating every accomplishment, and most importantly, for patiently listening to me talk about dopamine for the last 5 years!

TABLE OF CONTENTS

LIST OF TABLES

LIST OF FIGURES

Chapter 1: Electrochemical methods for the detection of catecholamines *in vivo* and *in vitro*

(Invited review, submitted in part to the Journal of Analytical Methods)

1.1 Introduction to neurochemical measurements by electrochemistry

Dopamine, norepinephrine, and epinephrine make up a class of neurotransmitters called catecholamines.[1] By definition, these are organic structures that consist of a benzene ring with two hydroxyl groups at the 3- and 4-positions, as well as an amine group side chain.[2,3] Their synthesis pathway is interconnected such that epinephrine is derived from norepinephrine, which itself is made from a dopamine.[1] Together, this class of neurotransmitters have been linked to the proper regulation of various biological functions such as the fight-or-flight response, control of respiration, cardiovascular regulation, and the sleep-wake cycle. These neurotransmitter systems also mediate cognitive processes involved in attention, reward recognition, and memory, such that dysfunction in these systems give rise to attention deficit hyperactivity disorder, addiction, schizophrenia, and posttraumatic stress disorder.[1,4,5] Therefore, it has become imperative in both clinical and laboratory settings to be able to accurately detect and monitor catecholamine levels as they can serve as diagnostic tools for a variety of medical conditions.

Historically, detection of catecholamines has been an analytical challenge due to several factors. As the physiological concentrations of these neurotransmitters are quite low in the brain, very sensitive techniques are required to make accurate and precise measurements.[2,6] Additionally, measurement from biological samples such as brain tissue or blood requires techniques that can separate analytes of interest from complex matrices with ease and

reproducibility. Catecholamine compounds are also unstable in neutral and basic environments; therefore, sample preparation conditions need to be optimized to prevent oxidation or decomposition of analytes during the process of quantification.[2,7] Two well established methods of catecholamine detection and quantification that meet the abovementioned criteria and challenges are: 1) fast-scan cyclic voltammetry (FSCV) and 2) microdialysis sampling coupled with separation by high performance liquid chromatography (HPLC) or capillary electrophoresis (CE) with electrochemical detection. The purpose of this mini-review is to explore the recent advances made in the field of catecholamine detection *in vitro* and *in vivo*, with specific attention given to the techniques of FSCV and separation methods coupled to electrochemical detection.

1.2 Fast Scan Cyclic Voltammetry (FSCV)

FSCV is an electrochemical technique that detects analytes, such as catecholamines, by utilizing their inherent electroactivity.[8,9,10] Although carbon-fiber microelectrodes are sensitive enough to detect non-stimulated burst firing ('phasic' release), typically measuring catecholamines from either slices or *in vivo* requires a bipolar stimulating electrode for eliciting release of neurotransmitters via electrical stimulation.[11,12] A carbon-fiber microelectrode is used for the detection of analytes based on their characteristic oxidation and reduction potentials in reference to a Ag/AgCl electrode. The carbon-fiber microelectrode is inserted into the brain region of interest and a potential is applied as a waveform optimized for the detection of one particular analyte. For example, to detect dopamine, a triangular waveform is applied that is first held at a potential of -0.4 V, ramped up to +1.2 V, then brought back down to -0.4 V at a scan rate of 400 V/s. This technique allows for the detection of a specific analyte based on

the region in which measurements are being made, as well as the potential at which it oxidizes, so no additional separation component is required. Additionally, the spatial resolution afforded by the size of the carbon-fiber (typically about 7 µm in diameter and 150 µm in length) and the millisecond temporal resolution enables functional analysis of both neurotransmitter release and uptake dynamics *in vivo* and in oxygenated brain slices (*in vitro)*.

One drawback of slice and anesthetized *in vivo* FSCV is that it can only measure differences in analyte levels, making it difficult to estimate absolute extracellular concentrations. Although FSCV cannot measure basal dopamine levels, *in vivo* FSCV can detect and measure spontaneous dopamine transients that arise from brief but intense phasic firing of dopamine neurons.[13,14] Additionally, FSCV is limited to detection of analytes that are easily oxidizable/reducible and requires that these redox potentials are within the range supported by carbon-fiber microelectrodes. Finally, FSCV measurements can only be made from "living" tissue within a 6 - 8 hour time frame, making it difficult to compare concentrations of neurotransmitters in different regions or to perform any type of longitudinal study. Many researchers, therefore, are working towards making improvements to overcome these challenges.

1.2.1 Method Improvements

Over the past few years, several refinements have been made to improve detection of biological analytes, more specifically neurotransmitters, at the carbon fiber microelectrode that is used in FSCV. Detection of neurotransmitters is dependent on the surface properties of the carbon fiber.[15] Thus, one of the simplest modifications that can be made to the carbon-fiber microelectrodes is to alter their surface chemistry. The Venton group has been leading the way in developing and characterizing how various types of carbon nanotubes (CNT) influence

sensitivity and detection of dopamine at these electrodes. For example, Jacobs *et al.* used a dip-coating method to modify the electrode, which meets their ideal criteria of a CNT-modified electrode that can be easily and reproducibly made at low cost.[16] Three types of functionalized single-walled carbon nanotubes (SWCNTs) were evaluated for their ability to measure dopamine, serotonin, and ascorbic acid by FSCV. Although the dip-coating method sufficiently covered the electrodes, high variability in the coverage was reported. Even so, Jacobs *et al*. successfully demonstrated two- to six-fold increased oxidation currents for both dopamine and serotonin using carboxylic acid and amide functionalized SWCNTs, but only carboxylic acid functionalized SWCNTs showed a significant 4.5 times increase in sensitivity to ascorbic acid. The detection of the neurotransmitters was not improved by functionalization of electrodes by octadecylamine modified SWCNTs. Additionally, improved selectivity was observed when detecting positively charged analytes versus negatively charged analytes based on the charge of the functional group on the nanotubes used. Jacobs *et al*. concluded that there was room for improvement when attaching SWCNTs to the surface of a carbon fiber electrode, in particular regarding reproducibility using this method to modify an electrode. Overall, the Venton lab demonstrated a simple method to modify the electrode surface by dip-coating, which affords the freedom to pick and choose different functional groups for surface alteration based on the analyte of interest.

In a follow up study, the Venton group modified the coating protocol to generate a more uniform self-assembled forest of SWCNTs on the surface of disk electrodes, but this time exclusively using the carboxylic acid functionalized SWCNTs.[17] These electrodes demonstrate improved sensitivity and limits of detection for dopamine at both 10 and 90 Hz, with additional

evidence of a nine-fold improvement in temporal resolution without loss in sensitivity. Compared to bare electrodes, they demonstrated 36-fold higher oxidation currents when detecting dopamine. Compared to the abovementioned dip-coating method, the sensitivity towards dopamine was 34-fold higher. The SWCNT-modified electrodes were evaluated using an expanded analyte set including the catecholamines epinephrine and norepinephrine, which exhibited the same trends of higher oxidation currents. The authors conclude that this method of depositing a dense forest of SWCNTs on carbon fiber electrodes shows a significant improvement of the electrode surface for the detection of catecholamines.

Aside from the surface, modification of catecholamine detection at the electrode can also be achieved by altering other parameters, such as the applied potential. An increase in sensitivity towards dopamine detection has also been demonstrated by Roberts *et al.* by applying an additional waveform to pretreat the electrode before the detection waveform is used.[18] In this work, cycling for an additional 5 minutes using an extended triangle waveform, from -0.5 V to +1.8 V, prior to voltammetric detection was shown to increase carbonyl and hydroxyl groups on the surface of the electrode. The result was an improvement in sensitivity, as demonstrated by a six-fold increase in the slope of the graph plotting increasing concentrations of dopamine detected versus peak anodic current. The Wightman group used a similar approach, this time extending the applied potential window of the detection waveform.[19] In this work, carbon fiber microelectrodes and pyrolyzed photoresist film (PPF) carbon electrodes were used in conjunction with extended waveforms to improve adsorption of analytes on the surface of carbon electrodes. The resultant oxidative etching of the electrodes established that the carbon surfaces could be renewed, enabling detection of

analytes and complex environments that would heretofore irreversibly foul electrodes. Although not as common, the contribution of scan rate on sensitivity and selectivity of catecholamine detection has also been evaluated. Most researchers who use FSCV use a "standard" scan rate of about 400 V/s, Keithley *et al.* evaluated the effect of ramping the scan rate of the standard applied waveform to 2400 V/s.[20] The faster scan rate led to a four-fold increase in detected oxidation current of dopamine, without the increase in time associated with extended waveforms that have been applied by others to improve detection current.[19] When an extended voltage window with a positive limit of +1.3 V was used in conjunction with this faster scan rate, the shape of the waveform was adjusted as well, such that the shape of the waveform resembled a sawhorse. The sawhorse waveform demonstrated improved limits of detection in vitro, from 5.3 nM to 0.96 nM. In other studies, increasing the frequency of the waveform from 10 Hz to 60 Hz improved the temporal resolution of FSCV.[21] At standard scan rate of 400 V/s, this allowed for an improvement in temporal resolution so that it was equivalent to constant potential amperometry, showing maximal response 67 ms after stimulus, compared to the 200 ms delay observed at 10 Hz. Although this increase in the frequency resulted in lower observed oxidation currents than when the waveform is applied at 10 Hz, the measured concentration of dopamine was equivalent. Despite lower signal current, the signal-to-noise ratio was maintained by increasing the scan rate to 2400 V/s.

Most of the research for the FSCV method development has focused on parameters and physical alterations to the working electrode. However, it is equally appropriate to give attention to the challenges associated with the reference electrode. To that end, Hashemi *et al.* have improved the reference electrode's ability to be implanted for extended periods of time

without producing a shift in potential.[22] Despite using sintered Ag/AgCl electrodes, which have thicker chloride plating than reference electrodes made in house, *in vivo* measurements made as early as 4 days after implantation typically show a +0.2 to +0.3 V shift in analyte peaks. Since voltages are used to identify the analyte, it is critical to address the shift in analyte potential. By fabricating the reference electrode with a Nafion-coating, these modified reference electrodes were stable for up to 28 days for *in vivo* FSCV measurements.

1.2.2 Electrode Design

An area that has attracted increasing interest is developing FSCV-compatible microelectrode array that allow simultaneous detection of neurotransmitters within a specific brain region. A prototype of this microelectrode array has demonstrated dopamine detection at four different channels, which could be controlled by individual waveforms, suggesting the potential for detection of multiple neurotransmitters simultaneously in the future.[23,24] In more recent work from the McCarty group, a similar fabrication method was used to create an electrode array that detects background and slowly changing extracellular dopamine levels.[25] In this microarray design, a square potential waveform applied to the two outer electrodes allowed for rapid adsorption and desorption of dopamine/dopamine-ortho-quinone. This small change in dopamine concentration could be measured by the middle electrode, where a triangular FSCV waveform was applied, enabling the possibility of future detection of tonic dopamine release *in vivo.*

A limitation of monitoring neurochemicals in their native environment with electrochemical methods is the inability to monitor longitudinal changes for greater than a 12-24 hour period. Such detection, for example from days to months, requires electrodes that are both

biocompatible and stable when implanted for long periods of time. In light of that requirement, Phillips and coworkers have developed silica encased carbon fiber microsensors that demonstrated excellent viability *in vivo* for up to 4 months after implantation.[26] This design modification of using silica versus glass as the outer casing enables repeated measurement of neurotransmitters in the same subject over time. An advantage of silica cased electrodes that can be implanted for long periods of time is that they will provide a better understanding of dynamic changes over the course of disease progression and other progressive, time sensitive models.

1.2.3 Pushing Boundaries

Optimization of various parameters and technological advances of FSCV over many years has made it a well-established technique for detection of neurotransmitters in the rodent brain, both in slices and in freely moving animals. In addition to new avenues being pursued in rodent studies, researchers have also been approaching new fronts in models used for studying catecholamines/monoamines, such as PC12 Cells, *Drosophila*, and human blood platelets.[27-30] Recent advancements and innovations have also been made in the pursuit of utilizing FSCV to better understand neurochemical dynamics in the human brain. There are numerous challenges when adapting a method from animal models to utilization in human studies. One of the biggest challenges is developing a microelectrode that will be approved by the Food and Drug Administration. Applying FSCV in human studies, Kishida *et al.* used modified carbon fiber microelectrodes for detection of dopamine.[31] These FSCV electrodes were modeled after electrophysiology electrodes used during deep brain stimulation and therefore were expected to be safe for human patients, able to withstand sterilization, compatible with current

neurosurgery equipment, and capable of detecting physiological dopamine. This work is the first to demonstrate sub-second detection of dopamine in the striatum of an awake human.

In order to further develop FSCV for application in human patients, there is a desire to have the experimental scientist and the instrumentation out of the surgery room to give the physicians and surgical team enough room to interact without the confines of instrumentation. Thus, the Garris group, in collaboration with researchers at the Mayo Clinic, has developed the Wireless Instantaneous Neurotransmitter Concentration Sensing System (WINCS), which shows great promise, not only for further facilitating animal research sans the constraints of wiring, but also for future intraoperative use in monitoring neurotransmitter release in conjunction with deep-brain stimulating electrodes.[32] They have gone on to integrate the WINCS with carbon nanofiber multielectrode arrays to improve spatial resolution of neurotransmitter detection when employing this system.[33] Nearly all the proof-of-concept work with humans started with using WINCS to evaluate dopamine since dopamine is the most well-characterized neurotransmitter in the field of electrochemical detection. However, an ultimate goal within the electrochemical community is to optimize the parameters of any new technique so that it can eventually be applied to other neurotransmitters as well. In particular, their work has focused on measuring the neuromodulator adenosine using FSCV, which was originally pioneered by the Venton lab. Lee *et al.* have taken advantage of the electroactive properties of adenosine to demonstrate the feasibility of measuring both dopamine and adenosine using WINCS in proof-of-concept experiments with animal models.[34]

Historically, FSCV has been used exclusively to measure dopamine. However, there is a renewed interest in modifying and developing FSCV for detection of other monoamines as well.

Norepinephrine is structurally related to dopamine, but until recently, little has been done with using FSCV to probe norepinephrine dynamics. The Wightman lab demonstrated that FSCV can be used to measure norepinephrine in the bed nucleus of the strial terminalis (BNST).[35] These findings have since then been extended to demonstrate that norepinephrine can be detected in the BNST while dopamine is concurrently detected in the nucleus accumbens.[36] Although beyond the scope of this review, other researchers have also applied the technique of FSCV recently towards the quantitation and pharmacological study of other neurotransmitters and neuromodulators such as serotonin, adenosine, and hydrogen peroxide as well.[30,37-39]

1.3 Microdialysis Sampling Coupled to Separation with Electrochemical Detection

Other modes of electrochemical detection can also be useful in quantifying catecholamines, such as for detection following separation of microdialysis samples. Microdialysis is an *in vivo* technique that uses a probe implanted in the brain region of interest to collect samples from freely moving animals.[40] Although both the size of the probe (for example about 240 μm in diameter and 2 mm in length typical for mouse brain measurements) and the temporal resolution (on the order of minutes) of this technique are worse than FSCV, the ability to determine basal extracellular levels of multiple neurotransmitters in a single sample, as well as the ability to perform multi-day experiments make this a comparable and complementary technique. The microdialysis probe is inserted following stereotaxic surgery using a guide cannula to target the specific brain region of interest. Perfusion of physiological buffer devoid of the analyte of interest through the inlet of the probe generates a concentration gradient at the semipermeable membrane of the tip. Small molecules under the molecular-weight cutoff limit of the membrane diffuse down their concentration gradient towards the probe and after

sufficient equilibration time, are collected through the outlet. Dialysate samples can be collected off-line and frozen until further analysis or on-line, in which case the dialysate is directly fed into the separation and detection set-up. Regardless of which method is used, separation of the complex mixture into multiple analytes is typically accomplished using either HPLC or CE coupled to a detector.[2,41,42] For the scope of this review, only methods using electrochemical detectors will be discussed.

1.3.1 HPLC Separation

For HPLC separation, the primary components required for separation and detection of catecholamines are a solvent reservoir, pump(s), an injector, column, electrochemical detector, and a computer to collect and analyze the data.[41] Optimization of the mobile phase, type of column, type of detector, and applied potential allows for the targeted study of specific neurotransmitters. Once the dialysate is injected on to the HPLC, it is carried through the column by the mobile phase where it interacts with the stationary phase of the column. Due to the physical properties of each of these components, the analytes are separated based on their interaction with the column, resulting in varying retention times for different analytes. Analyte peak area is determined by integration and quantified against known standards. Separation by CE requires a high voltage power supply, the capillary, source and destination buffer reservoirs, a detector, and data collection and analysis system.[42] CE relies on the different electrophoretic mobilities of each analytes to separate them as they travel through the capillary from the anode to the cathode. Upon detection, peaks are depicted on an electropherogram based on their migration times.

In recent years, advances to the method of HPLC analysis of catecholamines has stemmed from improvements to the column itself. By altering the density of the C_{18} moieties, the Atlantis T3 column retains polar compounds better, a feat that was difficult to accomplish in the past with the conventionally used hydrophobic stationary phase.[2,43,44] Alternatively, using columns with porous silica rods such as the C_{18} monolithic column results in better separation of the catecholamines norepinephrine and epinephrine.[2,45] Advancements in column technologies have led to improved sample through-put and sensitivity using traditional, commercially available electrochemical detectors when it comes to HPLC analysis. Although improvements for catecholamine analysis are found through improved separation, advancements in the detection of other neurotransmitters have also been made in recent years. As those studies are beyond the scope of this review, they have not been included in this discussion.

1.3.2 Electrophoresis Separation

True progress is being made when it comes to utilizing electrophoretic separation of microdialysis samples, especially in the pursuit of lab-on-a-chip designs. The pioneering work of the Martin group in 2008 produced the first report of a microchip system that combined microdialysis sampling with microchip electrophoresis coupled to electrochemical detection.[46] Biological measurements were demonstrated via detection of stimulated dopamine from PC 12 cells. Sampling dopamine standards through the same process allowed for quantification of dopamine, as well as identification by matching migration times. Others have gone on to explore novel materials for fabrication in an effort to produce lower cost, portable, yet effective microchips for catecholamine detection.[47,48] Novel methodologies have also been applied to optimize the electrode; for example, in the work by Johnson *et al.,* epoxy-encapsulated

electrodes have been devised to allow for the variation of the electrode if required.[49] They also demonstrated the ability of using carbon-fiber and glassy carbon electrodes in conjunction with their epoxy-encapsulated microchip systems for the separation and detection of a mixture of catecholamines.

Developing the first step in catecholamine separation and detection, the Kennedy group has been working towards improving the temporal resolution of microdialysis sampling so that analysis can be done on the order of seconds to more closely match the dynamic behavior of neurotransmitter systems. With that goal, their work generates discrete sample plugs of the dialysate stream to decouple temporal resolution from factors such as flow rate and tubing size. [50] Using immiscible oil, 2 nL dialysate plugs are generated and collected into a capillary, which are then fed into a microfluidic chip for analysis. This methodology was shown to bring down temporal resolution (0.1-2 seconds); additionally, the storage, stability, and analysis of these samples were also assessed and reported.[51] Although this technique employs CE coupled to laser-induced fluorescence, not electrochemical detection, we believe the improvement in microdialysis sampling is noteworthy, and may in the future be translated into the field of electrochemical detection of catecholamines. Further exploring nano level methodologies, Wu *et al.* have devised a novel nanocapillary electrophoretic electrochemical (Nano-CEEC) chip to achieve zeptomole limits of detection of neurotransmitters with a total sampling-to-detection time of 15 min.[53]

Most remarkably, the study of catecholamines by electrochemical methods has advanced to combine the techniques of FSCV and CE to make measurements in a single *Drosophila* larva with nM detection limits.[53] Such innovative coupling of well-studied techniques allows

researchers to combine the benefits of each to make breakthrough discoveries in unconventional biological models, such as the *Drosophila* larva.

1.4 Conclusions

Although well established for neurotransmitter detection, FSCV and HPLC/CE separation paired with electrochemical detection are constantly being optimized to utilize their capability of quantification and detection to its fullest potential. In this review we have presented some of the recent noteworthy advances made in catecholamine detection using electrochemical detection methods. As methodology is key for any technique, improvements in methods have also been highlighted. Improvements in sensitivity and limits of detection mentioned herein allow for the extension of these techniques to *in vivo* systems beyond traditional rodent models. Strides made in applying FSCV to human studies pave the way for translating laboratory research results to clinical therapeutics by providing a standardized platform with which drugs can be evaluated. Overall, the advancements presented herein demonstrate that despite being well-established technique, researchers across the field are successfully finding novel ways to improve and utilize these methods for the detection of catecholamines.

Chapter 2: Manganese and Dopamine

2.1 Neuronal Communication

Communication in the brain occurs through a combination of electrical and chemical signals. Although that is a simple and straightforward description, the complexity of neuronal communication stems from each of the individual aspects of this process. When one unravels all the different combinations associated with signal transduction, factoring in which types of neurons are involved, which part of the brain the signal originates from, what kind of message is being passed on, where the message is being received, which chemicals are released, *etc*., the number of total outcomes is breathtaking. Indeed, for an organ that is the control center for every function in our body, an intricate and precisely regulated network of communication is befitting.

Neurons can be found in one of several thousand varieties, each with their own structure and function.[1] Conventionally, neurons are represented in the form depicted in Figure 2.1, which highlights the components common to most, if not all, neurons. Comparable to other cells, the central structure of a neuron is the cell body (soma), which contains the nucleus and all other major organelles. Stemming from the soma are the dendrites, which are branched structures responsible for receiving signals from other neurons. These signals are sent via the axon, which is found as a single projection extending from the cell body, terminating at the axon terminal, which may or may not be branched. Distinction amongst neurons occurs based on several factors, such as the level of branching of dendrites, the location of the axon with respect to the location of the dendrites, how far the axon projects from the cell body, and how many axon terminals are

present. Regardless of type of neuron, neuronal communication occurs via the same mechanism – conversion from electrical to chemical signal.

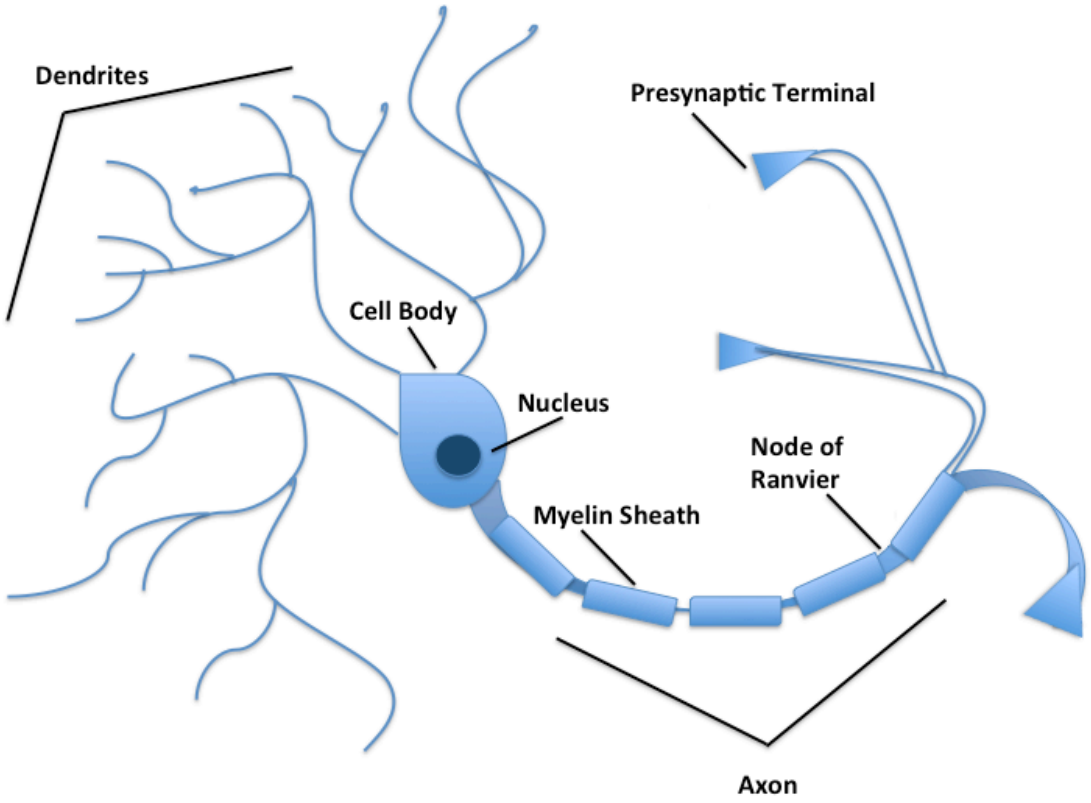

Figure 2.1: Schematic depiction of the primary components of a neuron.

The propagation of an action potential is central to the success of communication between neurons. Neurons have a negative resting potential, around -70 mV, compared to their external environment due to the uneven pumping of positive and negatively charged ions present on either side of the neuronal membrane.[1,4] An external stimulus has the ability to change that potential to a less negative one, which is called “depolarization” of the membrane potential. If this depolarization is significant enough and passes a certain threshold, then an action potential is generated (Figure 2.2). This manifests as a complete, all-or-none depolarization and repolarization of the neuron. This action potential migrates down the axon, facilitated by the myelin sheath that encompasses the axon, until it reaches the axon terminal. The activation of the neuron by this electrical signal causes the terminal to release stored chemicals. These chemicals further propagate neuronal communication by traveling across the synapse to the dendrites of the target neuron. The synapse is a junction created from the connection made by the axon terminal (termed the presynaptic terminal) of one neuron and the dendritic terminal of a different neuron (called the postsynaptic terminal). The two terminals do not physically touch; hence chemicals are used to transmit information. The two ends of the synapse are held tightly together by a variety of proteins and astrocytes to generate this ~ 20 - 40 nm space.[1] Once the chemical transmitters act on the receptors of the postsynaptic neuron, downstream signaling then carries out the intended function of the communicated signal, either at the postsynaptic neuron or by once again converting to an electrical signal and passing it on further.

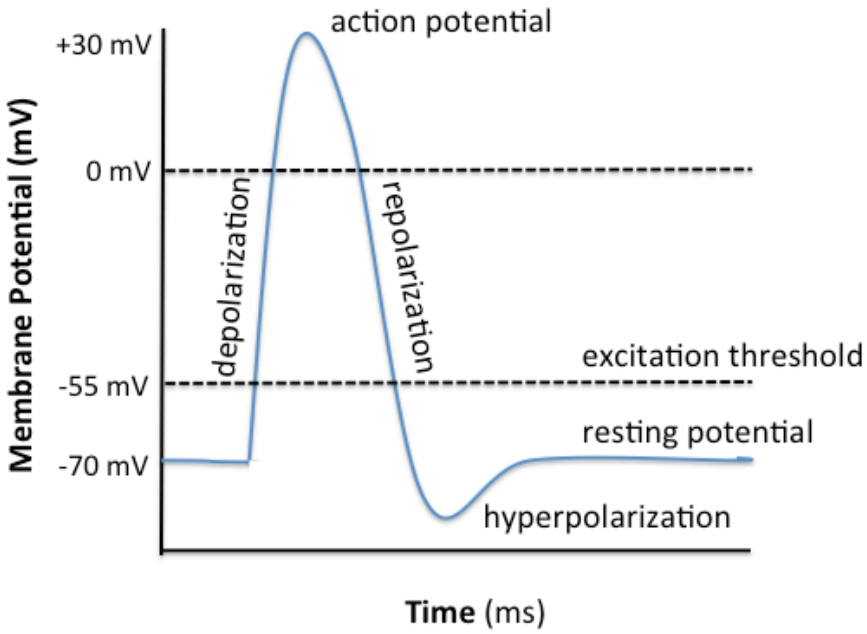

Figure 2.2: The membrane action potential over time.

2.2 Dopamine

The chemicals that transmit signals across the synaptic cleft are neurotransmitters. Correlated with different aspects of biological functioning (Table 2.1), neurotransmitters are chemical messengers that are synthesized and stored in the neuron. The most well characterized neurotransmitter in the mammalian brain is the catecholamine dopamine (3,4-dihydroxyphenethylamine). Dopamine neurons are found in the midbrain and project out to various regions of the forebrain through several different pathways (Figure 2.3).[1,4] Dopaminergic neurons of the mesolimbic pathway have cell bodies in the ventral tegmental area with axon terminals in the nucleus accumbens, while the mesocortical pathway also originates at the ventral tegmental area but terminates at the cortex.[1,4] Finally the mesostriatal (also called nigrostriatal) pathway projects from the substantia nigra to the caudate putamen.[1,4]

Dopamine is synthesized in the neuron (Figure 2.4) by a multi-step pathway starting with tyrosine, subsequently forming 3,4-dihydroxy-L-phenylalanine (L-DOPA) by tyrosine hydroxylase, which is converted to dopamine by aromatic amino acid decarboxylase (AADC; Figure 2.5).[1,4] Once synthesized, dopamine is packaged into vesicles via the vesicular monoamine transporter (VMAT), where it is stable at an acidic pH.[1] The sequestered dopamine is localized near the nerve terminal and upon sufficient action potential, an influx of calcium ions triggers activation of the vesicles, causing them to fuse with the terminal membrane and release their contents into the synaptic space. Once released dopamine interacts with its receptors on the pre- or postsynaptic neuron. There are five dopamine receptors, D1 – D5, that are grouped into two families. The D1 and D5 receptors make up the D1 family, while the D2, D3, and D4 receptors comprise the D2 family.[1,4] All five receptors are categorized as G protein-coupled receptors (GPCRs), which means

that when dopamine binds to one of them, they initiate a response in a specific G protein. D1 family receptors are coupled to G_S proteins, which stimulate adenylyl cyclase activity and increases concentration of the second messenger cyclic adenosine monophosphate (cAMP).[1,4] Conversely, D2 receptors are coupled to G_i/G_o proteins, which inhibit adenyly cyclase and therefore, cAMP production. D2 and D3 receptors also function as inhibitory autoreceptors, meaning they are also found on the presynaptic neuron from where they regulate extracellular dopamine levels by feedback inhibition signaling.[1,4] Dopamine in the synaptic space will not only interact with its receptors, but dopamine can also be metabolized by one of several different pathways (Figure 2.6).[1,4] If acted on by the enzyme monoamine oxidase, dopamine is converted to dihydroxyphenyl-acetic acid (DOPAC). Through a different pathway, catechol-*o*-methyltransferase can form 3-methoxytyramine (3-MT). Either of these products (DOPAC or 3-MT) can subsequently interact with the opposite enzyme; both pathways lead to the formation of homovanillic acid (HVA). Any remaining dopamine that has not diffused away from the synaptic cleft is taken back up into the cytoplasm of the presynaptic neuron by the dopamine transporter (DAT), a transmembrane protein, to be recycled.

Neurotransmitter	Primary Function
Acetylcholine	muscle control, memory formation, sensory response
Dopamine	reward, motor behavior, learning
Norepinephrine	fight-or-flight response
GABA	central nervous system inhibition
Glutamate	long term potentiation, memory
Serotonin	mood regulation, sleep, muscle control

Table 2.1: Common neurotransmitters and their biological functions.[1,4]

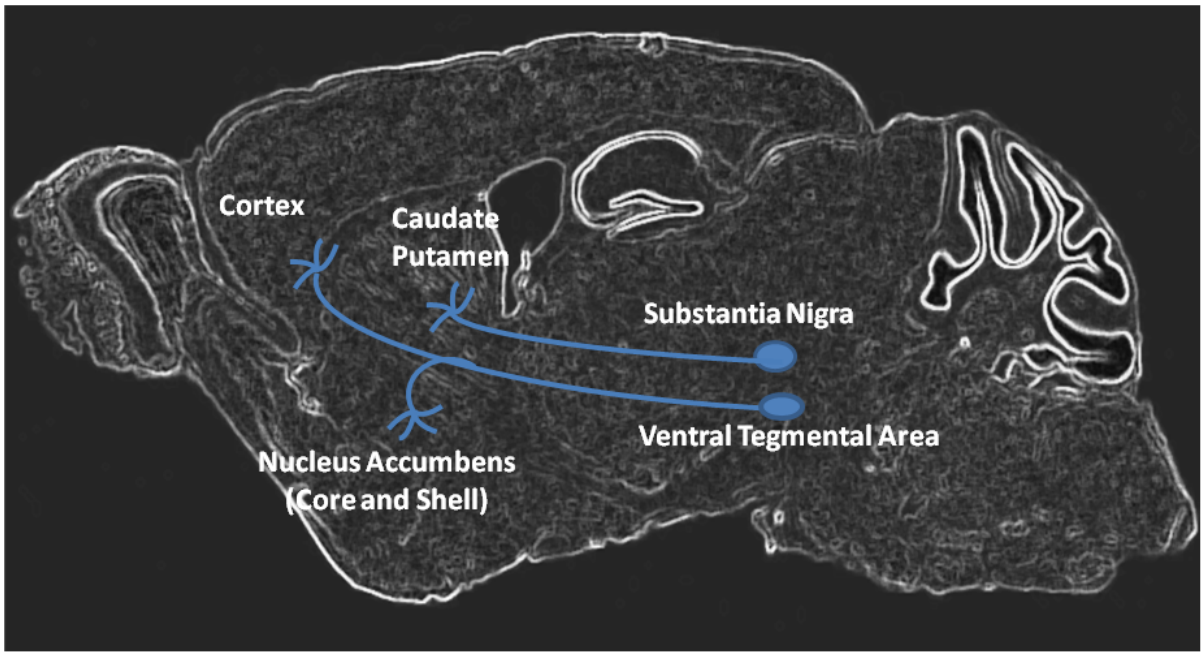

Figure 2.3: Dopamine Pathways. Sagittal rodent brain slice adapted from Paxinos *et al.* showing three major dopamine projection pathways extending from the midbrain to the forebrain.[1,54]

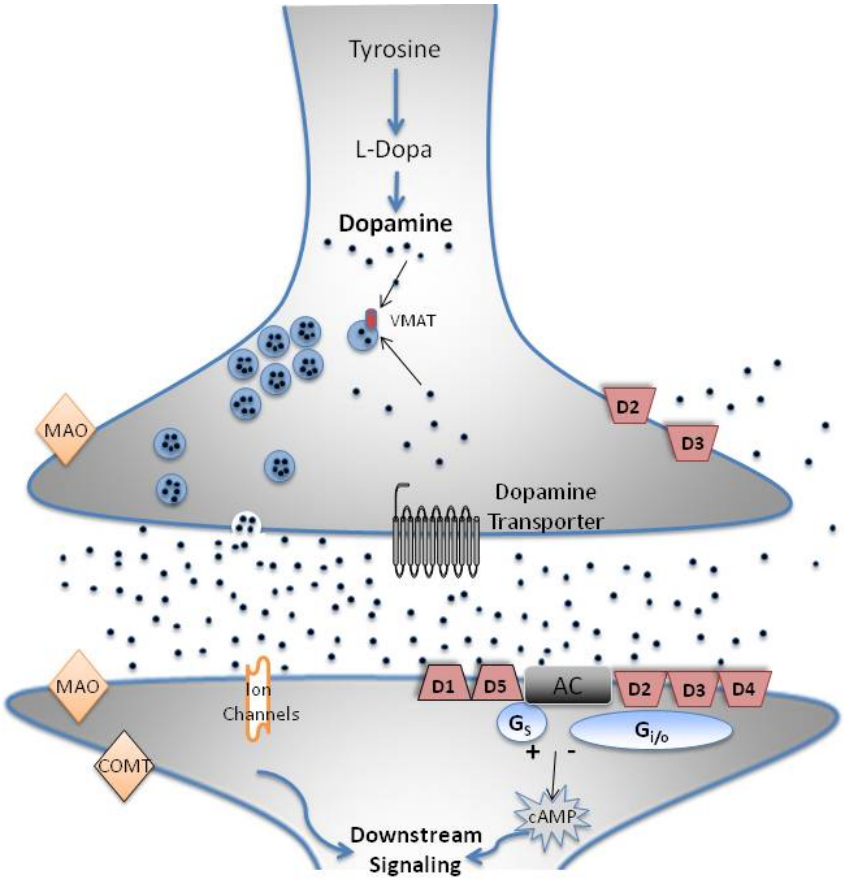

Figure 2.4: Dopamine Neuron. Schematic of synapse between dopamine presynaptic and postsynaptic neurons.

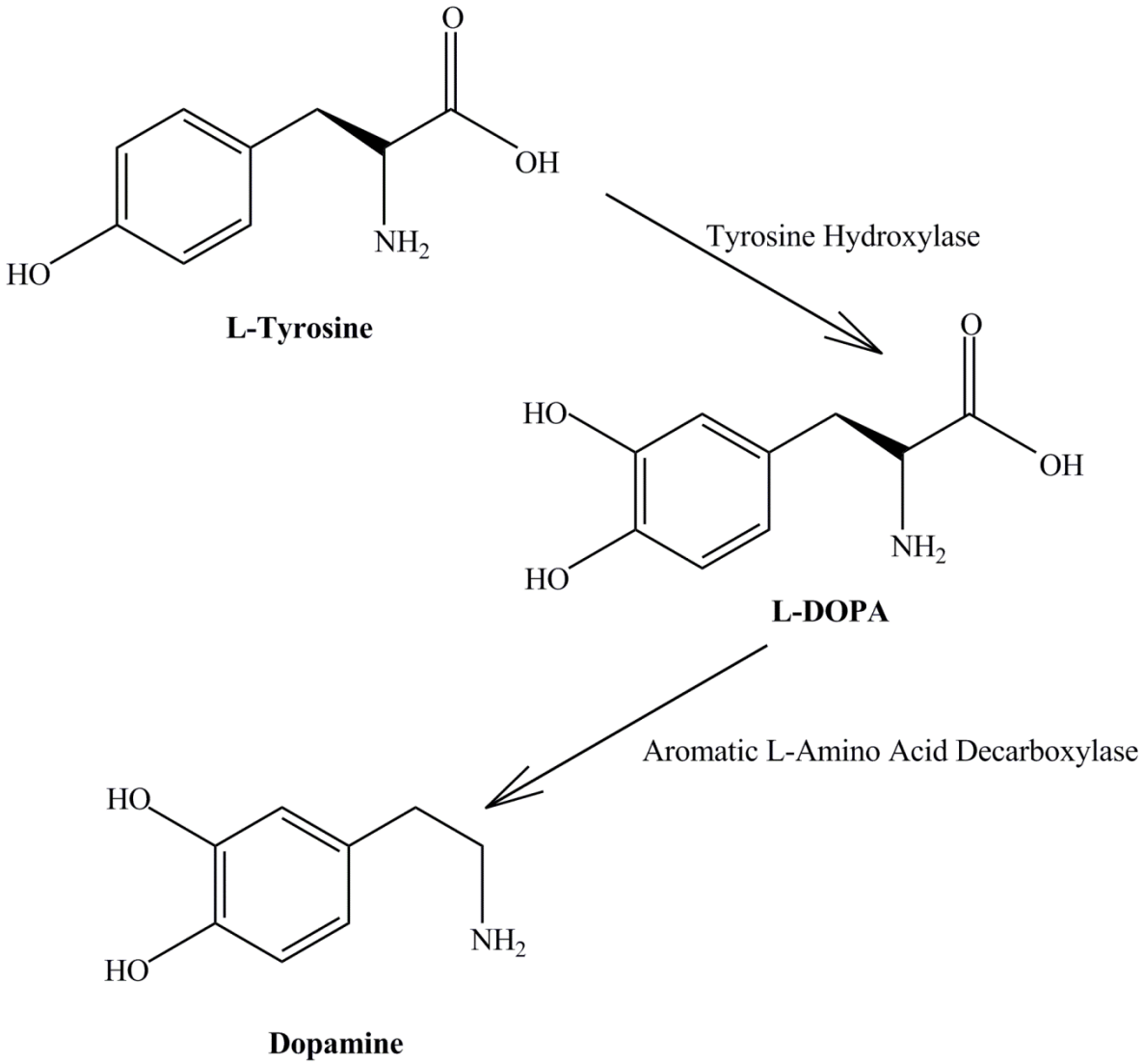

Figure 2.5: Biosynthesis pathway of dopamine.

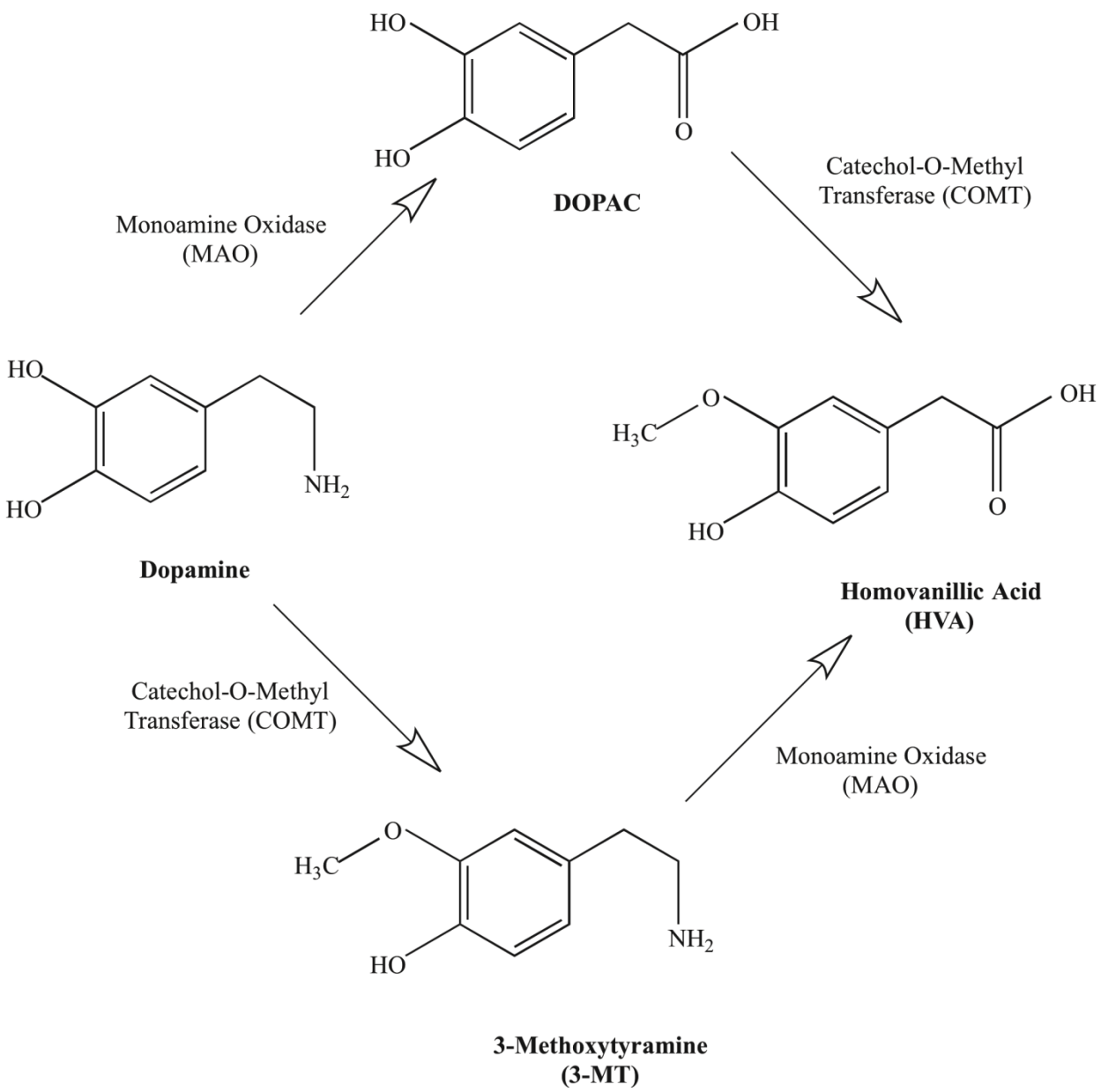

Figure 2.6: Metabolism pathways of dopamine.

The importance of the dopamine neurotransmitter stems from the multitude of functions it regulates in the human body. The dopaminergic system plays a critical role in motor movement, learning, reward, pleasure, cognition, and motivation behavior, just to name a few.[1,4] Dysfunction in the dopamine system leads to a variety of disorders, the best known of which is the neurodegenerative movement disorder of Parkinson's disease.[1,4] In addition to deficits in movement, both slowness and impaired initiation, patients of this disease exhibit depression, apathy, and cognitive decline. As a progressive disorder, most symptoms of Parkinson's disease don't manifest until at least 70% of striatal dopamine projection neurons have degenerated.[1,4] Other movement disorders connected to neuronal dysfunction in the striatum include Huntington's disease and dystonia.[1,4] Non-movement diseases that have been linked to dopamine system malfunction include schizophrenia, attention deficit hyperactivity disorder, and addiction.[1,4] Most critical to the work presented herein, the symptomatology of the neurological disorder manganism also strongly implicates striatal dopamine in its etiology.[55,56]

2.3 Manganism

First reported in 1837, manganism is a movement disorder characterized by motor deficits and a progression of symptoms very similar to Parkinson's disease, such as speech deficits, muscular rigidity, "intention tremors," bradykinesia, and gait changes.[55,57,58] Although many symptoms of manganism appear to be similar to those found in Parkinson's patients, it is still a point of contention as to whether the two are related. By one hypothesis, "Mn poisoning" is believed to be a precursor to the onset of Parkinson's in later years.[59] This is suggested because aside from the similarity in symptoms, both appear to act on the same brain region, the basal ganglia[60]. Certainly studies such as the one shown by Racette *et al*., in which welders exposed to

Mn developed Parkinson's disease an average of 17 years earlier than controls, suggest that Mn exposure may increase the risk of Parkinson's development.[61] However, the lack of a substantial number of such clinical studies still leaves room for questions when accepting the link between the two neurological disorders. Alternatively, the opposing hypothesis rejecting a correlation between the two disorders cites as its main piece of evidence that the two appear to act on different pathways and regions in the brain. While it is true that the basal ganglia, a group of brain regions that includes the caudate putamen (CPu), nucleus accumbens (NAc), the globus pallidus, the subthalamic nucleus, and the substantia nigra pars reticulate and compacta, is implicated in both, Mn accumulates primarily in the globus pallidus, CPu, and NAc whereas Parkinson's is associated with an 80% degeneration of the nigrostriatal pathway, primarily of dopamine neurons in the substantia nigra pars compacta[19] and CPu.[4,62] Interestingly, such significant degeneration of dopamine neurons has not yet been correlated with the onset of manganism. Moreover, subtle differences in the symptoms also exist between these two neurological diseases, for example between the "intention tremors" of manganism patients that occur when movement is attempted and the "resting tremors" of Parkinson's patients that occur without any intended movement at all[13]. In spite of this debate, the preferential accumulation of Mn in dopamine rich regions, as well as the cognitive and movement symptoms associated with the disorder, point to the dysregulation of the dopamine system as the primary candidate to explain how Mn disrupts the brain in patients afflicted with manganism.[56,63] When relaying the relevance of studying the relationship between manganism and dopamine to better strategize approaches for treatment, it is imperative to understand that although disorders such as Parkinson's disease are more widespread and well known, the more common day-to-day

exposure to manganese makes more people susceptible to developing this disease as compared to Parkinson's, which requires genetic predisposition and vulnerability to some degree.

2.4 Manganese

As manganese is an essential trace element, it is necessary for the human body for many functions such as immunological response, reproduction, and bone growth.[55,58,64,65] Manganese is found in a variety of foods, such as grain, rice, nuts, and tea, as well as in parenteral nutrition solutions for neonates, therefore meeting the low dose daily requirements by diet is not difficult to accomplish.[65] As a metal, the most well known use of manganese is in iron and steel production.[66] It also serves an important function in alkaline batteries as the electron accepting cathode.[67] Additionally, it can be found in pesticides, as well as in gasoline in the form of the antiknock agent methylcyclopentadienyl manganese tricarbonyl.[55] The onset of manganism has been suggested to be due to long term exposure to the metal, which can accumulate in the body and brain through one of several different routes.

2.5 Sources of Manganese Overexposure

Occupational exposure appears to be the leading cause of excess manganese inhalation, with occupations in welding, mining, and battery assembly being the worst offenders.[66-69] Recently, a study also showed that environmental exposure to children living in an area with high rates of electronic waste recycling resulted in significantly elevated blood manganese levels.[70] Environmental factors such as industrial pollution and residency in contaminated areas has also been reported to increase manganese exposure.[71] Once inhaled or ingested, the method by which ingested manganese passes through the blood brain barrier is not fully understood; however, the roles of several transport mechanisms have been suggested, including the divalent

metal transporter 1 (DMT-1).[72-75] DMT-1 is a non-exclusive transporter as it can also bind iron, and interestingly, iron deficiency has been linked to manganism vulnerability.[76,77] An additional connection between manganese and iron stems from the preferential accumulation of manganese in the basal ganglia, as that region is already rich in both metals and therefore more likely to accumulate them.[78] Even if all modes of environmental exposure can be avoided, studies have reported that medical conditions such as liver or kidney failure that impair clearance of metals from the body can result in accumulation of dietary manganese and eventually result in the same type of basal ganglia accumulation and neurological symptoms.[79-81] For similar reasons, conditions such as alcoholism, which can impair the liver's ability to properly function and clear toxins from the body, have been suggested to be risk factors for the development of manganism.[82]

2.6 Research Model and Objectives

For the purposes of this work, a sub-acute manganese treatment protocol was adapted from Dodd *et al.* that results in significant manganese accumulation in the basal ganglia of mice via subcutaneous injections.[60] The overall aim of this work was to determine how basal ganglia manganese accumulation impacts striatal dopamine dynamics over a period of 21 days. Based on this treatment method, C57Bl/6 mice were administered three 0.1 mL subcutaneous injections of 50 mg/kg $MnCl_2$ over the course of 7 days, with no treatment for two days between each dose. A control group was given the same volume of saline on treatment days. All neurochemical and behavioral data from the saline group at each time point were collapsed to form a single control group, as these results were not different across time points. After the third dose, analyses of dopamine and behavior were done immediately after (24 hours later: day 1), a week later (day 7),

and three weeks later (day 21), to assess the short and long term effects of manganese accumulation. The three objectives of this research were to answer the following questions:

Research Objective I: Does excess accumulation of manganese result in changes to striatal dopamine release, uptake, or extracellular levels? Additionally, can time-dependent changes be observed by this protocol to correlate to the time-dependent development and progression of manganism?

Research Objective II: Are the attenuated dopamine release levels observed in Objective 1 due to impaired functionality or lower concentration of dopamine reserve pool vesicles?

Research Objective III: Do lower levels of dopamine in the striatum result in behavioral abnormality after the intermittent manganese treatment protocol?

Chapter 3: Dopamine Monitoring By Fast Scan Cyclic Voltammetry (FSCV)

Two out of the three research objectives for this thesis work were achieved using the technique of fast scan cyclic voltammetry (FSCV) therefore more in depth background and methodology are provided here. Methodology of other techniques is provided within the relevant chapters. For a step by step instructional video and corresponding literature, see our publication:

Maina, F.,* Khalid, M.,* Apawu, A.,* and Mathews, T.A., "Presynaptic Dopamine Dynamics in Striatal Brain Slices with Fast-Scan Cyclic Voltammetry" *J Vis Exp*, 59, pii: 3464. doi: 10.3791/3464 (2012). *indicates co-first authors.[83]

3.1 Fast Scan Cyclic Voltammetry Background

FSCV is one of the primary methods used today to study dopamine neurotransmission. In contrast to neuroanalytical techniques like microdialysis, FSCV provides the advantage of better temporal and spatial resolution, selectivity without an additional separation component, and the capability of analyzing neuronal functionality in real time.

Electrochemical methods such as voltammetry rely on the charge-transfer process at an electrode surface to characterize the sampling environment.[84] More specifically, this method quantitates the concentration of oxidizable species based on the current generated by their redox reaction. Although Jaroslav Heyrovsky developed the Nobel Prize winning method of using applied voltage to both identify and quantify organic molecules, it was Ralph Adams who applied it for the purpose of measuring neurotransmitters in the rodent brain.[86] By using biocompatible carbon-based electrodes for FSCV induces less tissue damage than other methods of neurochemical analysis. The versatility of FSCV lies in the variety of substances it

can monitor simply by varying the parameters of the applied potential and the brain region from which measurements are made.

For the detection of dopamine, a sweeping triangular waveform is used that spans the potentials at which dopamine is known to oxidize and its oxidation product is known to reduce. At scan rates upward of 400 V/s, this 8 - 9 ms waveform can be repeated approximately 10 times every second, allowing for temporal resolution capable of making dynamic measurements of the neurotransmission process.[84] During this two-electron process (Figure 3.1), a current is generated, the integral of which over time equals charge (Q). Using Faraday's law (Equation 3.1), that charge can be related back to the moles of dopamine undergoing the redox process, thereby giving a concentration of dopamine found in the vicinity of the electrode. The electrode surface therefore provides a platform for the exchange of electrons. [15]

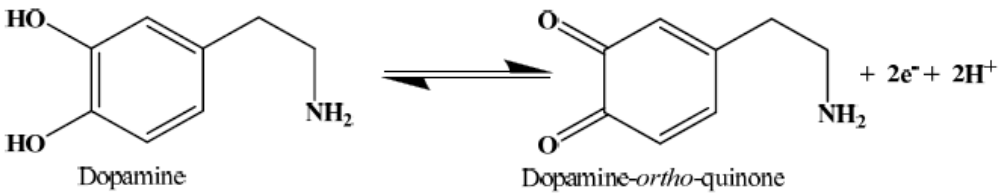

Figure 3.1: Oxidation-reduction reaction of dopamine.

$$Q = nFN$$

Equation 1: Faraday's law
Q: total charge (Coulombs)
n: number of moles of electrons transferred per molecule
F: Faraday's constant (9.649×10^4 Coulombs/mole)
N: number of moles of analyte being detected

Carbon-fiber microelectrodes are most commonly used for detection of catecholamines in the brain. In the cylindrical form, such as the ones used in this work, the typical working surface of the electrode spans about 50 – 200 μm in length, with a diameter of 7 μm. These dimensions contribute to the excellent spatial resolution provided by this technique to measure from discrete anatomical regions, as well as the minimal tissue damage that is induced. Unfortunately, the size of these electrodes, though smaller than microdialysis probes, is still not small enough to sample directly from the synaptic cleft (Figure 3.2). Therefore, it is important to understand that measurements from FSCV are also being made in the extracellular space. An advantage that the carbon microfiber electrodes have is their ability to rapidly respond to changes in extracellular environment and relate them back to release and uptake events of dopamine. Additionally, using pharmacological agents, functionality of autoreceptors and the dopamine transporter can also be assessed.[8,9,84] Unfortunately, post-synaptic receptor activity cannot be discussed, as this technique can only monitor presynaptic events.

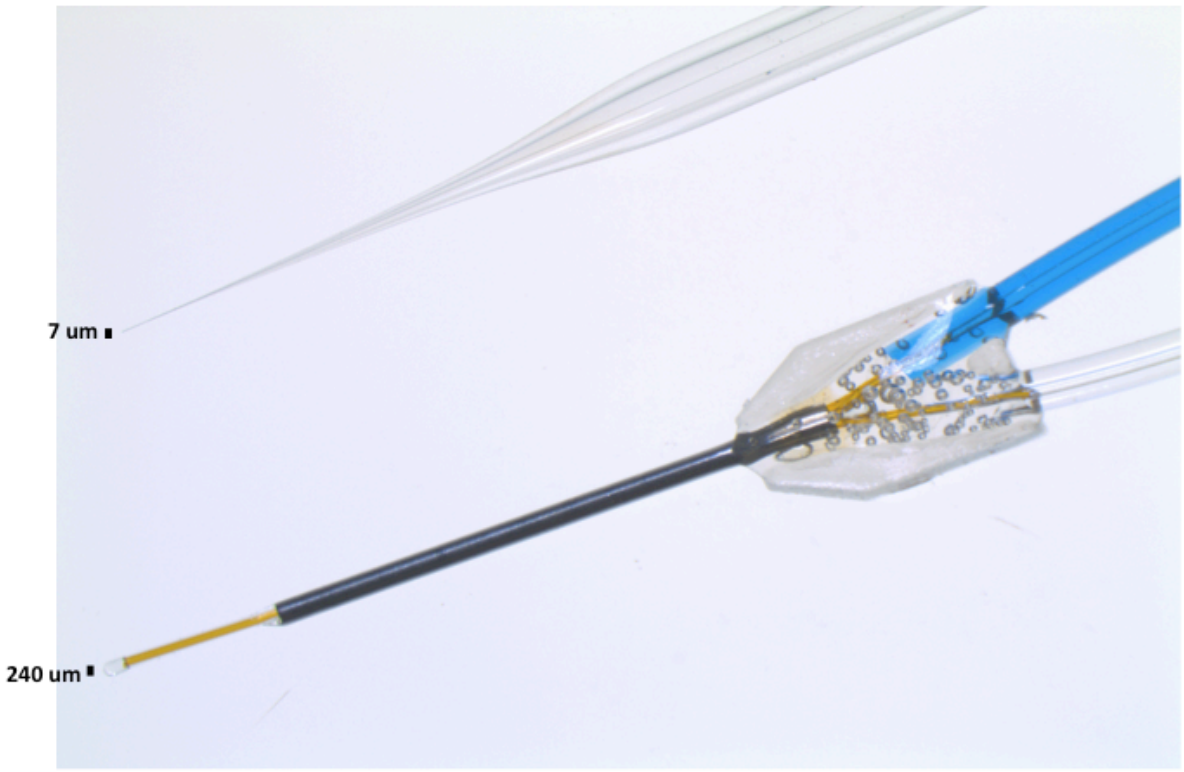

Figure 3.2: Size comparison of carbon-fiber microelectrode and microdialysis probe. For measurements in a mouse brain, diameter of carbon-fiber electrode (7 µm, top) as compared to diameter of microdialysis probe (240 µm, bottom).

Development of FSCV over the course of several decades has optimized it for use in both *in vitro* (slice) and *in vivo* experiments. While monitoring of neurotransmission in freely moving animals enables researchers to correlate brain activity with behavioral experiments, there are several advantages to performing FSCV in slices as well. First, working with slices allows for multiple experiments and pharmacological experiments to be performed on the same animal, within the same day without having to account for clearance times in between drugs as typically multiple slices for a particular brain region can be generated. Second, local manipulations to a particular brain region assess their effects on dopamine neurotransmission without contributing effects from other brain regions/neuronal projections. Third, conditions pertaining to stimulation, temperature, and pH are under the control of the researcher. Finally, multiple brain regions can be tested within the same slice since there is not trailing damage from placement of the electrode. For these reasons, our analysis of the dopaminergic system using FSCV was done using slice experiments.

3.2 Electrode Fabrication and Calibration

For all experiments, cylindrical carbon-fiber microelectrodes were used that were fabricated in-house. In this process, vacuum suction aspiration is first used to thread a carbon fiber (diameter 7 µm; Goodfellow Oakdale, PA) through a borosilicate glass capillary (length 10 cm, o.d. 1.2 mm, i.d. 0.68 mm; A-M systems, Carlsborg, WA). The capillary is melted in half at the center to create two electrodes, each with a tapered end of approximately 4.4 mm and a tight seal around the fiber using an electrode puller (Narishige, Tokyo, Japan; setting - 90.7 main magnet, 23.2 sub-magnet, and 53.4 heater). A microscope (Olympus, Tokyo, Japan) is then used to cut the extending carbon fiber to a length of 50 – 200 µm. Before use, the electrode is back-

filled with a 150 mM KCl solution and a lead wire is then inserted (Squires Electronics, Cornelius, OR) to help connect the electrode to the headstage of the potentiostat.

Each electrode is calibrated before use to determine sensitivity, as well as afterwards to obtain a calibration factor for data analysis. Calibration is done using a flow t-cell that has 3 ports. A Ag/AgCl reference electrode is also inserted through one side via a self-made hole. Tubing is used to connect the inlet to a syringe pump set to a flow rate of 2 mL/min for the modified- artificial cerebrospinal fluid (aCSF; see Section 3.3). A second port is connected to a 10 cc syringe that is filled with the calibration dopamine solution. The third port at the top is where the electrode is lowered into during calibration. Dopamine standard of 3 μM is made up in modified aCSF (see Section 3.3) at the time of calibration and filled into the syringe. The dopamine signal is recorded at least three times, and the current is averaged. To obtain a pre-calibration factor, the average is divided by 3 (to account for the concentration of standard being 3 μM). Only electrodes above a specific threshold calibration factor (10 nA/μM) are used for experiments. After each experiment, the process is repeated, and that post-calibration factor is used for data analysis.

The reference electrode, which can be used multiple times before requiring replacement, is also fabricated in-house. For that process, a 250 μm silver wire (A-M Systems, Carlsborg, WA) is chloridized in 1 M HCl for 5 - 10 minutes to form a layer of AgCl on the surface.

To elicit dopamine release, a commercially available bipolar tungsten stimulating electrode (Plastics One, Roanoke, VA) is also required.

3.3 FSCV Solutions

For all experiments, the following three versions of artificial cerebrospinal fluid (aCSF) are required, all three made in ultrapure (18 MΩ cm) water:

1. Modified aCSF for electrode calibrations. Can be made in advance and kept unrefrigerated for up to one week. Concentrations of components are as follows (in mM): 2.5 KCl, 126 NaCl, 1.2 NaH_2PO_4, 2.4 $CaCl_2$, 1.2 $MgCl_2$, and 25 $NaHCO_3$ (pH 7.4).
2. Sucrose aCSF for slicing (see Section 3.4). Once prepared, requires at least 20 minutes of oxygenation and can be stored in the refrigerator at 4 °C for up to 1 week.[86] Consists of (in mM): 180 sucrose, 30 NaCl, 4.5 KCl, 1.0 $MgCl_2$, 26 $NaHCO_3$, 1.2 NaH_2PO_4, and 10 D-glucose (pH 7.4).
3. Recording aCSF for data acquisition (see Section 3.5).This aCSF must be prepared daily before experiments and kept oxygenated by bubbling with 95% O_2/5% CO_2 at room temperature. Contained (in mM): 126 NaCl, 2.5 KCl, 2.4 $CaCl_2$, 1.2 $MgCl_2$, 25 $NaHCO_3$, 1.2 NaH_2PO_4, 11 D-glucose, and 0.4 ascorbic acid (pH 7.4).

3.4 Brain Slices

Once solutions are made, the mouse is sacrificed by CO_2 asphyxiation in a small gas chamber, followed by decapitation using scissors. The brain is rapidly removed and sliced using a Vibratome (St. Louis, MO). Coronal slices of 400 µm thickness are cut until the brain region of interest is identified. For all experiments, striatal brain slices were obtained to utilize the brain region of the caudate putamen (CPu). Slices are then allowed to acclimate in oxygenated recording aCSF at room temperature for at least 1 hour before using for experiments

3.5 Data Acquisition

After incubation, the brain slice is moved to a custom made recording chamber continuously perfusing with oxygenating aCSF and set to 32^{o}C. The carbon-fiber and stimulating electrodes are lowered onto the slice as shown in Figure 3.3A while the reference electrode is connected to the headstage via an alligator clip and is making contact with the aCSF bathing the slice. The stimulating electrode should rest on top of the slice while the carbon-fiber electrode is inserted about 75 μm deep into the slice, 100 - 200 μm away from the bipolar stimulating electrodes. Electrical stimulation parameters are set in TarHeel CV software (ESA Biosciences, Inc., Chelmsford, MA) to apply a single pulse stimulation (monophasic, 350 μA, 60 Hz, and 4 ms pulse width) to evoke dopamine release.[87] The slice is stimulated every 5 minutes while a potential is applied at the carbon fiber electrode in the shape of a triangular waveform (Figure 3.3B). Initially, the potential is held at -0.4 V vs. Ag/AgCl reference electrode to facilitate adsorption of dopamine onto the electrode. The potential is then ramped up to +1.2 V then brought back down to -0.4 V at a scan rate of 400 V/s. This process generates a stable charging current that is digitally subtracted out from the data files so only current from dopamine oxidation is recorded. During the upward scan, at approximately +0.6 V, dopamine is oxidized to dopamine-ortho-quinone (Figure 3.3C). On the downward scan, at approximately -0.2 V, dopamine-ortho-quinone is reduced back to dopamine. If a dopamine signal is obtained, collection is continued at that location of the electrode every 5 minutes until at least three stable values are obtained. A signal is considered stable if three consecutive readings are within 10% of each other. If signal is not obtained, the electrode is moved to a different location and

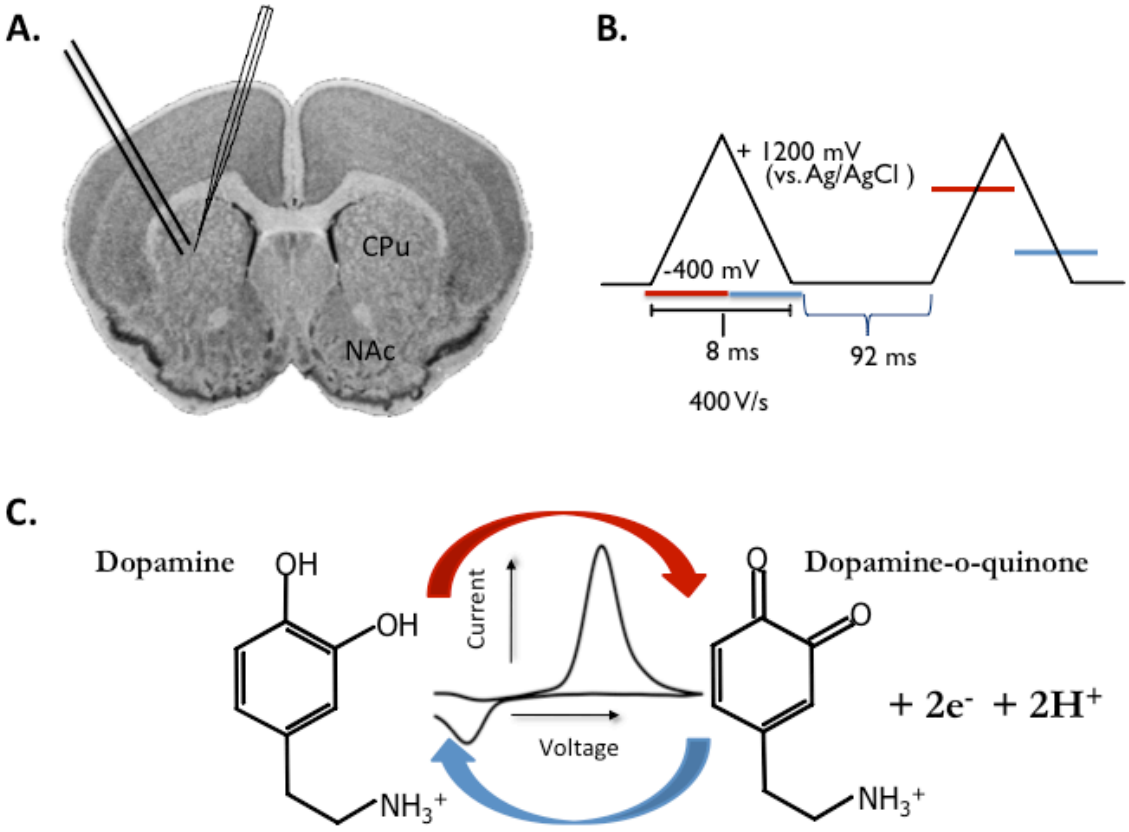

Figure 3.3: Schematic of FSCV data acquisition. A) Coronal brain slice displayed to portray placement of carbon-fiber microelectrode and stimulating electrode in brain region of interest, the caudate putamen. **B)** Waveform applied to working electrode for dopamine detection. Starting from -400 mV, potential is ramped up to +1200 mV and then brought back down to -400 mV vs. Ag/AgCl at a scan rate of 400 V/s. This waveform lasts for approximately 8 ms and is repeated every 100 ms. **C)** Visual representation of redox reaction occurring at the electrode's surface oxidizing dopamine to dopamine-ortho-quinone before reducing it back to dopamine in a two electron process that generates the current vs. voltage cyclic voltammogram shown in center.[54]

the process is repeated. Only after obtaining stable signal are any pharmacological agents perfused over the slice (using a pump set at a flow rate of 1 mL/min).

3.6 Data Analysis

FSCV data is presented in one of three ways. Primarily, a cyclic voltammogram can be generated which shows the applied potential against the current generated by the redox process (Figure 3.4). The locations of the peaks, corresponding to the potentials at which the neurotransmitter oxidizes and reduces, serve as a way to identify which neurotransmitter is being detected. In the case of dopamine, the peaks are found at +0.6 V and -0.2 V. Alternatively, the generated current can be plotted against time to examine the release and uptake properties of the neurotransmitter of interest (Figure 3.5). The ascending phase on the left represents predominantly the release of the neurotransmitter; the maximum peak height is converted to a concentration by using the post calibration factor and LVIT analysis software. The descending phase on the right is associated with the uptake of dopamine, which can be analyzed to determine how fast the transporter is taking dopamine back up into the neuron (V_{max}, µM/sec). A false color plot can also be generated, which combines the parameters of time (x), applied voltage (y), and current (z) in one plot (Figure 3.6). The characteristic oxidation and reduction current peaks of dopamine can be seen by the green and blue regions at +0.6 mV and -0.2 mV, respectively.

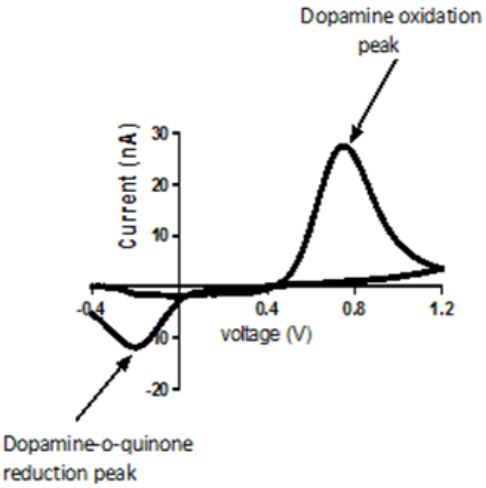

Figure 3.4: Representative cyclic voltammogram of dopamine.

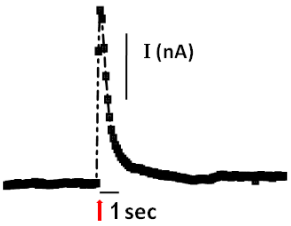

Figure 3.5: Representative current versus time trace of dopamine. Red arrow indicates time of stimulation.

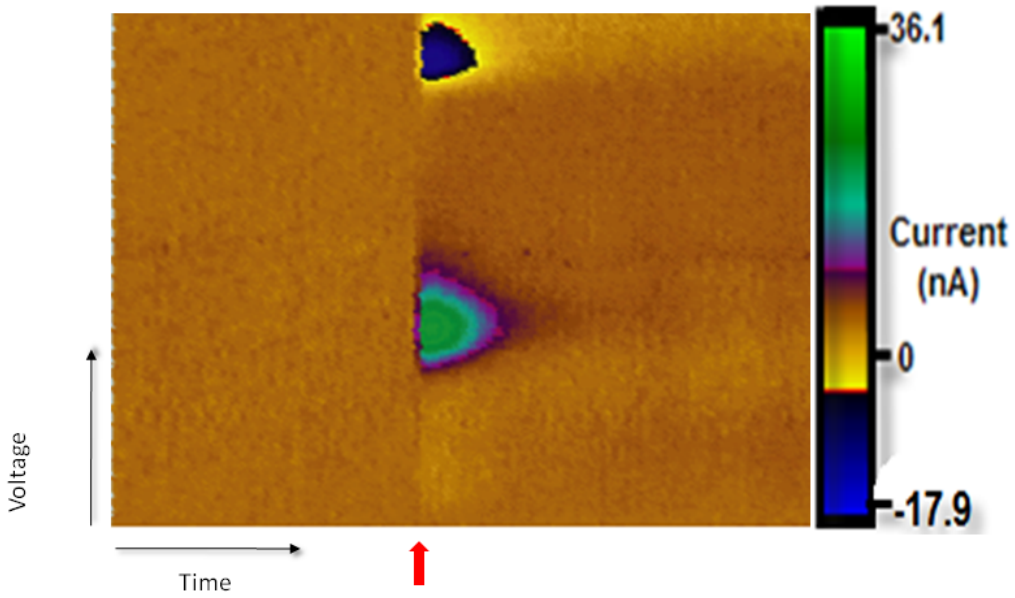

Figure 3.6: Color plot depicting dopamine oxidation and reduction peaks in false color. Red arrow indicates time of stimulation.

Current versus time traces obtained from experiments are analyzed using Labview software (National Instruments, Austin, TX). Based on Michaelis-Menten kinetics (Equation 3.2), traces are fit by nonlinear regression to obtain values for three parameters.[8,9] The concentration of dopamine released per pulse ([DA], nM) is correlated to the height of the trace. The V_{max} value (μM/s) estimates the rate at which dopamine is taken back up into the transporter and is visually expressed by the decay of the current trace on its right side. The affinity of dopamine for the dopamine transporter is related to the K_m value and for the purposes of our analysis, is fixed at 0.16 μM. The other two parameters are varied for the purposes of obtaining a fit with an R^2 value greater than 0.9.

$$\left(\frac{d[\mathrm{DA}]}{dt}\right)_{uptake} = \frac{-V_{\max}[\mathrm{DA}]}{K_{\mathrm{m}} + [\mathrm{DA}]|}$$

Equation 3.2: Michaelis-Menten based equation for nonlinear data fitting.

Chapter 4: Altered Striatal Dopamine Release Following a Sub-acute Exposure to Manganese

Adapted and Updated from:
Khalid, M., Aoun, R.A., Mathews, T.A., "Altered Striatal Dopamine Release Following a Sub-acute Exposure to Manganese," *J. Neurosci. Methods,* 202(2), 182-191 (2011)[88]
(Copyright License Number: 3143730589208)

4.1 Introduction

Manganese (Mn) is a key component for cellular function, immunological response, adenosine triphosphate (ATP) regulation, digestion, and reproduction.[55,64] Mn is also required for metalloenzymes such as superoxide dismutase and glutamine synthetase.[65] Normal levels of Mn intake by dietary consumption are around 2-5 mg per day and regulating homeostatic levels of Mn is crucial for sustained functioning of the body in several aspects.[65] Mn deficiency has been linked to fertility problems, birth defects, stunted growth, and impaired formation of bones.[65] On the other end of the spectrum, overexposure to Mn can lead to accumulation in the brain and subsequent neurotoxicity. High exposure can occur through occupations in welding, mining, and battery assembly, amongst others.[66-69] Elevated Mn levels can also result from medical conditions such as liver or renal failure or iron deficiency, both of which inhibit the clearance of Mn from the body.[76,77,79-81] Manganism, the resultant neurological disorder caused by overexposure to Mn, leads to a progression of symptoms that mimic those of Parkinson's disease. In the early stages of manganism, general symptoms such as headaches, hypersomnia, psychosis, irritability, anorexia, and apathy begin to appear.[89] As the disease progresses, working memory impairment, reduced attention concentration, and speech deficits

manifest.[89-91] The final symptoms to emerge are primarily motor deficits, such as muscular rigidity, "intention tremors," dystonia, bradykinesia, and gait changes.[55,62]

Clinical magnetic resonance imaging has demonstrated that preferential accumulation of Mn occurs in the dopamine (DA) rich regions of the basal ganglia.[92] Although the method by which Mn passes through the blood brain barrier is not fully understood, calcium channels, transferrin, the divalent metal transporter 1 (DMT-1), and N-methyl-D-aspartate (NMDA) have been suggested to regulate blood brain barrier transport of Mn.[72-75]

Despite the similarities between the symptoms of manganism and Parkinson's disease and the evidence implicating Mn overexposure in the onset of Parkinson's disease, these two neurological disorders appear to act on different pathways and regions in the brain.[61] Within the basal ganglia, excess Mn accumulation associated with manganism occurs primarily in the globus pallidus, caudate putamen (CPu), and nucleus accumbens (NAc).[62,93,94] In contrast, Parkinson's disease etiology is primarily associated with a greater than 80% loss of nigrostriatal dopamine neurons in the CPu, which originate in the substantia nigra pars compacta, as well as the appearance of Lewy bodies.[95] This significant degeneration of DA neurons in the substantia nigra pars compacta is not observed with the onset of manganism.[94,96,97] Furthermore, manganism patients show no difference in radiolabeled fluorodopa uptake (as measured by positron emission tomography, PET), while Parkinson's patients show reduced uptake.[62,98] Paired with the clinical differences seen in symptoms between the two disorders, such as the "resting tremors" of Parkinson's patients versus the "intention tremors" of manganism's, this information suggests that manganism is distinct from Parkinson's. [62] As a result, there is a need for further studies to better understand how Mn specifically acts upon the DA system, without

relying on the findings of Parkinson's studies as an indirect means to understand the alterations occurring in the DA system upon Mn exposure.

Previous studies performed on non-human primates and rats have indicated several impairments of the DA system as a result of Mn administration.[99-104] Decreases in amphetamine-induced DA release have been observed in non-human primates (via PET), emphasizing that excessive accumulation of Mn impairs DA release.[99,100] However, reports of alterations in other presynaptic components of DA dynamics have been inconsistent. For example, some studies show an increase in DA transporter expression/binding upon excess Mn exposure, while others show a decrease or no change.[99,101,105,106] Additionally, the influence of Mn toxicity on the DA D2 autoreceptor shows variable effects, ranging from decreased to increased expression to no effect at all.[99,107,108] The inconclusive evidence obtained thus far begs for a more in depth analysis of the effect of Mn exposure on the presynaptic DA system.

In this study, we used several complementary analytical techniques to probe the effect of a sub-acute manganese (II) chloride ($MnCl_2$) exposure on DA dynamics in C57Bl/6 mice over a period of three weeks. The integration of three different techniques allows for a novel methodological approach to correlate Mn tissue levels with the functionality of the DA system. Tissue content analysis quantified intracellular Mn and DA levels present in the brain after treatment was halted. Using *in vivo* microdialysis, the consequences of Mn treatment on striatal extracellular DA levels, as well as levels of its metabolites, 3,4-dihydroxyphenylacetic acid (DOPAC) and homovanillic acid (HVA), were assessed. Additionally, fast scan cyclic voltammetry (FSCV) was used to characterize DA dynamics, specifically DA clearance, electrically-evoked DA release, and functionality of presynaptic DA D2 autoreceptors. Although

our results demonstrate no serious deleterious effects from sub-acute administration of $MnCl_2$ on DA tissue content levels, the microdialysis and voltammetry results highlight subtle but significant alterations on the DA release mechanism.

4.2 Materials and Methods

4.2.1 Animals

C57Bl/6 mice were obtained from Jackson Laboratories and bred in-house for all experiments. Mice were group housed (3-4 animals per cage) at Wayne State University's animal care facilities. A 12 h light/dark cycle was used with food and water available *ad libitum*. Tissue content and microdialysis studies were performed on males only, weighing 23-25 g. Voltammetry experiments were conducted on both male and female mice weighing 23-33 g. All protocols and animal care followed guidelines set by the National Institutes of Health Office of Animal Care and Use and were approved by the Wayne State University Institutional Animal Care and Use Committee.

4.2.2 Manganese Treatment

Mice were injected subcutaneously with manganese (II) chloride tetrahydrate ($MnCl_2.4H_2O$) in a sub-acute treatment based on a published protocol shown to significantly increase Mn concentrations in the basal ganglia.[60] Briefly, animals were randomly assigned to two treatment groups and injected with either 0.1 mL of Mn (50 mg/kg, in saline) or saline (0.9% NaCl). This treatment was repeated every third day for a week, for a total of 3 treatments on days 1, 4, and 7. After the last injection, neurochemical analyses by three different techniques were conducted at three time points, 1, 7, and 21 days later, to assess both the short and long term effects of Mn exposure.

4.2.3 Tissue Content Analysis for Neurotransmitter and Metal Detection

Brain tissue samples were analyzed for metal accumulation, DA, and its metabolite DOPAC. Briefly, mice were sacrificed by cervical dislocation and brains were removed, dissected, and weighed. To determine which acid provided optimal recovery for *both* DA and Mn from the CPu, samples were homogenized in 400 µL of either 0.1 M HNO_3 or 0.1 M $HClO_4$. Overall, HNO_3 provided the best recovery (Table 1) and it was used to prepare all subsequent tissue samples. For all experiments, tissue homogenates were centrifuged for 15 min at 12,000 g at 4 °C in 400 µL of 0.1 M HNO_3. Metal levels for Mn, Cu, and Fe were assayed using graphite furnace atomic absorption spectrometery (GFAAS). DA and DOPAC were detected in the supernatant using high performance liquid chromatography (HPLC) coupled to an electrochemical detector.

All tissue samples were analyzed for Mn, Cu, or Fe using GFAAS as previously described. [109-111] After tissue samples were homogenized and centrifuged, they were diluted with 0.2% HNO_3 and 5 µg/mL $Mg(NO_3)_2$ was added as a matrix modifier. Each sample (20 µl) was injected onto a pyrocoated graphite atomizer tube with an integrated L'vov platform within a GFAAS system (Perkin Elmer, Uberlingen, Germany) equipped with an electrothermal atomizer and an autosampler. The detection of each metal was achieved using an element specific hollow cathode lamp. The lamp was operated at 20 mA, with a wavelength of 279.5 nm (Mn), 324.8 nm (Cu), or 248.3 nm (Fe). The slit width was 0.2 nm for both Mn and Fe and 0.7 nm for Cu. The GFAAS parameters were optimized to obtain the highest absorbance value and maximum pyrolysis temperature possible without loss of analyte. Metal peak areas were integrated using PerkinElmer WinLab32 software and quantified against known standards.

To assay tissue samples for the neurotransmitter DA and its metabolite DOPAC, tissue samples were homogenized and centrifuged as described above. DA and DOPAC from each sample supernatant (20 μL) were separated and detected in a single chromatogram using a Shimadzu LC-20AD HPLC (Shimadzu, Columbia, MD) with electrochemical detection (ESA 5011 cell; +220 mV relative to a Pd reference electrode). The isocratic separation of analytes was achieved using a Luna C_{18} (100 x 3 mm) column with 3 µm particles (Phenomenex, Torrance, CA) with the same mobile phase used for microdialysis sample separation (see section 2.5) at a flow rate of 0.55 mL/min.[112] Neurotransmitter peak areas were integrated using Shimadzu LC Solutions software and quantified against known standards.

4.2.4 Microdialysis Surgery

Male C57Bl/6 mice (5-8 weeks old) were anesthetized with Avertin (20 mL/kg) by intraperitoneal injection.[113] Once anesthetized, eyes were protected with sterile ophthalmic ointment and the skin over the skull was shaved and sterilized with Betadine and alcohol. A small incision was made above the skull, which was cleaned and dehydrated with 10% H_2O_2. Mice were placed on a stereotaxic frame for implantation of a guide cannula (CMA/Microdialysis, Chelmsford, MA) targeted to the dorsal striatum (coordinates in mm: A +0.8, L -1.3, V -2.5 from Bregma), based on the Paxinos mouse atlas.[54] The guide cannula was secured in place using fast drying dental cement (Teets, Diamond Springs, CA). Following dialysis experiments, mice were euthanized by carbon dioxide asphyxiation and brains were removed for histological confirmation of probe placement.

4.2.5 Microdialysis

Approximately 6 hours after surgery, the dummy cannula was removed and the microdialysis probe (CMA/7, 2 mm length, 240 μm diameter, Cuprophane, 6 kDa MW cutoff; CMA/Microdialysis, Chelmsford, MA) was inserted and perfused overnight with artificial cerebrospinal fluid (aCSF; in mM: 145 NaCl, 3.5 KCl, 2.0 Na_2HPO_4, 1.2 $MgCl_2$, 1.0 $CaCl_2$, pH 7.4) at a flow rate of 1.1 μL/min. After the dialysis probe was inserted, the dialysate outlet was inserted into a microcentrifuge tube on ice and an overnight sample (collection period ~ 12 hours) was collected. The next morning, this sample was analyzed by GFAAS to determine extracellular Mn levels in saline- and Mn-treated mice. Concurrently, at least three metabolite baseline samples were collected at 20-minute intervals to measure extracellular DOPAC and HVA levels. Next, at least 3 baseline samples were collected to measure extracellular concentrations of DA. After the collection of baseline samples, the saline- and Mn-treated mice were divided into two groups for two different types of experiments: (1) zero net flux analysis or (2) stimulation of DA release with 120 mM KCl aCSF.

The quantitative microdialysis method of zero net flux was performed to determine basal extracellular DA levels in saline and Mn-treated mice. A programmable gradient infusion pump (CMA/402) was used to perfuse 5, 10, and 20 nM DA (prepared in aCSF) through the microdialysis probe to the striatum for 90 minutes each.[114-117] Typically, when using this method, the amount of analyte being perfused into the microdialysis probe is not measured, as it is assumed that DA_{in} equals the targeted concentration chosen for perfusion. Prior to the *in vivo* experiments, an *in vitro* calibration was performed to more accurately determine the actual DA_{in} values.[117] Dialysate DA concentrations were determined following perfusion of 5, 10,

and 20 nM DA via the same set up, only in the absence of the animal. Since DA is easily oxidized to its ortho-quinone, the DA stock standard solution (1 mM) was prepared in 0.1 M perchloric acid, 10 µg/mL ascorbic acid, and 10% methanol, and aliquots (250 µL) were stored at -80°C. [118] Zero net flux solutions were made fresh daily by successive dilution of the stock standard solution in aCSF containing 200 µM ascorbic acid.

Microdialysis samples (20 µL) were manually injected onto a Luna 100 x 3 mm, C_{18}, 2.6 µm column (Phenomenex, Torrance, CA) for separation of DA and its metabolites (DOPAC and HVA), followed by electrochemical detection using an ESA 5041 cell (ESA Coulochem III, Chelmsford, MA) with an applied potential of +220 mV relative to a palladium (Pd) reference electrode (Szapacs et al., 2004). A guard cell (ESA 5020) was placed in line before the injection loop and set at a potential of +350 mV. The isocratic separation was achieved using a mobile phase that consisted of 75 mM of NaH_2PO_4, 3.0 mM 1-octanesulfonic acid, 0.125 mM EDTA, 9.0 % acetonitrile, and 0.2-0.5 % triethylamine (pH ~ 3.0). A flow rate of 0.4 mL/min was used to detect the neurotransmitters in a single chromatogram within 20 minutes. DA and its metabolite peak areas were integrated using Shimadzu LC Solutions software and quantified against known standards.

In a second cohort of mice, isotonic aCSF containing 120 mM KCl (in mM: 120 KCl, 30.5 NaCl, 2.0 Na_2HPO_4, 1.2 $MgCl_2$, 1.0 mM $CaCl_2$, pH 7.4) was perfused through the probe for 20 minutes following baseline sample collections. [117,119] Immediately after the 20 minutes of high K^+ stimulation, the perfusate was switched back to standard aCSF. This influx of K^+ depolarizes neurons, inducing exocytosis and subsequently increasing extracellular DA levels. The effect of 120 mM K^+ on extracellular DA levels was determined in both saline- and Mn-treated mice.

These samples were analyzed by HPLC and electrochemical detection as described for zero net flux experiments above. Additionally, the area under the curve (AUC) for high K^+ DA release was calculated from 80 to 140 minutes (Figure 4.3, inset) for all animal groups.

4.2.6 Fast Scan Cyclic Voltammetry

For *in vitro* fast scan cyclic voltammetry (FSCV), mice were sacrificed by decapitation following CO_2 asphyxiation. The brain was immediately removed and placed in pre-oxygenated (95% O_2/5% CO_2) high sucrose aCSF (in mM: 180 sucrose, 30 NaCl, 26 $NaHCO_3$, 10 D-glucose, 4.5 KCl, 1.0 $MgCl_2.6H_2O$, 1.2 NaH_2PO_4, pH 7.4) on ice for 5-10 minutes. [86] Coronal 400 µm thick slices that encompassed the striatal brain region (which includes the CPu and NAc) were prepared using a vibrating tissue slicer (Vibratome®, St. Louis, MO). Slices were kept in a continuously oxygenated reservoir of aCSF (in mM: 126 NaCl, 25 $NaHCO_3$, 11 glucose, 2.5 KCl, 2.4 CaCl, 1.2 NaH_2PO_4, 1.2 $MgCl_2$, 0.4 ascorbate, pH 7.4) for at least one hour before use. At the time of the experiment, a brain slice was transferred to a custom-made submersion chamber (Custom Scientific, Denver, CO) that was continuously perfused with aCSF and kept at 32^oC.

For all experiments, a two-electrode system was employed in which a Ag/AgCl reference electrode was paired with a carbon-fiber working microelectrode, inserted ~ 75 µm deep into the slice. Carbon-fiber microelectrodes were made by first aspirating carbon fiber (diameter = 7 µm, Goodfellow, Oakdale, PA) through a glass capillary (A-M Systems, Carlsborg, WA). The capillary was subsequently heated using a micropipette puller (Narishige, Tokyo, Japan) to form two electrodes, each with a tight seal at the glass-fiber junction. The exposed length of the carbon fiber was cut to approximately 50-200 µm. Each electrode was then filled with 150 mM KCl and a lead wire (Squires Electronics, Cornelius, OR) to complete the electrical connection.

Using a ChemClamp potentiostat (Dagan Corporation, Minneapolis, MN), potential was applied at the carbon-fiber microelectrode in the shape of a triangular waveform, initially held at -0.4 V. That potential was ramped up to +1.2 V, then back down to -0.4 V at a scan rate of 400 V/s. This waveform was repeated every 100 ms. To evoke DA release in slice, a bipolar stimulating tungsten electrode was placed approximately 100-200 µm away from the carbon-fiber microelectrode, controlled by TH software (ESA Inc., Chelmsford, MA). An electrical stimulation was applied to the slice by a single pulse (monophasic, 350 µA, 60 Hz, 4 ms width) every 5 minutes.

DA release and uptake measurements were made after slices were allowed to equilibrate in the submersion chamber for at least 30 minutes. For receptor characterization, dose-response curves were generated using pre-drug values for each animal as their own controls. DA dynamics were analyzed only after subtracting out the background current. Electrode calibration was performed post-experiment using a flow injection system. The electrode was calibrated with a 3 µM DA solution in aCSF to obtain a calibration factor, which was later used to convert the current to a concentration. A Michaelis-Menten based set of equations were used to fit the current versus time profile of each release event to quantify the maximum concentration of DA released per pulse ($[DA]_p$), as well as the rate of uptake by the DA transporter (µM/s; V_{max}).[8,87,120,121]

Data obtained from FSCV experiments can be presented in one of three ways, as depicted by representative plots in Figure 4.5. The top traces in Figure 4.5A are current versus time plots. The rise phase of the peak is predominately indicative of electrically-evoked DA release (amplitude), which is converted from current (y-axis) to a concentration (µM) using the

aforementioned calibration factor. The descending phase of the peak (decay of peak returning to baseline) represents DA uptake rates (μM/s). The insets show the respective cyclic voltammograms, which plot the measured current (y-axis) against the potential (x-axis) applied to the electrode. The voltammograms are used to confirm the detection of DA by the location of the oxidation peak of DA at +0.6 V and reduction peak of dopamine-ortho-quinone at -0.2 V. Below the two-dimensional plots is an all inclusive three-dimensional color plot which combines time (x-axis), applied voltage to the working electrode (y-axis), and generated current (z-axis; color scale). The characteristic oxidation current of DA is revealed as a bright green mark (an increase in current that corresponds to the amount of dopamine being oxidized) at approximately +0.6 V on the y-axis.

4.2.7 Chemicals

Components of the mobile phase and neurotransmitter standards were either of HPLC grade or the highest quality obtained from Sigma-Aldrich (St. Louis, MO) and Fisher Scientific (Pittsburgh, PA). Concentrated HNO_3, $HClO_4$, boric acid, triethylamine, and citric acid were purchased from EMD (Gibbstown, NJ). All standards for calibration curves used in GFAAS and HPLC analysis were prepared fresh daily.

4.2.8 Statistical Analysis

Data was analyzed using GraphPad Prism software (GraphPad, La Jolla, CA). All values are expressed as means ± standard error of mean (SEM) with a difference of $P< 0.05$ considered statistically significant. Comparisons of two means were analyzed by Student's *t*-tests. When comparisons of three or more means were made, a one way analysis of variance (ANOVA) was

performed. Two-way ANOVA with Bonferroni post-test was used when testing for interaction of multiple variables.

4.3 Results

4.3.1 Tissue Content Protocol and Analysis

The levels of striatal Mn, Fe, and Cu were analyzed by GFAAS first to assess the extent to which the acid used for tissue treatment influences metal recovery. Levels of DA and DOPAC were concurrently determined from acid-digested tissue by HPLC. The striatum was similarily homogenized in two different acids, 0.1 M HNO_3 or 0.1 M $HClO_4$ (Table 4.1). Striatal Mn levels were unaffected by the choice of acid used for homogenization ($P = 0.1203$), as were levels of DA ($P = 0.4809$) and DOPAC ($P = 0.0542$). Striatal Cu ($P < 0.0001$) and Fe ($P < 0.0001$) levels were significantly reduced when the tissue was treated with $HClO_4$ as compared to HNO_3. For this reason, HNO_3 was selected for all subsequent tissue content experiments.

Typically, metal levels in brain tissue are measured following sample digestion with a strong acid at 60 °C. However, high heat can degrade biological molecules, such as neurotransmitters, necessitating the use of cold acid solutions.[111] To determine if lower temperatures and acid content would be suitable for the recovery of trace metals, the striatum was divided in half and the sides were either homogenized in 0.1 M HNO_3 at room temperature or digested overnight at 60 °C in pure HNO_3. No difference was observed in the Mn levels extracted from homogenized tissues (0.92 ± 0.03 ng/mg wet weight; n = 6) compared to the overnight digested samples (0.96 ± 0.04 ng/mg wet weight; n = 6; $P = 0.38$; Table 4.1). Since similar Mn levels, as well as comparable levels of other trace metals (Table 4.1), were recovered from both tissue

preparations, the cold acid homogenizing assay was chosen for all measurements so that parallel neurotransmitter analyses could also be performed.

Employing the optimized tissue content protocol discussed above, Mn levels in the striatum were measured using GFAAS at three time points (day 1, 7, and 21) after repeated Mn treatment (Figure 4.1). Analysis by one-way ANOVA indicated a significant difference in Mn tissue content in Mn-treated mice compared to saline controls ($F_{3,33} = 112.9$, $P < 0.001$, n = 7; Figure 4.1A). On day 1 a 260% increase in Mn levels was observed in mice treated with Mn compared to saline controls ($P < 0.001$); this increase is similar to that reported by Dodd *et al.* [60] at the same time point. Mn accumulation persisted for up to 21 days after treatment, revealing a 150% ($P < 0.001$) and 30% ($P < 0.05$) increase on days 7 and 21, respectively. The same tissue homogenate was used to concurrently detect DA tissue levels, which primarily reflects the content of intraneuronal stores. No difference in intracellular striatal DA levels was observed between Mn and saline treated mice at any of the time points of analysis ($F_{3,36} = 0.60$, $P = 0.62$, n = 7-8; Figure 4.1B).

Analyte	$HClO_4$ (ng/mg wet weight)	HNO_3 (ng/mg wet weight)	
	homogenized	homogenized	overnight digested
Mn	1.0 ± 0.1	1.0 ± 0.1	1.0 ± 0.1
Cu	6.0 ± 0.4 [a]	16 ± 0.6	16 ± 2.2
Fe	16 ± 1.0 [a]	40 ± 0.8	43 ± 1.7
DA	8.0 ± 1.0	9.4 ± 2.0	ND
DOPAC	1.0 ± 0.2	2.2 ± 0.4	ND

Table 4.1: Analysis of trace metals, DA, and the DA metabolite DOPAC in dorsal striatum tissue homogenized with HNO_3 or $HClO_4$. Within the HNO_3 group, homogenization is compared to overnight digestion of tissue as a preparation method. All data reported as average (n = 5 - 6) of wet tissue weight (ng/mg) ± SEM. DA and DOPAC levels cannot be detected by overnight digestion and are therefore reported as 'not determined' (ND). (a) $P < 0.001$ compared to homogenized sample in HNO3 group (two-tailed Student's t-test).

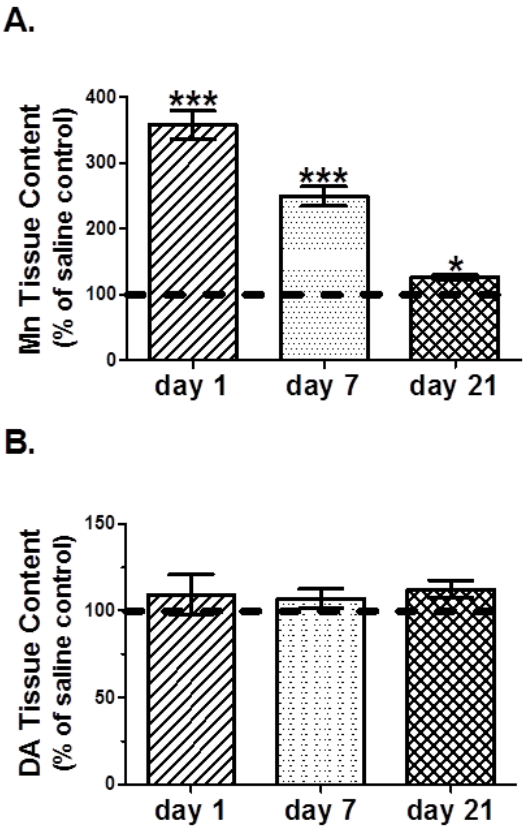

Figure 4.1: Striatal tissue A) Mn and B) DA levels in saline- and Mn-treated mice. Dashed line indicates the normalized values for saline-treated mice (set as 100%). Results are means (n = 7-8) expressed as percentage of saline-treated mice. *$P < 0.05$, ***$P < 0.001$ compared to control group (one-way ANOVA).

4.3.2 Microdialysis

In vivo microdialysis was used to determine whether the accumulation of Mn observed in striatal tissue influences the concentration of DA in the extracellular space of freely moving animals. Striatal extracellular DA levels (analyzed without correction for probe recovery) showed a significant difference between treatment groups ($F_{3,15} = 14.13$, $P = 0.0003$; Figure 4.2). Extracellular DA concentrations averaged from three baseline samples were not different between saline-treated mice (3.1 ± 0.1 nM; n = 10) and Mn-treated mice when DA was measured 1 (3.3 ± 0.1 nM; n = 6) or 21 (3.1 ± 0.3 nM, n = 8) days after Mn treatment. However, striatal DA levels were significantly decreased 7 days after Mn treatment (2.1 ± 0.1 nM; n = 8; $P < 0.01$).

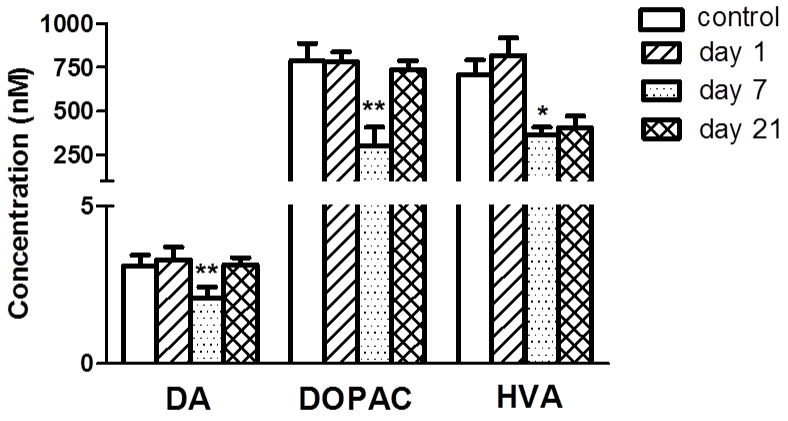

Figure 4.2: Baseline dialysis levels of DA and its metabolites DOPAC and HVA in the striatum of saline-treated versus Mn-treated mice. Results are reported as mean (n = 5 - 10) concentrations (nM) ± SEM. *$P < 0.05$, **$P < 0.01$ compared to respective controls (one-way ANOVA).

Since a decrease in extracellular DA levels was observed only at the day 7 time point, we set out to determine if this DA decrease is actually persistent across all time points but is perhaps masked by other presynaptic events. Others have established that the method of zero net flux can expose alterations in extracellular DA levels that are masked by transporter-mediated changes in *in vivo* probe recovery.[122,123] Therefore, zero net flux was utilized to evaluate DA levels at the day 1 and 21 time points, in addition to confirming the changes observed in extracellular levels at day 7. Basal DA levels in saline-treated mice, determined with zero net flux analysis, were similar at all time points and therefore the data were collapsed into one representative group labeled saline controls. The average extracellular DA levels (corrected for probe recovery) for this combined saline control group were 10.1 ± 1.1 nM (n = 8). Using zero net flux, a significant main effect of Mn treatment on extracellular DA in the striatum was revealed ($F_{3,25}$ = 7.871, P = 0.009, Figure 4.3). In mice treated with Mn, striatal DA levels were 6.9 ± 1.2 nM (n = 6) and 9.7 ± 1.6 nM (n = 6) 1 and 21 days after Mn treatment, respectively, which are not different from those observed in the saline control group. However, similar to the results using conventional microdialysis, Mn-treated mice showed a significant reduction in extracellular DA levels to 3.0 ± 0.4 nM (n = 6; $P < 0.05$) 7 days after cessation of sub-acute treatment.

In zero net flux experiments, the extraction fraction (E_d), determined from the slope of the regression lines, gives an approximation of the probe recovery.[116] The average E_d for saline controls (0.41 ± 0.05 nM) was not found to be significantly different (one-way ANOVA) from the extraction fraction at day 1 (0.31 ± 0.03 nM; $P < 0.01$), day 7 (0.38 ± 0.02 nM), or day 21 (0.34 ± 0.06 nM; $P < 0.01$) in Mn-treated mice.

Together, conventional and quantitative microdialysis results indicate that extracellular DA concentrations in the dorsal CPu are more susceptible to the effects of Mn accumulation at the intermediate time point of analysis (day 7) post-Mn exposure. In contrast, the relative recovery rate of DA was altered on days 1 and 21 (but not on day 7), suggesting Mn treatment has different time-dependent biological effects on DA neurotransmission.

Extracellular levels of the DA metabolites DOPAC and HVA were also evaluated to determine if Mn overexposure results in alterations in DA metabolism (Figure 4.2). One-way ANOVA demonstrated that DOPAC levels were significantly different due to Mn treatment ($F_{3, 19}$ = 8.24; P = 0.002). On day 7, extracellular DOPAC in saline-treated mice was 800 ± 100 nM (n = 5), but only 300 ± 100 nM (n = 5) in Mn-treated mice. Similarly, striatal HVA levels showed a significant decrease after treatment ($F_{3, 18}$ = 7.00; P = 0.004). Dialysate samples analyzed from saline- and Mn-treated mice at the day 7 time point had mean HVA levels of 700 ± 80 nM (n = 6) and 400 ± 40 nM (n = 4), respectively. No differences in DOPAC or HVA levels were seen at any other time points. Thus, changes in extracellular levels of DA metabolites were only observed 7 days after Mn treatment, which is consistent with our baseline dialysate DA analyses.

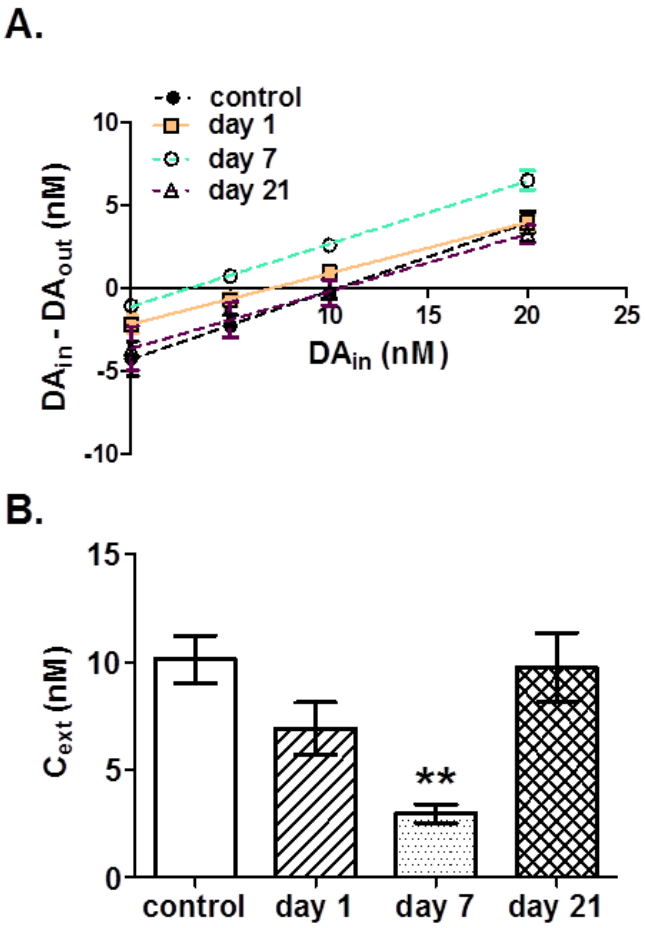

Figure 4.3: Extracellular DA levels determined by zero net flux microdialysis (n = 5). A) Striatal DA levels (C_{ext}), corrected for *in vivo* probe recovery, are represented by the x-intercepts of the plotted linear regression lines. **B)** Summary of extracellular DA levels corrected for *in vivo* probe recovery in saline- and Mn-treated mice. $^{**}P < 0.01$ compared to control group (one-way ANOVA).

To investigate whether Mn treatment affects stimulated DA release, extracellular DA levels were assessed by *in vivo* microdialysis following reverse dialysis with high-K^+ aCSF. Twenty minute perfusion of high-K^+ aCSF (120 mM KCl) maximally elevated extracellular DA levels (46 ± 5 nM) to ~15-fold above the baseline levels (3.1 ± 0.1 nM; n = 10) observed in saline-treated mice. Conversely, Mn treatment attenuated stimulated DA release at all time points. DA levels in Mn-treated mice were only increased to approximately 22 ± 2 (n = 6), 24 ± 4 (n = 8), and 29 ± 5 (n = 8) nM at 1, 7, and 21 days after Mn treatment, respectively (Figure 4.4). Two-way ANOVA showed a significant main effect of treatment ($F_{1, 126} = 13.19$, $P < 0.001$) and time ($F_{8, 126} = 83.57$, $P < 0.001$) as well as a significant interaction ($F_{8, 126} = 13.02$, $P < 0.001$), indicating Mn treatment significantly altered high-K^+ evoked increases in extracellular DA at all time points.

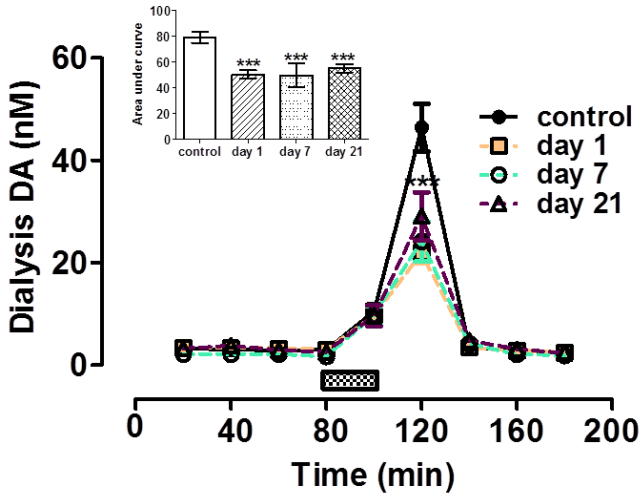

Figure 4.4: Extracellular DA levels determined by *in vivo* microdialysis. Time vs. DA concentration plots of high K^+ stimulated DA release. Black bar indicates 20 min time fraction in which 120 mM KCl aCSF was applied. Results are means (n = 6 - 10) of DA concentration (nM) ± SEM. Inset compares area under curve upon high K^+ stimulation in saline- (control) versus Mn-treated mice. *** $P < 0.001$ compared to control group (two-way ANOVA).

4.3.3 Fast Scan Cyclic Voltammetry

Due to the slow temporal resolution of microdialysis (20 minute sample intervals), this technique mainly detects net changes in the extracellular levels of DA and its metabolites. To assess various aspects of neuronal DA dynamics on a sub-second time scale, FSCV was utilized. FSCV enables the investigation of dopamine system functionality by quantifying DA release and uptake. Electrically-evoked DA release was measured in the CPu of saline and Mn-treated mice 1, 7, and 21 days after treatment. Additionally, the rate at which the DA transporter recycles extracellular DA back into the presynaptic neuron was compared between the control group and Mn-treated group at all three time points using a calculated V_{max} value. Since DA release and uptake were comparable across all treatment time points for the saline-treated mice, these data were collapsed into a single control group. This control group (n = 6) had an average DA release of approximately 1.7 ± 0.04 μM and an average uptake rate of 4.1 ± 0.2 μM/s. Analysis with one-way ANOVA determined electrically-evoked DA release was significantly different in Mn-treated mice compared to controls on day 21 ($F_{3,23}$ = 4.486; $P < 0.05$; Figure 4.5B), when stimulated release was recorded to be 0.6 ± 0.04 μM (n = 6), exhibiting approximately a 66% attenuation in signal. Neither day 1 levels of released dopamine (1.9 ± 0.3 μM; n = 6) nor day 7 levels (1.6 ± 0.4 μM; n = 6) showed any significant change from the control group. Additionally, the rate of DA uptake in the dorsal CPu was not altered in Mn-treated mice at any time point (average approximately 4.5 ± 0.09 μM/s; $F_{3,23}$ = 2.413; P = 0.0968; Figure 4.5C). Since all FSCV experiments examine dopamine release and uptake, when all animals were combined for analysis, the same trend was reproduced even in larger testing groups (n = 31 – 72/group; Figure 4.6)

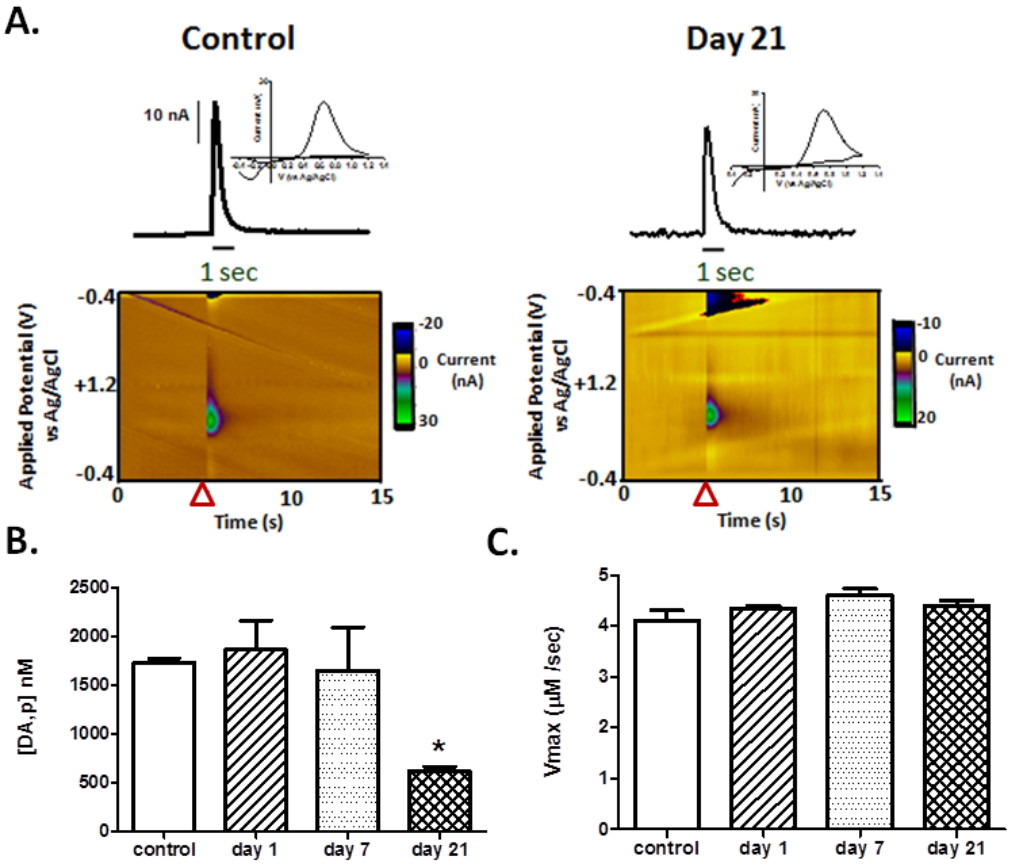

Figure 4.5: Electrically evoked DA release and uptake from the dorsal CPu as measured by FSCV. A) Representative concentration vs. time and false color plot of saline- and Mn-treated mice on day 21. Central figures show color plots integrating time, applied potential, and current as false color 3D plots. Red triangle represents time point of electrical stimulation (5 s). Current vs. time traces (converted to concentration vs. time using post-experiment electrode calibration) shown above, with inset showing characteristic DA current vs. voltage voltammograms. Summary of **B)** electrically evoked DA release and **C)** DA uptake rates in the CPu of saline- (control) and Mn-treated mice. Data are mean (n = 6/group) ± SEM expressed as DA,p (µM) or Vmax (µM/sec). **P* < 0.05 compared to control group (one-way ANOVA).

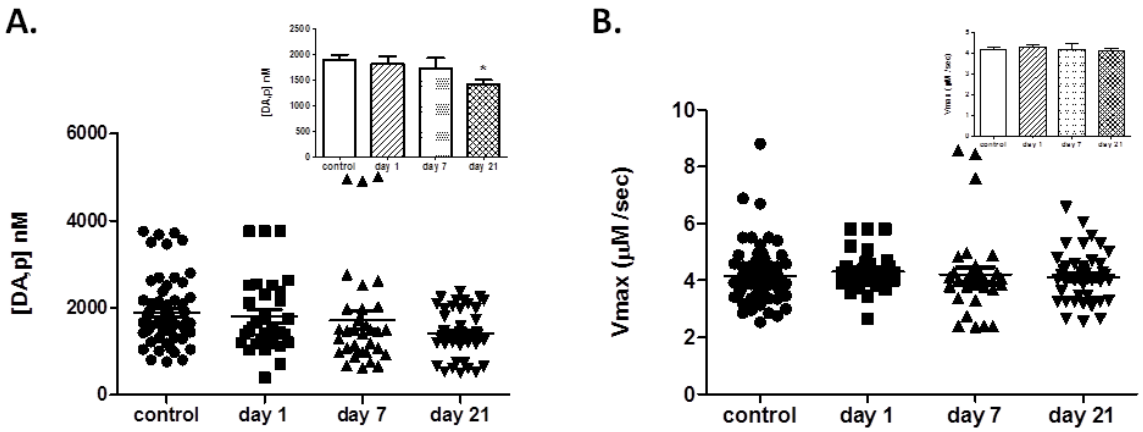

Figure 4.6: Scatter plot demonstrated reproducible trends in DA release and uptake in greater sampling population. A) FSCV measured DA release (n = 31 - 72/group) demonstrating reproducible trend of day 21 attenuation in release (inset), as well as precision of measurements. **B)** DA uptake rates are not different when samples are recorded from a larger population (n = 31 - 72/group; one-way ANOVA).

To test if alterations in the functionality of DA D2 autoreceptors caused the differences in DA levels detected following Mn treatment, the effect of the D2 receptor agonist quinpirole on electrically-evoked DA release was measured in slices from saline- and Mn-treated mice.[124-126] Dose-response curves were generated by perfusing increasing concentrations of quinpirole (0.001 to 10 μM) over the brain slice at 30-minute intervals (Figure 4.7). [125] For all treatment groups, quinpirole decreased electrically-stimulated DA release ($F_{7, 66}$ = 119.5; $P < 0.0001$). The concentration at which the pre-drug value of DA release was reduced by 50% from the maximum response (IC_{50}) was determined for each of the treatment groups. The IC_{50} for saline-treated mice was 71 ± 12 nM (n = 10) and 60 ± 12 nM (average) for Mn-treated mice, indicating that our protocol for Mn treatment does not affect the functionality of release-regulating presynaptic autoreceptors in the CPu ($F_{3,29}$ = 0.13; P = 0.94).

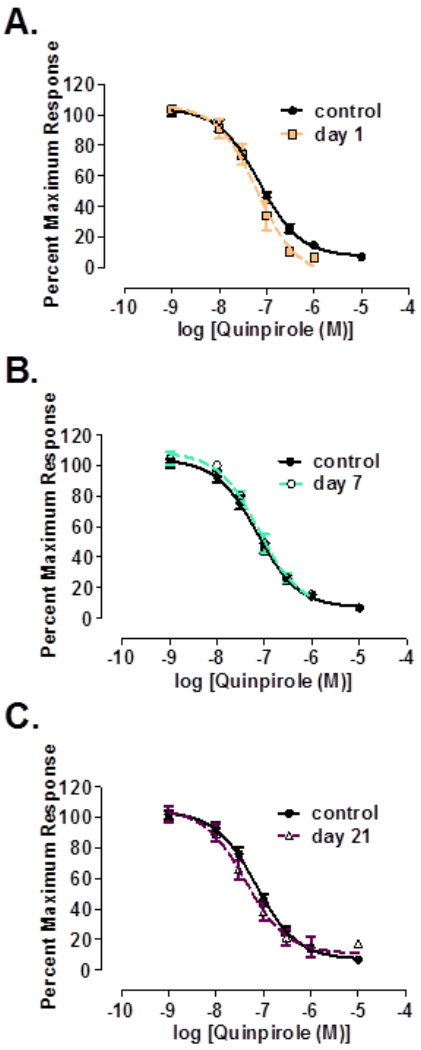

Figure 4.7: Quinpirole dose-response curves in the CPu. Dose-response curves generated by plotting the log concentration of quinpirole (M) vs. the maximal release of DA per pulse, as a percent of baseline response (defined as 100%). Dose-response curve of quinpirole on stimulated release in saline-treated controls versus Mn-treated mice shown for **A)** day 1, **B)** day 7, and **C)** day 21 (n = 3 - 10).

4.4 Discussion

Herein, we demonstrated that a sub-acute $MnCl_2$ exposure elevates striatal tissue Mn levels for at least 21 days after cessation of treatment compared to saline-treated mice. Despite being unable to detect changes in intraneuronal DA levels, both *in vivo* microdialysis and *in vitro* FSCV reveal Mn-induced baseline and stimulated release changes in extracellular DA, as well as differences in extracellular levels of the DA metabolites DOPAC and HVA. Contrary to literature reports, these alterations in release were not coupled with any compensatory changes in DA uptake or D2 autoreceptor functionality. [101,105,106,107,108]

Multiple administration methods (*e.g.* intraperitoneal, subcutaneous, inhalation, and oral), Mn salts (*e.g.* $MnCl_2$, $MnSO_4$, and $Mn(OAc)_3$), and doses (*e.g.* 25-100 mg/kg, >300 mg/kg, single- or multiple-dose regimes) have been used to study the subsequent neurological effects of Mn exposure.[55,59,127] The primary consideration in choosing an exposure protocol is whether or not the exogenous application of Mn results in a significant accumulation at the region of interest. In a review by Burton *et al.,* [55] it is suggested that cumulative doses any lower than 300 mg/kg do not significantly alter DA levels in the striatum of non-human primates. However in rodents, Dodd *et al.* [60] have shown that an intermittent, subcutaneous dose of 50 mg/kg $MnCl_2$ causes significant accumulation of Mn in the basal ganglia. Therefore, to better understand the impact of a sub-acute Mn exposure on DA dynamics, we adopted the protocol developed by Dodd *et al.* [60]

The development of a parallel detection method for Mn and DA in the striatum enabled a direct correlation between Mn accumulation and DA levels in the same tissue sample. This parallel analysis subsequently revealed that intraneuronal DA levels are not affected even

though persistent accumulation of Mn is observed in the striatum for up to 21 days after subcutaneous $MnCl_2$ exposure (Figure 4.1). This increase in Mn is in accordance with what was observed by Dodd *et al.*,[60] who also reported a significant effect on locomotor activity but conducted no analysis of the DA system. Our tissue content results indicate that there are no alterations in intracellular DA concentrations. However, there may still be underlying changes in DA dynamics that are masked by the inability of tissue content analysis to distinguish between intra- and extracellular DA levels.

In vivo microdialysis was used to determine whether sub-acute Mn treatment selectively altered extracellular DA, DOPAC, or HVA levels in the striatum at three discrete time points after Mn exposure. Extraneuronal DA, DOPAC, and HVA levels, without correction for probe recovery, showed no differences immediately (24 hours) or 21 days post-Mn treatment but were significantly reduced 7 days after sub-acute exposure compared to control mice (Figure 4.2). These results suggest that alterations in presynaptic DA dynamics are delayed, despite the immediate increase in striatal Mn levels observed by tissue content analysis. Furthermore, our results suggest that a sub-acute Mn exposure does not deplete intracellular DA, as total tissue DA levels in the striatum were unchanged despite reductions in extracellular DA levels. Since the tissue content of DA is mainly reflective of intraneuronal stores, this treatment protocol does *not* appear to be neurotoxic. However, the dialysate results from this study suggest that the presynaptic DA system is vulnerable to the effects of excessive Mn accumulation. Compared to previous studies that have examined the acute or long-term consequence of Mn on presynaptic dopamine dynamics, our study investigated more intermediate time points following Mn exposure. [101,103,104] Acute treatment was shown to alter extracellular DA levels,

while no difference was observed in extracellular DA levels in either the CPu or NAc 70 days following prolonged (20 consecutive days) postnatal Mn-treatment.[101,103,104] Although our study did not detect any immediate changes in extracellular DA levels as in the Serra and Vidal studies, which may be the result of differences in Mn concentration or duration of Mn infusion, our results suggest that sub-acute Mn exposure in adults has the ability to influence presynaptic DA dynamics; however, these impairments are apparent for only a restricted period of time.

To investigate whether Mn exposure results in other compensatory changes at presynaptic DA terminals, high K^+ was perfused (via reverse dialysis) into the striatum to measure DA efflux. Our results show that Mn-treated mice at all time points had an attenuated response to high K^+ infusion compared to controls. These results are consistent with the reduction in K^+ evoked DA release observed by Vidal *et al.* upon an intrastriatal infusion of Mn. [104] Furthermore, long-term consequences of Mn-treatment have been seen in the form of a blunted striatal response to cocaine induced DA efflux. [101] Additionally, Guilarte *et al*. [99,100] have shown a decrease in amphetamine-induced DA release upon Mn accumulation in non-human primates. Taken together, these results suggest that Mn profoundly influences the ability of exogenous compounds to evoke presynaptic DA release. In further support of this conclusion, when electrically-evoked DA release was monitored using FSCV, a blunted DA response was observed in Mn-treated mice that paralleled the alterations observed with *in vivo* microdialysis. Although the neurochemical techniques (microdialysis versus FSCV) and sample preparation methods (intact brain versus slice preparation) used to probe DA dynamics are different, together they suggest that sub-acute Mn exposure can induce severe impairments in presynaptic striatal DA

efflux. One thing to note is that FSCV only shows impairments 21 days after Mn-treatment whereas alterations in microdialysis results are seen at all time points. This difference may be attributed to the stimulation parameters used for each of these techniques. Specifically, the microdialysis high K^+ stimulation of 20 mins is six orders of magnitude greater in duration than the 4 ms electrical-stimulation applied to the slice when using FSCV. As a result, a stimulation longer in duration may be able to overcome any release-regulating impairments that are elucidated by shorter stimulation methods.

To better understand whether subtle but biologically significant alterations in extracellular DA occur at any other time points in Mn-treated mice, the microdialysis technique of zero net flux was used. Zero net flux microdialysis permits estimation of basal extracellular DA levels by infusing in various concentrations of DA to quantify the extracellular DA concentration (C_{ext}). C_{ext} is defined as the point where there is no net diffusion of DA between the extracellular space and the microdialysis membrane (the x-intercept).[129,130] This method also provides an approximation of *in vivo* extraction fraction (E_d) from the slope of the zero net flux regression line. [123,131] The present results obtained by zero net flux in the CPu agree with those without correction for extraction fraction, as a significant decrease in extracellular DA concentration was observed only 7 days after Mn-treatment in both cases. Notably, zero net flux results did not show a significant difference in E_d at any of the time points after Mn treatment (Figure 4.3). Since previous studies by Justice and co-workers have shown that pharmacologic inhibition of DA transporter-mediated uptake alters E_d, this finding suggests Mn treatment may not affect DA transport.[114,115,123,128-130] However, zero net flux studies in monoamine transporter knockout mice (heterozygous for DA and complete knockout for serotonin transporter) show no

difference in striatal E_d. [117,132] Thus, there is considerable debate on how E_d values correlate with transporter function.[117,133,134] A more direct method to measure the DA uptake function of the DA transporter is to use FSCV, which records the release and uptake of DA following electrical stimulation in brain slices with high temporal (100 ms) resolution.[8,87, 135] This method has been used to show that DA is typically cleared from the extrasynaptic space in less than one second in non-treated animals, highlighting the necessity of a higher temporal resolution technique to detect uptake changes.[8,87,135] In contrast to our zero net flux results, no difference in DA uptake rates between controls and Mn-treated mice was observed by FSCV. Specifically, our analysis of DA V_{max}, a quantification of the rate at which the DA transporter reuptakes DA into the presynaptic neuron, showed no difference compared to saline-treated mice (Figure 4.5). Previous studies have implicated the DA transporter for Mn transport into DA neurons.[100,101,105,106,136,137] However, there is uncertainty as to whether Mn directly interacts with the DA transporter or, once inside DA neurons, disrupts either presynaptic proteins or DA function.[99,100,105,136-138] Our FSCV results argue that Mn does not directly alter DA uptake, as no difference in uptake rates were observed. However, a significant concomitant reduction in stimulated DA release was measured by both microdialysis and voltammetry. Taken together, these results suggest that intracellular accumulation of Mn has the ability to either directly or indirectly influence presynaptic DA release dynamics for at least 21 days after sub-acute Mn treatment.

There is considerable evidence suggesting that Mn can alter DA D2 receptor binding and protein expression, but the lack of consistent findings across Mn treatments and animal models has made it difficult to ascertain the exact interaction between excess Mn and DA D2

receptors.[99,107,108] Since our study shows that a sub-acute Mn exposure reduces DA release dynamics with both microdialysis and voltammetry, we sought to determine if the impaired stimulated DA release was modulated by presynaptic release-regulating DA D2 autoreceptors. An advantage to using FSCV to probe DA D2 autoreceptor functionality is that brain slices exclude contributions from the DA D2 impulse-regulating receptors found on cell bodies, allowing for a selective evaluation of nerve terminal D2 autoreceptors that control exocytotic DA release.[83,139] The results from the present study show no difference in the half maximal inhibitory concentration (IC_{50}) values for the DA D2 agonist quinpirole, suggesting that a sub-acute Mn exposure does not affect DA D2 autoreceptor functionality in the CPu. Similarly, but using a different protocol, non-human primates treated with Mn for at least 27 weeks showed no alterations in D2 autoreceptor levels in the caudate or putamen, and a pre-weaning Mn exposure (21 days long) in rats also showed no differences in striatal D2 protein levels 3 and 86 days after treatment.[59,100140,141] However, there are other studies showing either an increase or decrease in DA D2 receptors after Mn treatment, and it is postulated that these variations in effects are due to the wide range of Mn treatment protocols and/or animal models that are used to evaluate potential Mn-DA interactions. [107,108]The results from this study with a sub-acute Mn exposure protocol suggest that there is no direct effect of Mn on DA D2 autoreceptor functionality in the CPu and furthermore, that the impaired DA release in these Mn-treated mice are not a result of DA D2 receptor dysfunction.

Intraneuronal Mn accumulation in DA neurons has numerous intracellular targets that could disrupt presynaptic DA release. For example, one target protein that receives considerable attention is α-synuclein which is a fundamental component of Lewy bodies (a hallmark of

Parkinson's disease).[142,143] The exact role of α-synuclein in neurotransmitter regulation has remained elusive, but there is increasing evidence that it is involved in modulating neurotransmitter release.[144-146] Mice that overexpress α-synuclein have impaired DA release, which does not appear to be a result of altered DA synthesis, vesicular activity, or DA transporter-mediated reuptake.[144] Interestingly, these DA system changes observed by Larsen *et al.* parallel our findings in which a reduction in DA release is observed with no change in uptake. Since Parkinson's disease and manganism are both linked to DA system dysfunction, manifested as a loss of motor control, it is plausible that α-synuclein is a common mediator in both diseases.[100,142,143] However, future experiments would need to be performed to affirm interactions between Mn and α-synuclein.

Although it is enticing to associate Mn with alterations in α-synuclein expression because of its similarities to Parkinson's disease, it is possible that the attenuated DA release is a result of dysfunction in other neuromodulators that would be susceptible to excess Mn accumulation and subsequently cause dysfunctions in DA transmission. [100,142] For example, in the presence of excess Mn, it is postulated that DA can be further oxidized, leading to an elevation in the amount of free radicals or hydrogen peroxide in the brain.[55,147-150] Hydrogen peroxide itself is a modulator of synaptic DA release.[151] If excess Mn causes an imbalance (increase) in hydrogen peroxide levels, then it is plausible that either this by itself or in combination with α-synuclein could lead to the reductions we observed in presynaptic DA transmission.

4.5 Conclusion

In summary, this work used several neurochemical techniques, which together, indicate that a sub-acute Mn exposure impairs stimulated DA release, with the most pronounced

alterations appearing 7 days after treatment. This is the first time that DA system dynamics have been monitored after Mn exposure at 3 discrete time points (early, intermediate, and late) in mice. Specifically, our results suggest that the DA system appears to be most susceptible to presynaptic alterations 7 days after Mn treatment. Specifically at this time point, *in vivo* microdialysis revealed a unique concomitant attenuation in striatal extracellular DA (both with and without probe correction), HVA, and DOPAC levels. The decreases in extracellular DA levels do not appear to be a result of altered DA uptake or DA D2 autoreceptor function. Most importantly, this effect on release is finite, as extracellular DA levels appear to rebound to control levels at a later time point of analysis (21 days). Taken together, these results suggest that Mn accumulation within the striatum can severely impair DA release dynamics, without showing signs of neurotoxicity.

Chapter 5: Behavioral Impact of Striatal Mn Accumulation

5.1 Introduction

Chronic exposure to manganese (Mn) results in motor impairments in clinical patients of manganism.[58,60,93] As dopamine's role in reward, learning, and movement is well documented, it is no surprise that a primary candidate for the study of Mn-induced neurotoxicity is the striatal dopaminergic system.[1,4,65,99,104,138] What *is* surprising is that to date, very few studies have been able to reproduce manganism-like behavioral changes in lab settings. Monkeys tested on learning tasks before and after dosing with $MnCl_2$ via inhalation, the method of exposure most similar to humans, show no difference in carrying out the task when compared to controls.[101,152] Similarly, rats exposed to manganese chloride using various doses and paradigms reveal no difference in open field locomotor activity when compared to saline controls.[101,153,154] In other rodent studies, when a baseline locomotor impairment is observed, contradictions in the results (increase versus decrease) beg for a more critical analysis.[60,140,155,156] A difference in locomotor activity is often revealed when comparing previously Mn-treated mice and saline-treated mice after the administration of a high dose of a psychostimulant such as amphetamine or cocaine.[101,154] A psychostimulant challenge may be an effective way to unravel subtle behavioral changes in animal models of manganism. [101,154,157]

Locomotor activity is often used as an indirect measurement of extracellular dopamine in the striatum.[158-160] As our previous Mn studies indicated a time-dependent change in dopamine release and in extracellular levels, we wanted to evaluate if the same correlation would hold true for the Mn-treated dopamine system of C57Bl/6 mice. The aim of this study, therefore, was to characterize the motor behavior of Mn-treated versus saline-treated mice to elucidate

any correlation between our observed neurotransmission alterations (Chapter 4) and potential changes in physical function due to the established subacute Mn treatment protocol.

5.2 Materials and Methods

5.2.1 Animals

All experiments conducted using both male and female C57Bl/6 mice weighing 20-30 g. Mice were purchased from Jackson Laboratories and bred-in house at Wayne State University's animal care facilities, where they were housed 3 - 4 mice per cage. Food and water was available *ad libitum*. All protocols and animal care followed guidelines set by the National Institutes of Health Office of Animal Care and Use and were approved by the Wayne State University Institutional Animal Care and Use Committee.

5.2.2 Manganese Treatment

Manganese (Mn) treatment was administered over the course of a week, every third day, on days 1, 4, and 7. Mn-treated group received 50 mg/kg dose subcutaneous injections of 0.1 mL manganese (II) chloride tetrahydrate ($MnCl_2.4H_2O$), made up in saline. Saline-treated control group received equivalent volume injections of saline (0.9% sodium chloride, NaCl). This treatment was adapted from Dodd *et al.*[60] due to its demonstrated ability to result in Mn accumulation in the basal ganglia. All behavioral tests were conducted after the last injection, either 24 hours later (day 1), 7 days later, or 21 days later.

5.2.3 Locomotor Activity Testing

Locomotor testing was done over the course of 2 hours, with the exception of tests in which methamphetamine was administered, which were conducted over the course of 4 hours. Throughout locomotor testing mice were kept in home cages to avoid behavioral changes due

to new environment stress. Animals were monitored in three categories: ambulatory distance (cm), stereotypic count, and vertical count. In addition to baseline behavior data, a methamphetamine injection (3 mg/kg, made in saline) was given intraperitoneally *(i.p.)* and the same three categories were subsequently monitored. All measurements made in static exposure chambers using 16-beam infrared emitter-detector arrays (Med Associates, St. Albans, VT) that measure beam breaks in the x, y, and z direction by software (Open Field Activity Software [SOF-811], Med Associates, St. Albans, VT). Beam breaks are translated into total distance traveled in the x and y direction (ambulatory distance, cm), repetitive behavior without change in x and y direction (stereotypical activity, counts), and beam breaks in z direction, translated to rearing behavior (vertical counts). All activity measurements were made in 60 second time blocks.

5.2.4 Beam Walk Testing

To perform the beam-walking test, mice were placed on a custom-built wooden plank (7/16 in x 36 in) 3 feet off the ground, angled at about 15° towards a safe box.[161] Mice were trained to walk across beam for three days before actual days of analysis (days 1, 7, and 21, as mentioned above). After three days of training, mice were video recorded while crossing the beam and time to traverse the length of the beam was recorded. Any mouse that did not cross the beam, fell off, or took more than 30 seconds was disqualified and excluded from the reported data of group.

5.2.5 Statistical Analysis

All data analyzed with GraphPad Prism software (GraphPad, La Jolla, CA). Values are expressed as means ± standard error of means (SEMs) with a difference of $P < 0.05$ considered

statistically significant. Comparisons of three or more means were made by a one-way analysis of variance (ANOVA). Two-way ANOVA with Bonferroni post-test was used when testing for interaction of multiple variables. Grubbs test (using GraphPad Outlier calculator online) used to exclude outliers in data sets with an alpha value set to 0.05.

5.3 Results

5.3.1 Baseline Ambulatory Distance

To evaluate the effect of Mn treatment on baseline locomotor activity, mice were placed inside the locomotor activity chamber while still in their homecages and movement in the x and y plane was recorded for two hours with no external stressors. The resultant data, summed up in 10-minute time blocks, is presented in Figure 5.1. All data for saline-treated controls on the respective days of analysis are combined to form one control group (n = 23). Compared to the control group, Mn-treated mice on day 1 had significantly lower locomotor activity (n = 9, two-way ANOVA, **$p < 0.01$ vs. control). Baseline distance traveled was not different from controls on days 7 (n = 6) or 21 (n = 5).

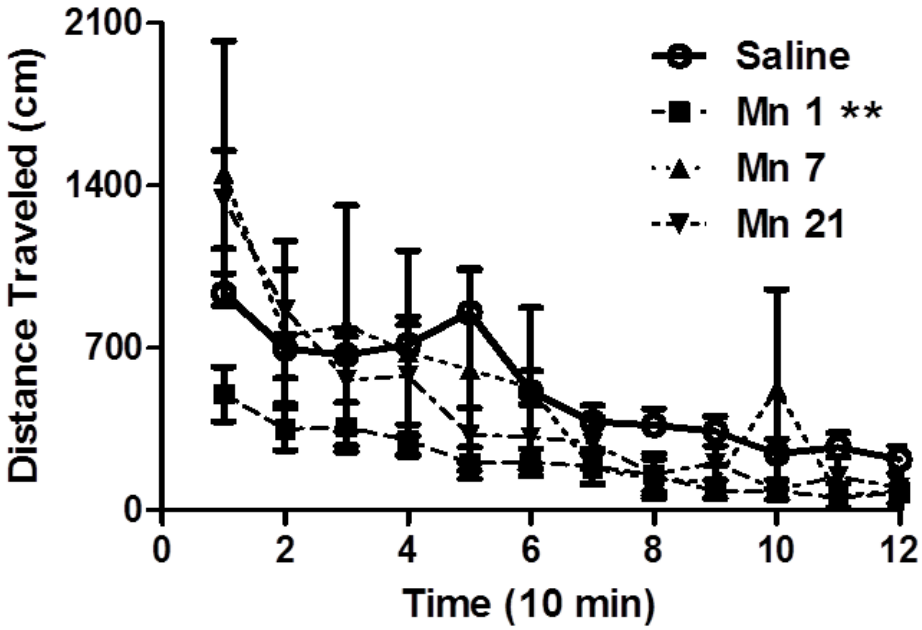

Figure 5.1: Baseline Ambulatory Distance. Distance traveled is plotted in cm on the y-axis and time blocks of 10 minutes are plotted on the x-axis for 2 hours of testing. Compared to saline-treated controls, Mn-treated mice show significant attenuation in homecage locomotor activity on day 1 (n = 5 - 23/group, two-way ANOVA, **p < 0.01 vs. control).

5.3.2 Baseline Stereotypy

Quantifying stereotypic counts during testing of ambulatory distance assessed potential impairment in repetitive movements of mice after Mn treatment. Mn- and saline-treated mice were compared by summing up total stereotypic counts over the course of two hours. Saline-treated mice (n = 26) exhibited an average stereotypic count of 17767 ± 1446. Mn-treated mice on days 7 (18111 ± 1966, n = 13) and 21 (18548 ± 1021, n = 8) were not different in stereotypic activity compared to saline control group (Figure 5.2). Significant impairment in repetitive movement was observed in Mn-treated mice on day 1 (12280 ± 1569, n = 16, one-way ANOVA, *$p < 0.05$ vs. control).

5.3.3 Baseline Vertical Counts

Vertical counts were quantified during locomotor testing to assess rearing behavior after Mn treatment. Mn-treated mice had an increase in vertical counts progressing from analysis on day 1 (450 ± 107, n = 11), 7 (1041 ± 159, n = 10), to 21 (2025 ± 541, n = 8). Compared to saline controls (825 ± 177, n = 21), rearing behavior on day 21 was significantly potentiated (one-way ANOVA, **$p < 0.01$ vs. control; Figure 5.3).

5.3.4 Ambulatory Distance – Psychostimulant Challenge

Ambulatory response to a methamphetamine challenge was monitored in both Mn-treated and saline-treated mice. A 3 mg/kg *i.p.* dose of methamphetamine caused an increase in locomotor activity across all groups (Figure 5.4). Analysis by two-way ANOVA revealed a significant effect of Mn treatment on day 7 (n = 10, * $p < 0.05$) compared to control group (n = 17), exhibiting a blunted increase (Figure 5.4C). Neither day 1 (n = 13; Figure 5.4B) nor day 21 (n = 7; Figure 5.4D) showed a difference in psychostimulant challenged behavioral response.

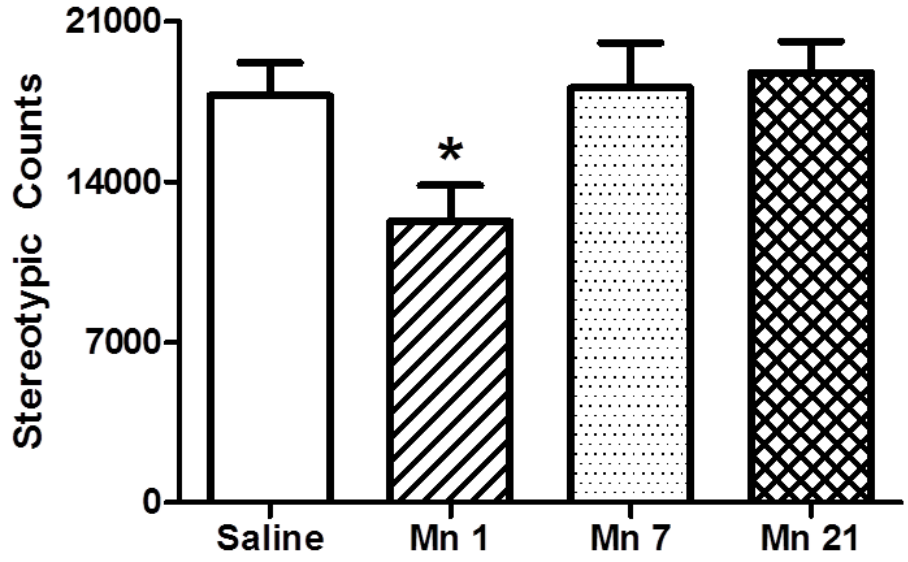

Figure 5.2: Summation of Baseline Stereotypic Counts Over Two Hours. Measure of repetitive movements, indicative of stereotypic behavior, shows impaired stereotypy in mice treated with Mn 1 day after treatment cessation (n = 6 - 26/group, one-way ANOVA, *$p < 0.05$ vs. control).

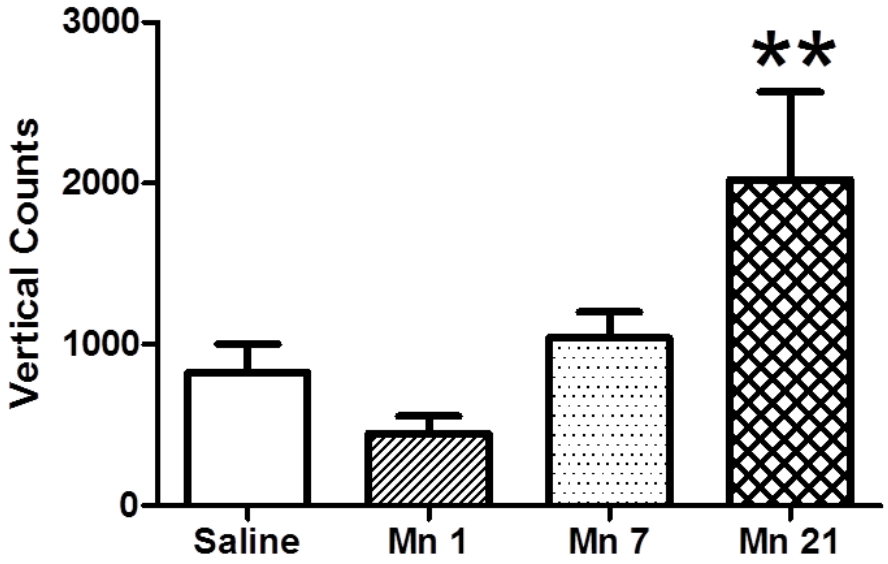

Figure 5.3: Baseline Vertical Counts after Mn Treatment. Summation of baseline vertical counts over two hours shows increased vertical counts in mice treated with Mn 21 day after treatment cessation (n = 5 - 22/group, one-way ANOVA, **p < 0.01 vs. control).

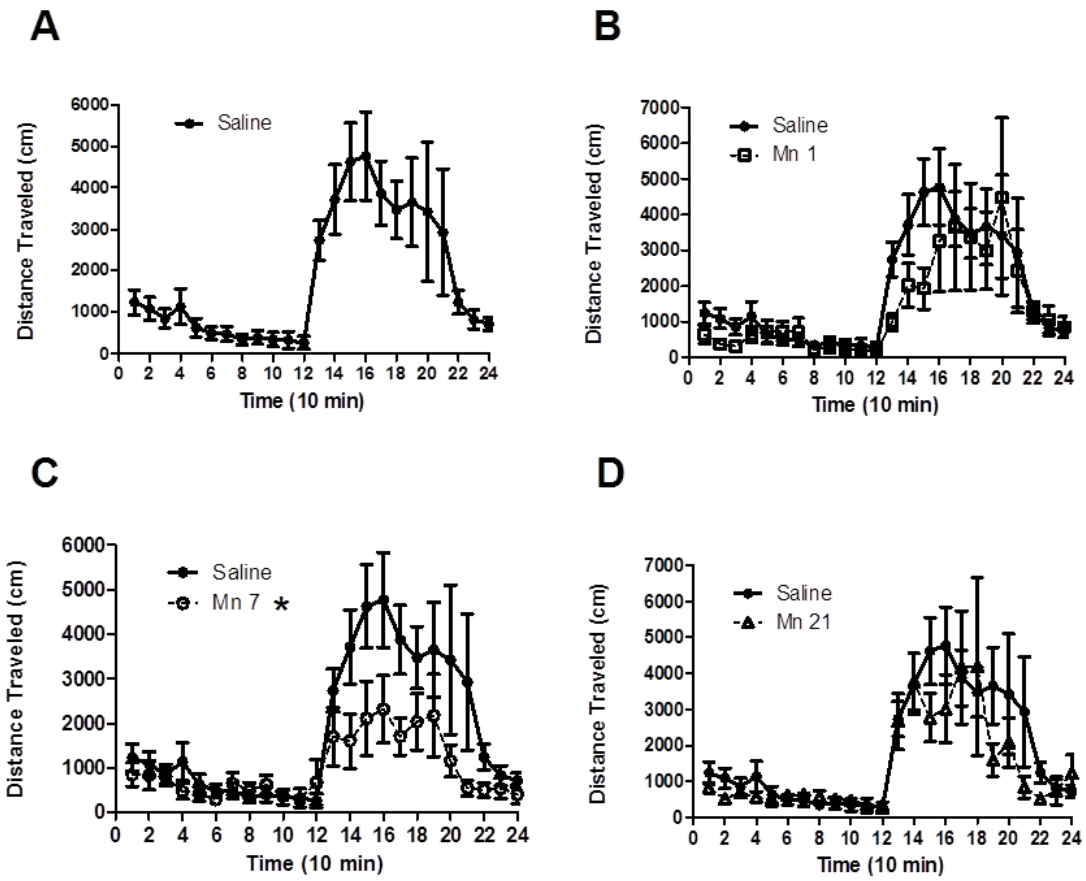

Figure 5.4: Locomotor Activity after Methamphetamine Challenge. After two hours of baseline collection, mice were challenged with a 3 mg/kg i.p. injection of methamphetamine, and subsequent locomotor effects were monitored for another two hours. **A)** Ambulatory distance traveled by saline-treated mice (n = 17). **B)** Compared to saline-treated controls, Mn-treated mice 1 day after treatment (n = 13). **C)** Methamphetamine Mn-treated mice on day 7 had a blunted locomotor response compared to the saline controls (Mn-treated: n = 10; two-way ANOVA, *$p < 0.05$ vs. control). **D)** Ambulatory distance traveled by mice on day 21 (n = 7) was not different when compared to saline controls.

5.3.5 Stereotypy – Psychostimulant Challenge

Three mg/kg *i.p.* injection of methamphetamine was used to elucidate effect of Mn treatment on repetitive behavior of mice in response to a psychostimulant (Figure 5.5). A main effect of methamphetamine treatment was observed by two way-ANOVA (n = 4 – 26/group, ***$p<0.001$), with baseline saline control values (17767 ± 1446, n = 26) increasing to 24594 ± 1807 counts (n = 17). Mn-treated day 1 stereotypic counts increase from 12280 ± 1569 (n = 16) to 23159 ± 1337 (n = 13), day 7 counts increase from 18111 ± 1966 (n = 13) to 26018 ± 4191 (n = 10), and day 21 stereotypic counts increase from 18548 ± 1021 (n = 8) to 28253 ± 2702 (n = 7). This data means that the expected increase in repetitive movements in response to the methamphetamine injection was observed across all groups of animals with no apparent difference in the meth-stimulated levels of stereotypy within the groups themselves.

5.3.6 Vertical Counts – Psychostimulant Challenge

Figure 5.6 shows measured changes in vertical counts upon methamphetamine administration. Average vertical counts of saline-treated mice increased from 1460 ± 656.8 (n = 22) to 3745 ± 1691 (n = 11). Mn-treated mice tested 1 day after treatment increased from 450 ± 107 (n = 11) to 1723 ± 568 (n = 8). Conversely, the vertical counts of mice tested on day 7 after treatment decreased from 1041 ± 159 (n = 10) to 420 ± 129 (n = 6). The same trend was observed in the group analyzed on day 21, decreasing to 729 ± 157 (n = 7) from 2025 ± 541 (n = 8). This divergent response to methamphetamine is unprecedented in any of our other behavior tests.

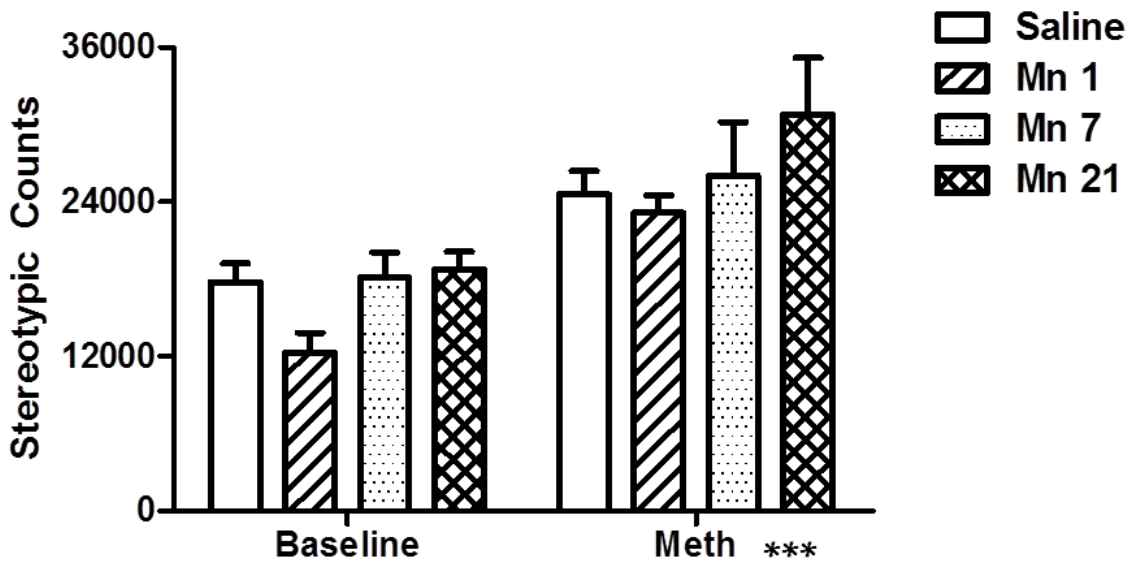

Figure 5.5: Summation of Stereotypic Counts after Psychostimulant Challenge. Effect of 3 mg/kg of methamphetamine on stereotypic counts as plotted compared to baseline. A main effect of increased stereotypy observed after methamphetamine (n = 4 – 25/group, two way-ANOVA***$p<0.001$).

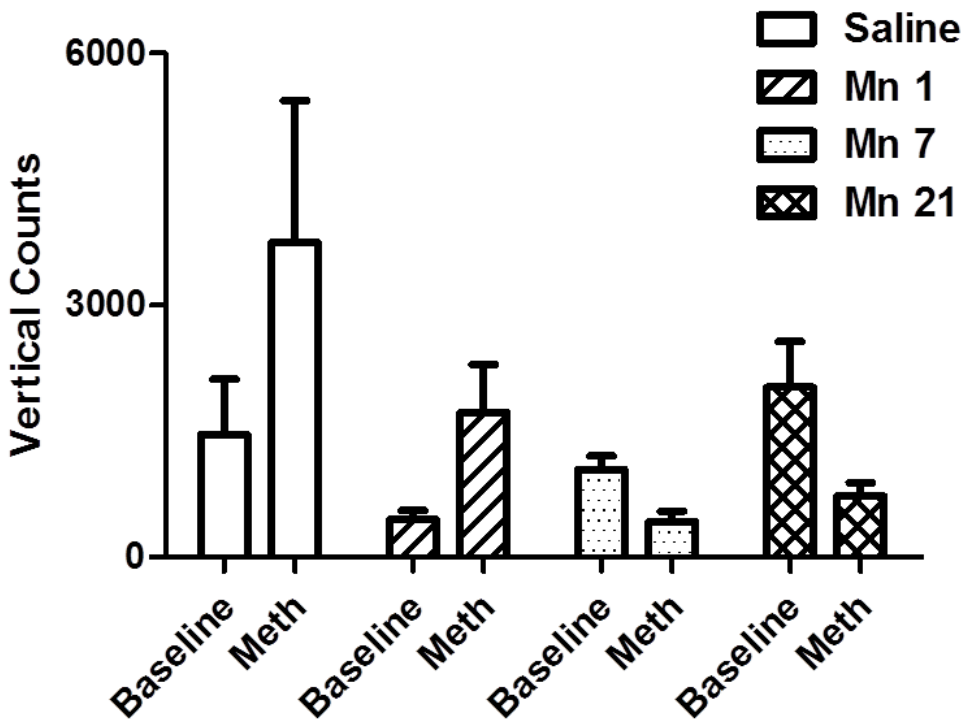

Figure 5.6: Summation of Vertical Counts after Psychostimulant Challenge. Effect of 3 mg/kg of methamphetamine on vertical counts plotted compared to baseline (n = 3 – 21/group, two way-ANOVA).

5.3.7 Beam Walk Balance Test

When data from saline-treated mice from all three time points were collapsed to form one control group (n = 21), the time to cross the beam was not different from the time it took Mn-treated mice to complete the same task at any of the three time points (n = 7, n = 7, and n = 5 on days 1, 7, and 21, respectively; Figure 5.7A). When comparing the number of mice that were disqualified from each group because they did not successfully complete the task, either due to falling, refusal to walk, or taking more than 30 seconds, Mn-treated mice on day 1 were almost 20% more likely to fail than the saline-treated controls (Figure 5.7B).

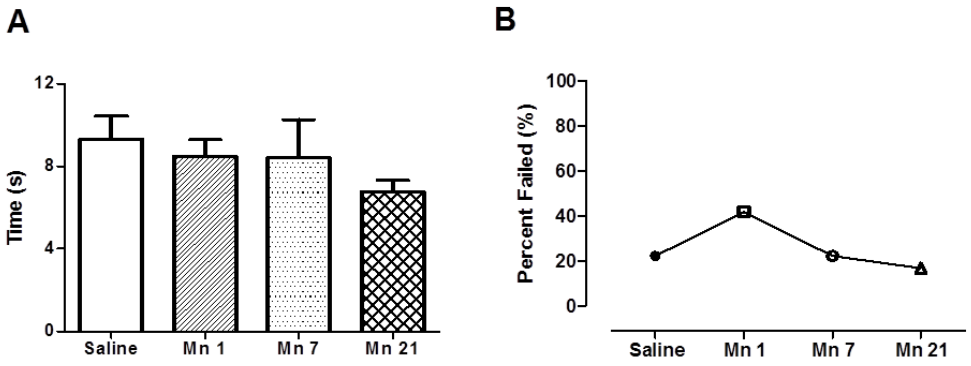

Figure 5.7: Beam Walk Assessment of Motor Coordination. A) Time required to traverse a narrow beam compared across Mn-treated groups and saline control. One way ANOVA shows no difference in beam walk time between Mn-treated and saline-treated controls. **B)** When comparing how many mice failed to complete the task in each group, Mn-treated mice on day 1 are 20% more likely to fail compared to saline controls.

5.4 Discussion

Since manganism is primarily characterized as a movement disorder, the aim of this study was to determine if our intermittent sub-acute Mn treatment protocol resulted in behavioral changes in mice treated with Mn over the course of a week. As locomotor activity is oftentimes considered to be an indirect measure of extracellular dopamine levels, we hypothesized that the attenuation in extracellular and stimulated dopamine observed by microdialysis and fast scan cyclic voltammetry would result in hypolocomotive mice after Mn treatment. Although behavioral studies have been conducted in animals treated with Mn in the past, it was imperative that we study the behavior of our mice after subcutaneous Mn injections for two reasons. First, although the literature reports behavioral observation of Mn exposed animals, the results obtained are far from conclusive.[60,101,140,153-156] While some report decreases in open field locomotor behavior, others are unable to elicit any phenotypic differences after Mn exposure. Furthermore, several researchers report hyperlocomotive activity in Mn-treated rodents compared to controls. As these studies that have reported hyperlocomotor activity vary greatly in their mode of Mn exposure (*e.g.* intraperitoneal or subcutaneous injections, oral administration, inhalation), duration of exposure (*e.g.* one week, twenty-one days, ten weeks, five months), and animal models used (*e.g.* mice, rats), their results cannot be directly extrapolated to predict the behavioral response of our treatment protocol in C57Bl/6 mice. Second, as our analysis timeline is unique, with neurochemical and behavioral analyses done 1 day, 7 days, and 21 days after treatment cessation, our interest lies in understanding the short and long term effects of Mn exposure, which is typically not reported in a single study.

Confirming our hypothesis, baseline locomotor activity data shows a decrease in X-Y direction movement. Contrary to our prediction, locomotor activity is blunted on day 1, while lower extracellular dopamine levels were recorded on days 7 (via microdialysis; Chapter 4) and day 21 (via fast scan cyclic voltammetry; Chapter 4). Although our subacute Mn dose is high enough to induce behavioral changes, the resultant locomotor activity effects may not be as straightforward as expected. Whereas in human patients the three stages of manganism symptoms culminate in motor deficiency as a late stage phenotype, our animal model reveals much earlier onset of impairment. Additionally, as opposed to human cases of manganism, this impairment does not appear to be permanent in murine studies, showing a return to normal activity by day 7 of analysis.

Consistent with the decline in ambulatory distance on day 1, stereotypic counts, indicative of repetitive behavior, were also lower on this day. This attenuation in stereotypy is postulated to be analogous to the rigidity observed in patients of manganism. Although no overt signs of rigidity were observed, we believe the inhibition of characteristic functionless rodent behavior that coincides with the time point of reduced horizontal movement signals the beginning of a bradykinesic state. Similar to ambulatory distance movements, stereotypical counts returned to control levels when tested one week after treatment cessation. This compensatory rescue is seen throughout our studies, both in neurochemical measurements and behavioral responses, demonstrating the ability of an intact neurological system to regulate homeostatic conditions in the face of an acute environmental insult such as our Mn treatment protocol.

The final baseline measurements made sought to assess potential changes in rearing behavior after Mn exposure. In this analysis, an increase in vertical counts on day 21 was

observed. Although the day that changes were seen in rearing behavior is different from all other behavioral measurements, this time point coincides with the changes in dopamine release as measured by fast scan cyclic voltammetry. Unlike all of our previous behavioral recordings, the vertical counts were *higher* than saline-treated controls. It is important to note that, although not statistically significant, a slight decrease in vertical counts was also observed on day 1, which would coincide with the day 1 impairments seen in the other two behavior tests.

All three aforementioned tests were repeated with the addition of a psychostimulant challenge. In addition to blocking the dopamine transporter, the psychostimulant methamphetamine acts as a releaser of dopamine.[1] As previously noted, an increase in extracellular dopamine has been correlated to hyperlocomotive activity; therefore, a 3 mg/kg *i.p.* challenge of methamphetamine is expected to access higher levels of intraneuronal dopamine stores. We hypothesized that due to the lower levels of stimulated and extracellular dopamine measured in previous experiments, this would not be possible for the Mn-treated mice at certain time points. The expected outcome was that although methamphetamine would significantly increase movement in saline-treated control mice, no potentiation of locomotor activity would be observed in Mn-treated animals. The acute challenge of methamphetamine resulted in a potentiation of ambulatory distance traveled in saline-treated mice and Mn-treated mice on days 1 and 21. As predicted, testing on day 7 after Mn treatment completion revealed blunted stimulation of movement. This blunted methamphetamine-induced activity coincides with the time point of lowest levels of extracellular dopamine, suggesting that mice on day 7 exhibit signs of an inability to access intraneuronal stores of

dopamine by methamphetamine. The most inexplicable trend in psychostimulant challenged behavioral response was seen in rearing behavior: both saline-treated and Mn-treated mice on day 1 showed an increase in vertical counts after methamphetamine stimulation, while day 7 and day 21 analysis revealed a *decrease*. The lower vertical counts despite a high dose of stimulant could simply be due to the increase seen in stereotypy; as there is a surge in repetitive behavior at those time points, there may be less interest in rearing.

Aside from activity chamber testing, the beam-walking test was used to characterize balance and coordination of Mn-treated mice, as well as an indicator of nigrostriatal damage. Thus, the beam-walking test has been used to assess the impact of Mn treatment on the basal ganglia.[162,163] There was no difference in coordination between Mn- and saline-treatment groups as the time required to traverse the beam was the same in both groups. These beam-walking data confirm that the subacute treatment protocol used for our work does not significantly damage the nigrostriatal pathway, which further substantiates our previous findings that recovery was demonstrated after impaired motor behavior. Interestingly, although no change is seen between groups overall, 20% more mice were observed to fail at the task (due to falling or noncompliance) than any other group on day 1. Supplementing the impaired locomotor and stereotypy data at the same time point of analysis, this would suggest the beginning of a bradykinesic state in Mn-treated mice on day 1.

Others have also reported similar locomotor impairment on day 1 in spite of a lack of parallel changes in dopamine levels.[156] In their work, however, GAD_{67}-GFP knock-in mice were used, which have γ-aminobutyric acid (GABA) neurons specifically labeled with green fluorescent protein for concurrent monitoring of the GABA system. This allowed them to

observe that although the dopamine system was not altered within twenty-four hours of manganese treatment, there *was* activation of GABA neurons. We believe that this could be the reason why our dopamine-focused characterization of manganese treated mice did not produce behavioral changes that agreed with the time points of neurochemical alterations. Future behavioral studies aim to monitor the GABA system as well to uncover potential connections between the two.

5.5 Conclusion

Overall, these locomotor and behavioral characterizations enabled us to better understand fine motor changes in C57 mice after an intermittent administration of $MnCl_2$. These behavior studies primarily revealed movement deficits within 24 hours after Mn treatment was completed. Although levels of movement were significantly decreased, typically within the first 24 hours, all attenuated values returned to control levels within the time course of this study. From this pattern, we can draw the conclusion that Mn exposure does impair motor behavior. However, at the Mn-levels administered in our study, the impact is reversible, as a return to control levels is observed within 7 days of the last treatment dose. To further probe and push the dopaminergic striatal system, mice were challenged with methamphetamine, which blunted stimulated ambulatory distance traveled on day 7, elucidating what we believe is an inability of the system to access additional intraneuronal dopamine pools. The hypothesis that dopamine reserve pools are altered after Mn treatment was then meticulously tested using fast scan cyclic voltammetry in our next study (Chapter 6).

Chapter 6: Investigation of Dopamine Reserve Pool after Manganese Treatment

6.1 Introduction

Thus far, our results have demonstrated that a sub-acute Mn treatment protocol results in lower dopamine extracellular levels and lower striatal dopamine release, without any compensatory changes in dopamine uptake or autoreceptor functionality. High potassium stimulation via microdialysis also revealed a blunted increase in dopamine extracellular levels as compared to the control group. Furthermore, there was an ineffectiveness in methamphetamine's ability to stimulate hyperlocomotor behavior in Mn-treated mice 7 days after treatment, an indication that methamphetamine may not be able to access additional stores of dopamine that are required to stimulate locomotor behavior. Together, these data suggest that the result of Mn accumulation in the striatum may be an intracellular change in dopamine regulation.

6.2 Vesicles: Key to Intraneuronal Regulation of Dopamine Release

6.2.1 Exocytosis

Once synthesized in the cell body, dopamine is packaged into secretory vesicles and stored in the nerve terminal.[1] Exocytotic release of neurotransmitters from these vesicles is a highly regulated and rapid five-step process.[1] In order for vesicles to release dopamine quickly at the signal of an action potential, they are first docked at the active zone of the nerve terminal. Second, vesicles are primed with adenosine triphosphate hydrolysis, which enables them to respond to calcium influx at the millisecond timescale. In the third step, upon influx of calcium, vesicles fuse to the plasma membrane and release their contents into the synaptic space. Afterwards, the membrane of the vesicle is retrieved and starts to be recycled by the process of

endocytosis. Finally, vesicles are recycled and re-loaded with neurotransmitters by the vesicular monoamine transporter (VMAT). There is considerable debate about the mechanism of this final step. In a recent review, Denker *et al.* report evidence for four different models of vesicle recycling.[164] In support of the "kiss-and-run" model, it has been shown that in some cases, synaptic vesicles only partially fuse to the membrane, after which the same individual vesicles are refilled for multiple rounds of exocytosis.[165-168] A second and more prominent theory argues in favor of full fusion of vesicles into the plasma membrane, after which vesicles are recycled in a method mediated by the protein clathrin.[169-171] The third model proposed, bulk endocytosis, suggests that after releasing dopamine, vesicles fused to the membrane generate new vesicles for recycling.[172-174] The fourth model called the endosomal sorting model suggests that the vesicles fused to the plasma membrane then fuse to a sorting endosome that generates new vesicles to store and release dopamine.[175-177] Although the fusion and recycling components of exocytotic release are important areas of dopamine regulation, don't believe that manganese treatment is disrupting this process. If that had been the case, we hypothesize that over time, we would stop seeing dopamine release altogether. On the contrary, our goal in examining dopamine vesicles of Mn-treated mice is to elucidate potential changes in vesicle storage and trafficking. As it has been shown by Stanwood *et al.* that manganese treatment leads to a 75% decrease in synapsin staining, a key protein in vesicle trafficking, we believe our impaired release results combined with the absence of change in intraneuronal levels of dopamine are due to malfunctioned vesicle trafficking.[178]

6.2.2 Dopamine Vesicle Pools

While in the axon terminal, dopamine vesicles have been shown to exist in three different pools: readily releasable, recycling, and reserve.[179] The readily releasable pool accounts for ~ 1 – 2% of the total vesicles which are docked at the "active site" of the neuron and release dopamine upon mild stimulation. The recycling pool, which replaces readily releasable pool vesicles as they are depleted, makes up 10 – 20% of the total vesicles. The reserve pool makes up the majority, accounting for ~ 80 - 90% of total vesicles, and is mobilized only if all other pools are depleted or upon prolonged stimulation.

A point of contention regarding the secretory vesicles is in understanding how these vesicles exchange between the three different pools, if at all. Additionally, it is unclear how "mobile" each of these pools are and therefore how they are recruited to the active zone for release. It has been well established that the family of proteins known as synapsins are in large part responsible for segregating the different pools of vesicles. It is hypothesized that regulating movement of vesicles from one area to another is also accomplished by synapsins.[1] A number of studies have been conducted to better understand patterns in mobility and immobility of vesicles, but with varying results. When studied by stimulated emission depletion microscopy, apparent vesicle movement is mostly random, but shows certain areas of immobility.[180,181] In mouse neuromuscular junctions, Gaffield and Betz report that vesicles are immobile at room temperature, but become mobile at physiological temperature.[182] Neuromuscular junction analysis reveals a pool of recycling vesicles that are mobile even at rest, while the reserve pool can only be mobilized after a strong stimulation.[183] In some cases, initially mobile vesicles were

observed to lose their mobility over time, regardless of which pool they were classified to be in.[184]

Together, these studies on the mobility of vesicles lend evidence to a high intermixing rate amongst vesicles proposed by Denker and Rizzoli.[164] They also suggest that the reserve pool is the compilation of "mature" vesicles, which are created after multiply endocytosed recycling vesicles lose their mobility. However, it is important to note that limited mobility does not mean these vesicles no longer release neurotransmitters. In fact, reserve pool vesicles are still capable of efficient exocytosis. [185,186]

6.3 FSCV Study of Dopamine's Vesicular Stores

We hypothesize that dysfunction in intracellular dopamine regulation after exposure to manganese stems from improper vesicle segregation and trafficking. Specifically, if the vesicles were unable to carry out their recycling and mobilization function due to striatal manganese accumulation, a change in normal rate of release of dopamine would be observed. External stimulation is used to study dopamine vesicular release, as such stimulation causes the neuron to release the contents of the vesicles docked at the terminal. *In vivo*, this dopamine would be released in response to a sufficient action potential and subsequent calcium influx. Changing the stimulation intensities can be used to tease apart the various subcategories of dopamine vesicles. In addition to external stimulation, the reserve pool has also been shown to mobilize by the administration of cocaine, a drug heretofore thought to act only as a dopamine transporter inhibitor.[187]

Slice fast scan cyclic voltammetry (FSCV) can be used to probe the model of distinct vesicle pools pharmacologically.[188] Using a variety of pharmacological agents, such as tetrabenazine

(TBZ), an inhibitor of the VMAT, alpha-methyl-p-tyrosine (α-MPT), a tyrosine hydroxylase inhibitor (inhibiting dopamine synthesis), amphetamine, a competitive dopamine transporter inhibitor that releases dopamine from vesicles, and cocaine, differences in dopamine release can be evaluated. The combination of synthesis and VMAT inhibitors allows for the differentiation of readily releasable versus reserve pool vesicles, as well as for the assessment of whether the attenuation of release is due to impaired loading of vesicles or in the mobilization of those vesicles to the neuron's docking site. Impaired release upon external stimulation suggests that Mn's mechanism of action may be caused by the hindrance of vesicle mobilization, or in the amount of dopamine available in reserve pool vesicles. An inability to retrieve dopamine from the reserve pool would explain the more extensive, long-term attenuation in release observed when stimulated with 120 mM of KCl for 20 minutes, which is considered to be a very strong stimulation. In this study, dopamine levels after depletion of the readily releasable and recycling pools in both saline- and Mn-treated mice were compared so as to evaluate the condition of the reserve pool and its ability to replace the depleted pools after significant Mn accumulation.

6.4 Materials and Methods

6.4.1 Animals

Male and female C57Bl/6 mice, either purchased from Jackson Laboratories or bred in house, were used for all experiments. Until ready for use, mice were housed (3-4 mice per cage) at the animal care facilities of Wayne State University. Food and water was available *ad libitum*. All protocols and animal care followed guidelines set by the National Institutes of

Health Office of Animal Care and Use and were approved by the Wayne State University Institutional Animal Care and Use Committee.

6.4.2 Chemicals

Components of artificial cerebrospinal fluid, $MnCl_2.4H_2O$, tetrabenazine (TBZ), α-methyl-p-tyrosine (αMPT), amphetamine, and cocaine were obtained from Sigma-Aldrich (St. Louis, MO) and Fisher Scientific (Pittsburgh, PA) and were of the highest quality available.

6.4.3 Manganese Treatment

All animals were divided into two groups: saline-treated controls and Mn-treated. The Mn group was given 0.1 mL subcutaneous injections of 50 mg/kg dose manganese (II) chloride tetrahydrate ($MnCl_2.4H_2O$) made up in sterile saline (0.9% sodium chloride, NaCl). Injections were given three times over the course of a week, on days 1, 4, and 7. Equivalent volume of saline was administered to control group on the same days. After treatment completion, experiments for neurochemical analysis were conducted 1, 7, and 21 days after final Mn injection.

6.4.4 Fast Scan Cyclic Voltammetry

The method of fast scan cyclic voltammetry is explained in detail in Chapters 3 and 4. A brief summary of the experimental details is included here as it was applied to the experiments conducted in this study. Acquisition of the brain slices containing the caudate-putamen, electrode placement, and collection of electrochemical data is as previously described.

Dopamine release and uptake measurements were made until at least three stable, consecutive baseline values were obtained. For the first set of experiments, once a stable dopamine signal was obtained, brain slices from treated mice (both saline and Mn) were

perfused with 10 µM TBZ, a VMAT inhibitor, while applying single pulse stimulations every 5 minutes to deplete the readily releasable pool. Successful dopamine depletion was observed by the complete loss of the dopamine signal. At that point, a combination of 10 µM TBZ and 20 µM amphetamine were perfused over the brain slice for 25 minutes. The purpose of the co-infusion of amphetamine is that it is capable of releasing cytosolic dopamine into the extracellular space by reverse transport.[139,189] Thus, with amphetamine on board, it is believed that the transporter is working in the opposite direction by transporting dopamine from the reserve pool of dopamine vesicles out into the extracellular space. A continuous 12.5-minute file was then collected without stimulation. The amplitude of the resultant peak was compared between saline-treated and Mn-treated mice at the three time points of analysis (day 1, 7, and 21 after treatment) to assess the intracellular levels of dopamine in the reserve pool.

For a more selective analysis of the reserve pool by using a drug that blocks dopamine synthesis, 50 µM α-MPT, a tyrosine hydroxylase inhibitor, was perfused onto the slices as single stimulations were applied to selectively deplete cytosolic and readily releasable pool dopamine. The reserve pool dopamine was again pharmacologically released using 20 µM amphetamine. After collecting a continuous file during perfusion without any electrical stimulation, maximum peak heights were compared to evaluate dopamine reserve pool content between saline- and Mn-treated mice.

In a third experiment, α-MPT and cocaine were used to determine if mobilization of the reserve pool was different between saline-treated and Mn-treated mice 1, 7, and 21 days after treatment cessation. By perfusion of the pharmacological agent α-MPT (50 µM), synthesis of dopamine was blocked, while single stimulation pulses depleted the readily releasable pool.

Once the dopamine signal was completely diminished, a 20 μM cocaine solution was co-perfused onto the slice (in addition to the 50 μM α-MPT) while electrical stimulations are continued every 5 minutes to mobilize the reserve pool vesicles. Saline- and Mn-treated mice were compared based on how long it took the stimulations to deplete this new, cocaine-induced signal of dopamine, as well as on the amplitude of the signal.

6.4.5 Statistical Analysis

All data analyzed with GraphPad Prism software (GraphPad, La Jolla, CA). Values are expressed as means ± standard error of means (SEMs) with a difference of $P < 0.05$ considered statistically significant. Comparisons of means were made by a one-way analysis of variance (ANOVA) with Dunnett's post-test to compare individual analysis time points to saline control group. Grubbs test (by GraphPad Outlier calculator online) was used to exclude outliers in data sets with an alpha value set to 0.05.

6.5 Results

6.5.1 Tetrabenazine/Amphetamine – Efflux after VMAT Inhibition

After depletion of the other two pools, as apparent by the diminished current versus time traces observed with FSCV (Figure 6.1C), amphetamine evoked efflux of reserve pool dopamine was quantified by measuring the amplitude of the resultant current (Figure 6.1). The average concentration of amphetamine-induced dopamine released in the saline-treated control group was 886 ± 202 nM (n = 8). After Mn treatment, analysis on day 1 revealed a dopamine concentration of 1207 ± 314 nM (n = 5) dopamine in the reserve pool. Neither this time point, nor results from day 7 (1425 ± 261 nM, n = 4) or day 21 (1325 ± 498 nM, n = 6) were different when compared to the saline group (Figure 6.2, one-way ANOVA, Dunnett's post-test).

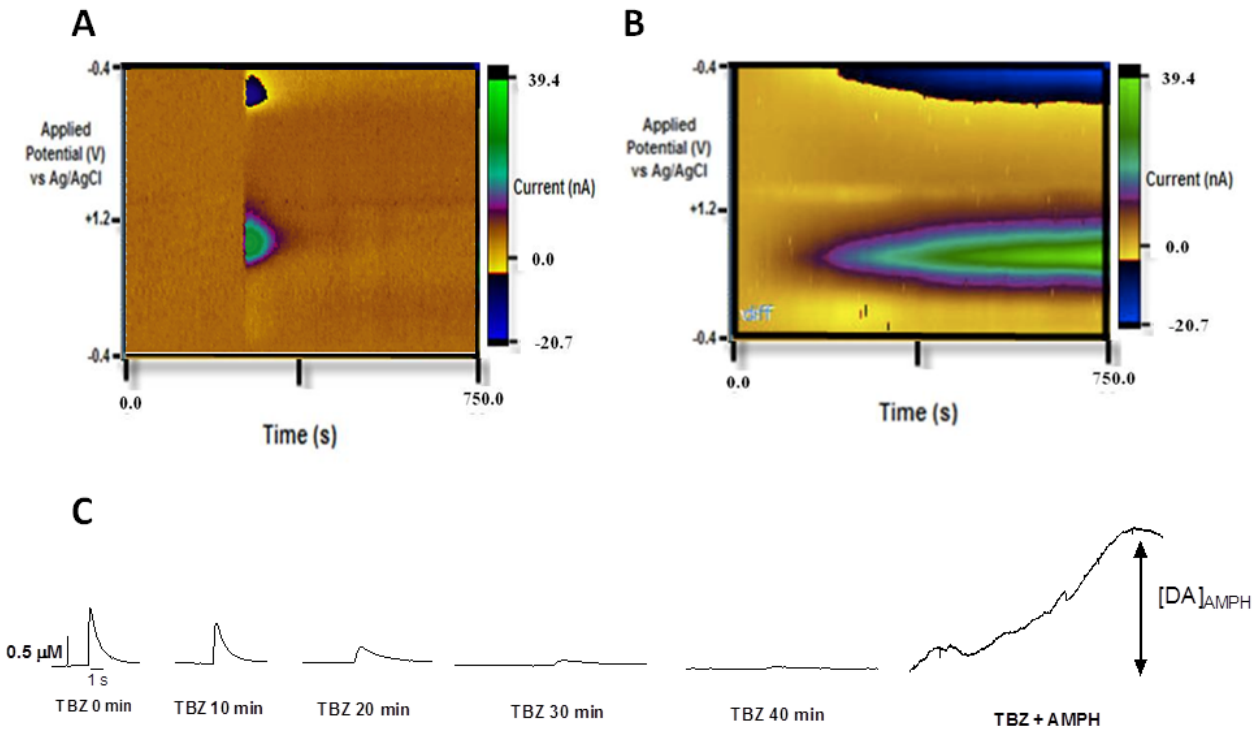

Figure 6.1: Representative FSCV data after TBZ and amphetamine perfusion. A) False color plot indicating pre-drug dopamine oxidation and reduction peaks. **B)** Representative color plot of Mn-treated mouse from day 1 analysis group. Note extended release and uptake profiles after perfusion of 20 µM amphetamine. **C)** Representative concentration versus time traces throughout tetrabenazine perfusion demonstrating diminishing dopamine signal as a result of blocking the vesicular monoamine transporter. The final panel illustrates how amplitude of amphetamine-induced dopamine efflux was measured.

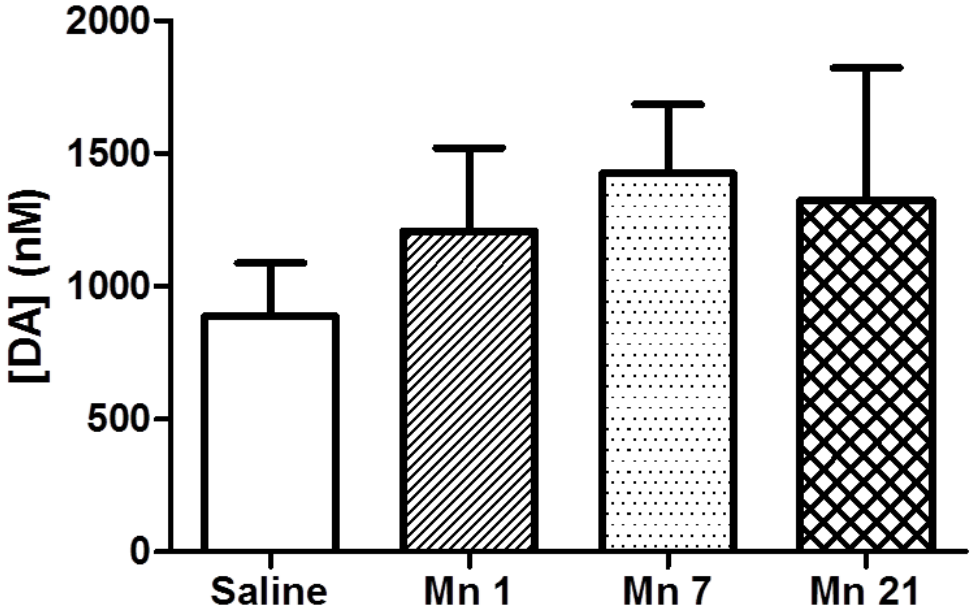

Figure 6.2: Maximum reserve pool dopamine released after TBZ and amphetamine perfusion. No change in quantity of dopamine released from reserve pool after readily releasable pool, recycling pool, and cytosolic dopamine depleted by VMAT inhibitor (tetrabenazine; n = 4 - 8/group).

6.5.2 α-methyl-p-tyrosine/Amphetamine – Efflux after Synthesis Inhibition

The concentration of dopamine in reserve pools was also evaluated using α-methyl-p-tyrosine (αMPT), a dopamine synthesis blocker. The amplitude of measured dopamine from the reserve pool was correlated to a concentration of 3469 ± 837 nM (n = 7). Brain slices from Mn-treated group revealed similar concentrations on day 1 (1696 ± 598 nM, n = 6), day 7 (1291 ± 493 nM, n = 4), and day 21 (3034 ± 931 nM, n = 6) of analysis (Figure 6.3). In agreement with the first analysis of reserve pool quantitation, none of the Mn-treated groups' time points were different from the saline-treated group (one-way ANOVA, Dunnett's post-test).

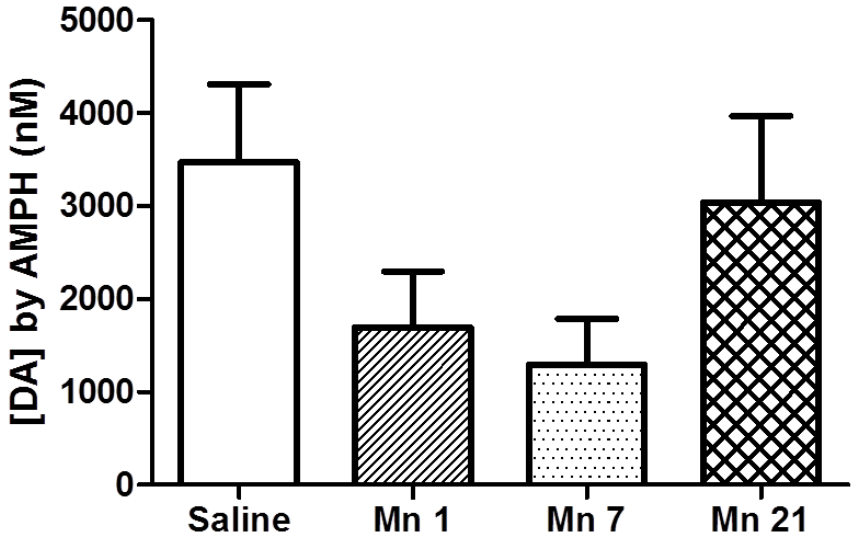

Figure 6.3: Reserve pool dopamine concentration after αMPT and amphetamine perfusion. No difference in quantity of dopamine released from reserve pool after readily releasable pool, recycling pool, and cytosolic dopamine depleted by synthesis blocker (α-methyl-p-tyrosine; n = 4 - 7/group).

6.5.3 α-methyl-p-tyrosine/Cocaine – Mobilization after Synthesis Inhibition

Cocaine acts on the reserve pool vesicles to mobilize them to the axon terminal for release, therefore this experiment was conducted to root out any potential impairment in the mobilization mechanism of vesicles as a result of Mn treatment. The amplitude of released dopamine was quantified, as well as the amount of time required to empty out the reserve pool (Figure 6.4), and compared across groups. Mn-treated mice on day 1 revealed a cocaine-mobilized dopamine reserve pool concentration of 385 ± 58 nM (n = 4). On day 7, an amplitude of 460 ± 82 nM (n = 5) was recorded and on day 21, 388 ± 53 nM (n = 5). All three values, while slightly lower, were not different from the concentration of dopamine in the control group (586 ± 109 nM, n = 7, one-way ANOVA, Dunnett's post-test, Figure 6.5). On average, the reserve pool of saline-treated mice was depleted in 38.6 ± 8.8 min. In comparison, the Mn-treated mice lost cocaine-induced dopamine signal in 23.8 ± 3.8 min (Mn day 1), 32.0 ± 7.7 min (Mn day 7), and 34.0 ± 4.3 min (Mn day 21). As illustrated in Figure 6.6, none of these depletion times were different from the saline group (one-way ANOVA, Dunnett's post-test).

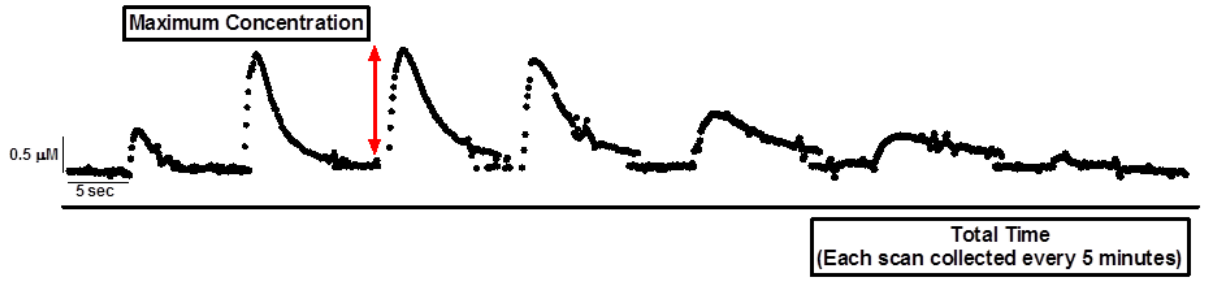

Figure 6.4: Time course of dopamine release changes upon cocaine perfusion. Concentration versus time traces during cocaine perfusion demonstrating time course of changes in dopamine signal. The arrow indicates how maximum amplitude is quantified, as well as total time for cocaine-induced dopamine signal to diminish to zero.

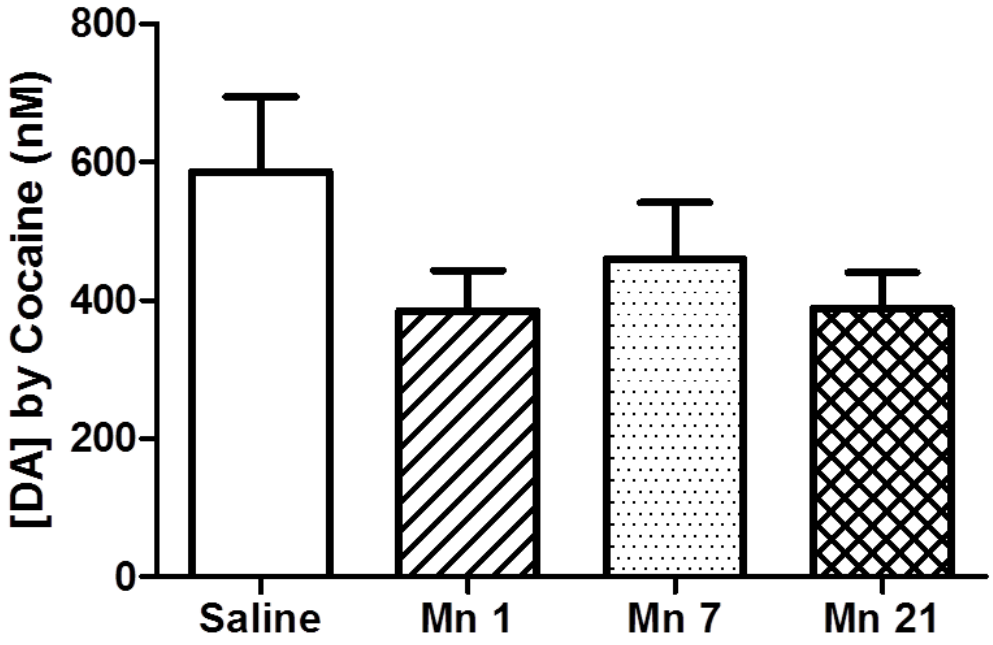

Figure 6.5: Reserve pool dopamine concentration after cocaine perfusion. No difference in quantity of cocaine-mobilized dopamine released from reserve pool after readily releasable pool, recycling pool, and cytosolic dopamine depleted by synthesis blocker (α-methyl-p-tyrosine; n = 4 - 7/group).

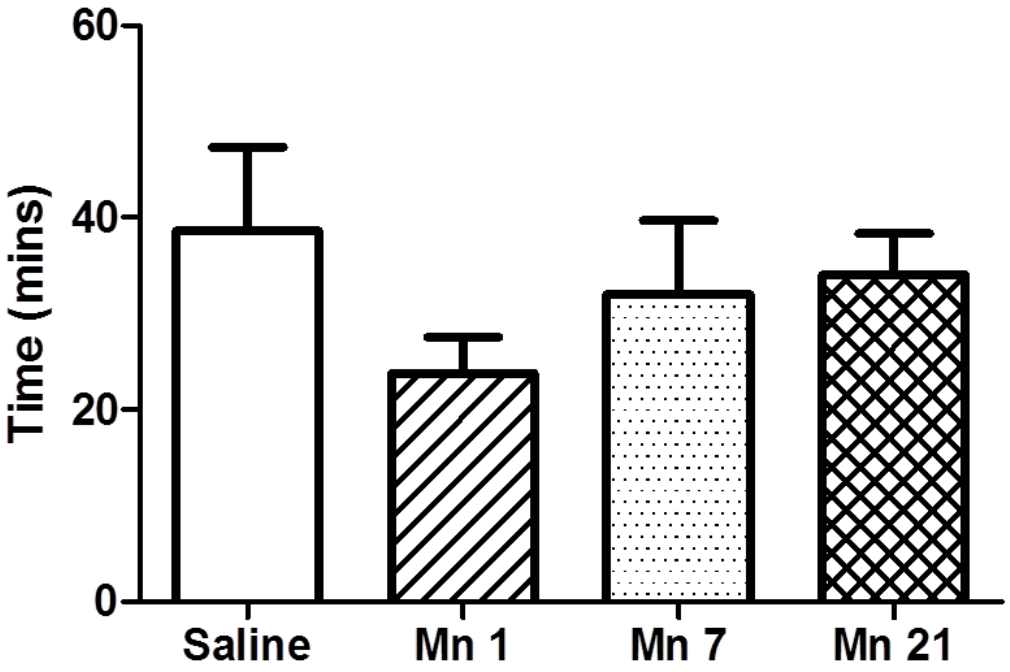

Figure 6.6: Maximum time required to deplete cocaine-mobilized dopamine reserve pool. Time to deplete reserve pool by cocaine mobilization not different between saline-treated or Mn-treated group at any of the three time points of analysis (n = 4 - 7/group).

6.6 Discussion

The mechanism of how manganese enters the neuron is not well understood. However, there is evidence to show preferential accumulation of manganese at subcellular organelles like the mitochondria and the Golgi apparatus.[190,191] As our data shows functional impairment of dopamine neurons without change in overall levels of dopamine content, our goal in this work was to probe intraneuronal aspects of dopamine regulation to uncover potential interactions of manganese with dopamine inside dopaminergic neurons. As quantal dopamine release is regulated by the exocytosis process, the results from our initial studies and evidence in the literature of synapsin loss after manganese treatment suggested that there may be dysfunction in the synaptic vesicles of our Mn-treated mice. Prior to inspection of the intraneuronal stores of dopamine, we hypothesized that the impaired dopamine release data were the result of either an inability of reserve pool vesicles to mobilize after Mn accumulation or a disparity in the number of vesicles available in the reserve pool as compared to the number of vesicles available *for release* in the reserve pool. The technique of FSCV provided a novel method for extracting both quantitative and dynamic information regarding vesicular stores which would not have been possible in the past using imaging or tissue analysis methods.

To elucidate the concentration of dopamine available in the reserve pool, reloading of new vesicles was blocked by inhibiting the VMAT. The average concentrations of dopamine in reserve pool vesicles after Mn-treatment were not found to be different. This measurement of dopamine available in the reserve pool is in agreement with our previous tissue content studies, where there were no differences in dopamine tissue content levels across Mn-treatment days. If we had found higher concentrations of dopamine packed into the reserve

pool vesicles, the lower release after Mn-treatment with no tissue content change in overall intracellular/extracellular levels could have been attributed to a greater amount of vesicles "maturing" into the reluctantly releasable reserve pool of vesicles.[164] The pitfall of using a VMAT blocker is that dopamine, serotonin, and norepinephrine all share the same transporter.[1] To target dopamine more selectively, a second study was conducted. This time, dopamine synthesis was directly blocked to eliminate contributions from the readily releasable and recycling pools so that the only dopamine present in the axon terminal would be from the reserve pool. In agreement with the first study, reserve pool concentrations were again found to be not different when comparing saline-treated and Mn-treated mice. As both these experiments proved our first hypothesis to be incorrect, we devised a study to examine the function of the vesicular system by assessing the synapsin-mediated mobilization of the reserve pool. However using FSCV, we were unable to detect any functional impairment in the mobilization of the reserve pool.

Together, the evidence presented in this chapter discredits the postulation that lower vesicular release of dopamine, as well as lower extracellular levels, are the result of abnormal reserve pool content or mobilization. To our knowledge, this is the first time that FSCV has been used to probe dopamine vesicular levels and mobilization after striatal manganese accumulation. Although this study suggests no dopamine impairments with recruitment and dopamine storage, it does not change the fact that the combination of our work firmly in the direction of presynaptic dopamine impairment. As such, there are several other hypotheses that have been proposed to link high levels of metals in the brain to aberrant presynaptic neurotransmitter dynamics.[192] In a review by Sadiq *et al.*, the authors discuss both presynaptic

and postsynaptic effects of metal toxicity at the synapse, citing studies of aluminum, arsenic, cadmium, lead, and manganese, to name a few.[192] Other metals, such as aluminum, cadmium, and lead affect voltage gated calcium channels via inhibition or downregulation.[193-199] It has been suggested that Mn's presynaptic actions also occur at sodium or potassium voltage gated channels. In voltage clamp experiments, Mn blocked tetrodotoxin sensitive and insensitive sodium channels.[200] The effect of Mn on potassium channels was shown to be divergent, with high concentrations (*i.e.* 10 mM) reducing channel currents while lower concentrations (*i.e.* 1 mM) increase their amplitudes.[201] These potassium and sodium channels act in a regulated manner to propagate action potentials, which in turn determine whether or not exocytotic release will occur. Thus, it is plausible to surmise that the Mn induced changes in dopamine release we have observed stem from the aforementioned irregular functioning of voltage-gated ion channels. Although purely conjecture at this stage, future experiments can be designed to further study this hypothesis.

Chapter 7: Summary and Conclusions

Research in the manganism field has made great strides in characterizing its symptomatology and understanding the risks associated with overexposure to the biologically essential trace element manganese. As a disorder of the brain, undoubtedly one of the most complex networks of communication in the human body, it is expected that manganism would be the result of dysfunction in many different neurotransmitter systems. Of those, a link between the dopaminergic system and manganism has been repeatedly established based on symptoms, the brain regions in which manganese accumulates, imaging studies, tissue studies, and other neurochemical measurements. Surprisingly little work has been done to assess dopamine functionality after high levels of manganese exposure. Furthermore, due to the wide range of exposure protocols and animal models used for the studies that are conducted, there is great disparity in the results obtained. Due to the analytical advantage granted by techniques such as fast scan cyclic voltammetry (FSCV) and microdialysis that allows for functional analysis of the brain in specific and discrete brain regions, it is now possible to take a multi-faceted approach to studying neurological disorders such as manganism.

The overarching goal of this work was to expose mice to manganese over the course of a short time period and then study its impact on the dopamine and behavioral system using a variety of complementary analytical techniques. A time dependent analysis regime was established to allow for short and long term study of the treated animals.

7.1 Neurochemical Characterization upon Sub-acute Manganese Treatment

The goal of our initial studies following the week-long intermittent dosing protocol was to assess if neurochemical alterations could be picked up in the striatum as tissue content studies

revealed significant accumulation of manganese for up to three weeks after treatment was completed. The results of these experiments are summarized below in Table 7.1. Parallel analysis of striatal tissue did not show any difference in the combined intra- and extraneuronal levels of dopamine. Even so, we hypothesized that some type of impairment on the dopaminergic system was bound to exist due to the significantly large increase in striatal manganese concentrations after treatment. When sampling the extracellular space using *in vivo* microdialysis, subtle differences in uncorrected baseline levels of dopamine were seen 7 days after treatment. Furthermore, when corrected for probe recovery using the microdialysis method of no net flux, the same time point was confirmed to have lower levels of dopamine compared to saline-treated controls. Furthermore, lower levels of dopamine's metabolites were observed 7 days after treatment, which continued to be low until the day 21 analysis. As there was a discrepancy between what dopamine tissue studies showed and what was revealed by the microdialysis results, we hypothesized that the change might be due to the release of dopamine from inside the neuron. To test this, we modified the aCSF solution to chemically stimulate treated animals with high concentrations of potassium using reverse infusion through the microdialysis probe. Indeed, impairment in how much dopamine could be released in response to the strong stimulation was observed in Mn-treated mice compared to the saline-treated group; in this case, attenuation of release was seen as early as 24 hours after treatment cessation and persisted until 21 days later.

Extracellular dopamine levels are not only affected by release of dopamine but also by its reuptake by the dopamine transporter. In order to assess the kinetics of transporter activity, as well as to look at release changes with better temporal resolution, we utilized FSCV to examine

these dopamine dynamics on the sub-second time scale. With a much lighter stimulation as compared to the high potassium study (both in terms of duration and intensity), we were able to elucidate release impairment only on day 21. However, no compensatory changes in dopamine uptake rates were observed due to Mn-treatment. A final attempt at uncovering the mechanism of extracellular regulation of dopamine levels was made by assessing the functionality of the presynaptic dopamine D2 autoreceptors. There was no difference in dopamine receptor functionality between the Mn-treatment groups and the saline controls, confirming that the alteration to dopamine neurotransmission was solely at the release mechanism of the neuron.

(vs. control)	Day 1	Day 7	Day 21
Intracellular DA	-	-	-
Microdialysis DA Baseline	-	↓	-
DA Metabolites	-	↓	↓
K+ Stimulated DA Release	↓	↓	↓
FSCV DA Release	-	-	↓
FSCV DA Uptake	-	-	-
DA Autoreceptor Functionality	-	-	-

Table 7.1: Summary of dopamine neurochemical analysis by microdialysis and FSCV.
Dash (-) indicates no change between Mn-treated animals and saline-treated controls.

7.2 Study of the Behavioral Impact of Manganese Exposure

Like Parkinson's disease, the movement impairment of manganism patients is one of its most characteristic symptoms. Furthermore, changes in striatal dopamine levels are oftentimes associated with changes in locomotor activity. The results from our initial experiments led us to hypothesize that the dopamine changes from our manganese protocol *should* manifest in changes in locomotor activity and coordination of treated mice as compared to controls (Table 7.2). When recording baseline locomotor activity, impaired movement in the X and Y direction was observed on day 1 after treatment. No differences in locomotor activity were seen at any of the time points at which dopamine was impaired. Furthermore, both stereotypic behavior and beam walk analysis supported the data from locomotor testing, suggesting behavioral impairments *before* any change in striatal dopamine release or extracellular levels.

Interestingly, Yang *et al.* have reported similar patterns of locomotor activity changes that do not match up with any correlated alterations in dopamine neuron activation. In fact, they observed behavioral changes at the same time point as our study, 24 hours after manganese chloride exposure. Furthermore, they did observe changes in neurons of a different neurotransmitter, γ-aminobutyric acid (GABA). Others have also reported GABA changes in response to manganese treatment protocols, which supports our expectation stated in the introduction that multiple neuronal systems should be affected to result in a neurological disorder as complex as manganism. The possibility of GABA dysregulation affecting locomotor behavior would also explain why our locomotor changes did not directly correlate to neurochemical dopamine changes recorded by FSCV and microdialysis, as our focus has been to better understand the dopamine system.

Another observation from the behavioral experiments was the inability of methamphetamine to stimulate behavior to the extent that would be expected (and is seen) in control animals. Methamphetamine's mechanism of action on dopamine neurons is to recruit additional dopamine from inside the neuron via the dopamine transporter, thereby creating a hyperlocomotive state. The inability of methamphetamine to induce hyperactivity would suggest unavailability of dopamine vesicles for release, which would explain why our intraneuronal tissue results did not reveal any difference in overall dopamine levels even though released and extracellular dopamine concentrations were attenuated. Since stronger stimulation resulted in greater impairment in release, this would suggest that access to the reserve pool is somehow affected by manganese accumulation. Therefore, the next step in understanding the mechanism between dopamine and Mn sought to take a deeper look at the vesicle pools of dopamine using FSCV.

(vs. control)	Day 1	Day 7	Day 21
Ambulatory Distance	↓	-	-
Stereotypy	↓	-	-
Vertical Count	-	-	↑
Ambulatory - Meth	-	↓	-
Stereotypy - Meth	-	-	-
Vertical - Meth	↑	↓	↓
Beam Walk Time	-	-	-
Beam Walk Failure Rate	↑	-	-

Table 7.2: Summary of behavior studies performed after sub-acute manganese treatment. Dash (-) indicates no change between Mn-treated animals and saline-treated controls.

7.3 Reserve Pool Analysis

To better understand the state of the dopamine reserve pool, pharmacological agents were used that would prevent more vesicles from being added to the reserve pool. Once the readily releasable pool and the recycling pool of dopamine vesicles were depleted, first by using a vesicular monoamine transport blocker (to prevent loading of new vesicles), then by using a dopamine synthesis blocker, we strategically forced the reserve pool contents to be released into the synaptic space by amphetamine efflux. Unfortunately, neither method revealed a change in the concentration of dopamine in the reserve pool of Mn-treated mice as compared to the saline-treated ones. Furthermore, our third study analyzing the mobilization of the reserve pool to the terminal for release using cocaine also did not reveal any impairment due to manganese exposure. This set of experiments, although disproving our hypothesis, did have the advantage of ruling out one theory of how manganese may be acting on the dopamine system. Without the spatial and temporal resolution of a technique like FSCV, such an intricate study of intraneuronal stores would not have been possible in the past.

7.4 Overall Conclusion and Future Directions

Overall, this work made great strides in characterizing the functional changes Mn induced upon the striatal dopamine system using a variety of neuroanalytical techniques. Furthermore, the time-dependent analysis of behavior allowed us to uncover data in support of the involvement of other neurotransmitters in locomotor impairment since changes in behavior were disparate from the changes we found in the dopamine system. Future experiments evaluating manganese's affect on the brain should evaluate GABA levels after manganese exposure to directly test this hypothesis. Other proposed mechanisms of neuronal impairment,

such as the generation of reactive oxidation species like hydrogen peroxide that have been shown to regulate dopamine release, should also be tested in future experiments to confirm or reject their validity.

REFERENCES

1. Nestler EJ, Hyman SE, Malenka RC (2009) Molecular Neuropharmacology: A Foundation for Clinical Neuroscience, 2nd ed. McGraw-Hill Companies.
2. Bicker J, Fortuna A, Alves G, Falcao A (2013) Liquid chromatographic methods for the quantification of catecholamines and their metabolites in several biological samples – A Review. *Analytica Chimica Acta* 768: 12-34.
3. Bergquist J, Sciubisz A, Kaczor A, Silberring J (2002) Catecholamines and methods for their identification and quantitation in biological tissues and fluids. *J Neurosci Methods* 113: 1-13.
4. Brady ST, Siegel GJ, Albers RW, Price DL (2012) Basic Neurochemistry: Principles of Molecular, Cellular, and Medical Neurobiology, 8th ed. Academic Press.
5. Charkoudian N, Rabbitts JA (2009) Sympathetic neural mechanisms in human cardiovascular health and disease. *Mayo Clin Proc* 84 (9): 822-830.
6. Fotopoulou MA, Ioannou PC (2002) Post-column terbium complexation and sensitized fluorescence detection for the determination of norepinephrine, epinephrine, and dopamine using high-performance liquid chromatography. *Anal Chim Acta* 462: 179-185.
7. Rosano TG, Swift TA, Hayes LW (1991) Advances in catecholamine and metabolite measurements for diagnosis of pheochromocytoma. *Clin Chem* 37: 1854-1867.
8. Wightman RM, Amatore C, Engstrom RC, Hale PD, Kistensen EW, Kuhr WG, May LJ (1988) Real-time characterization of dopamine overflow and uptake in the rat striatum. *Neuroscience* 25: 513-523.
9. Wightman RM, Zimmerman JB (1990) Control of dopamine extracellular concentration in rat striatum by impulse flow and uptake. *Brain Res Rev* 15: 135-144.

10. Michael DJ, Wightman RM (1999) Electrochemical monitoring of biogenic amine neurotransmission in real time. *Journal of Pharmaceutical and Biomedical Analysis* 19: 33-34.

11. Phillips PE, Robinson DL, Stuber GD, Carelli RM, Wightman RM (2003) Real-time measurements of phasic changes in extracellular dopamine concentration in freely moving rats by fast-scan cyclic voltammetry. *Methods Mol Med* 79: 443-464.

12. Robinson DL, Howard EC, McConnell S, Gonzales RA, Wightman RM (2009) Disparity between tonic and phasic ethanol-induced dopamine increases in the nucleus accumbens of rats. *Alcohol Clin Exp* Res 33(7): 1187-1196.

13. Owesson-White CA, Roitman MF, Sombers LA, Belle AM, Keithley RB, Peele JL, Carelli RM, Wightman RM (2012) Sources contributing to the average extracellular concentrations of dopamine in the nucleus accumbens. *J Neurochem* 121(2): 252-262.

14. Sombers LA, Beyene M, Carelli RM, Wightman RM (2009) Synaptic overflow of dopamine in the nucleus accumbens arises from neuronal activity in the ventral tegmental area. *J Neurosci* 29(6): 1735-1742.

15. Kissinger PT, Heineman WR (1996) Laboratory Techniques in Electroanalytical Chemistry, 2nd ed., revised and expanded. Marcel Dekker, New York.

16. Jacobs CB, Vickrey TL, Venton BJ (2011) Functional groups modulate the sensitivity and electron transfer kinetics of neurochemicals at carbon nanotube modified microelectrodes. *Analyst* 136: 3557-3565.

17. Xiao N, Venton BJ (2012) Rapid, sensitive detection of neurotransmitters at microelectrodes modified with self-assembled SWCNT forests. *Anal Chem* 84: 7816-7822.

18. Roberts JG, Moody BP, McCarty GS, Sombers LA (2010) Specific oxygen-containing functional groups on the carbon surface underlie an enhanced sensitivity to dopamine at electrochemically pretreated carbon fiber microelectrodes. *Langmuir* 26(11): 9116-9122.

19. Takmakov P, Zachek MK, Keithley RB, Walsh PL, Donley C, McCarty GS, Wightman RM (2010) Carbon microelectrodes with a renewable surface. *Anal Chem* 82: 2020-2028.

20. Keithley RB, Takmakov P, Bucher ES, Belle AM, Owesson-White CA, Park J, Wightman RM (2011) Higher sensitivity dopamine measurements with faster-scan cyclic voltammetry. *Anal Chem* 83: 3563-3571.

21. Kile BM, Walsh PL, McElligott ZA, Bucher ES, Guillot TS, Salahpour A, Caron MG, Wightman RM (2012) Optimizing the temporal resolution of fast-scan cyclic voltammetry. *ACS Chem Neurosci* 3: 285-292.

22. Hashemi P, Walsh PL, Guillot TS, Gras-Najjar J, Takmakov P, Crews FT, Wightman RM (2011) Chronically implanted, nafion-coated Ag/AgCl reference electrodes for neurochemical applications. *ACS Chem Neurosci* 2: 658-666.

23. Zachek MK, Park J, Takmakov P, Wightman RM, McCarty GS (2010) Microfabricated FSCV-compatible microelectrode array for real-time monitoring of heterogeneous dopamine release. *Analyst* 135:1556-1563.

24. Zachek MK, Takmakov P, Park J, Wightman RM, McCarty GS (2010) Simultaneous monitoring of dopamine concentration at spatially different brain locations in vivo. *Biosensors and Bioelectronics* 25: 1179-1185.

25. Dengler AK, McCarty GS (2013) Microfabricated microelectrode sensor for measuring background and slowly changing dopamine concentrations. *J of Electroanalytical Chemistry* 693:28-33.

26. Clark JJ, Sandberg SG, Wanat MJ, Gan JO, Horne EA, Hart AS, Akers CA, Parker JG, Willuhn I, Martinez V, Evans SB, Stella N, Phillips PE (2010) Chronic microsensors for longitudinal, subsecond dopamine detection in behaving animals. *Nature Methods* 7 (2): 126-129.

27. Zhang B, Heien ML, Santillo MF, Mellander L, Ewing AG. (2011) Temporal resolution in electrochemical imaging on single PC12 cells using amperometry and voltammetry at microelectrode arrays. *Anal Chem* 83: 571-577.

28. Makos MA, Han KA, Heien ML, Ewing AG (2010) Using In Vivo Electrochemistry to Study the Physiological Effects of Cocaine and Other Stimulants on the Drosophila melanogaster Dopamine Transporter. *ACS Chem Neurosci* 1: 74–83.

29. Vickrey TL, Venton BJ. (2011) Drosophila Dopamine2-like receptors function as autoreceptors. *ACS Chem Neurosci* 2: 723-729.

30. Ge S, Woo E, White JG, Haynes CL (2011) Electrochemical measurement of endogenous serotonin release from human blood platelets. *Anal. Chem* 83(7): 2598-2604.

31. Kishida KT, Sandberg SG, Lohrenz T, Comair YG, Sáez I, Phillips PE, Montague PR (2011) Sub-second dopamine detection in human striatum. *PLoS ONE* 6 (8): 1-5.

32. Kimble CJ, Johnson DM, Winter BA, Whitlock SV, Kressin KR, Horne AE, Robinson JC, Bledsoe JM, Tye SJ, Chang SY, Agnesi F, Griessenauer CJ, Covey D, Shon YM, Bennet KE, Garris PA, Lee KH (2009) Wireless Instantaneous Neurotransmitter Concentration Sensing System

(WINCS) for intraoperative neurochemical monitoring. *Conf Proc IEEE Eng Med Biol Soc*: 4856-4859.

33. Koehne JE, Marsh M, Boakye A, Douglas B, Kim IY, Chang SY, Jang DP, Bennet KE, Kimble C, Andrews R, Meyyappan M, Lee KH. (2011) Carbon nanofiber electrode array for electrochemical detection of dopamine using fast scan cyclic voltammetry. *Analyst* 136: 1802-1805.
34. Shon YM, Chang SY, Tye SJ, Kimble CJ, Bennet KE, Blaha CD, Lee KH. (2010) Comonitoring of adenosine and dopamine using the Wireless Instantaneous Neurotransmitter Concentration System: proof of principle. *J. Neurosurg*, 112: 539-548.
35. Herr NR, Park J, McElligott ZA, Belle AM, Carelli RM, Wightman RM (2012) In vivo voltammetry monitoring of electrically evoked extracellular norepinephrine in subregions of the bed nucleus of the stria terminalis. *J Neurophysiol* 107: 1731-1737.
36. Park J, Takmakov P, Wightman RM (2011) In vivo comparison of norepinephrine and dopamine release in rat brain by simultaneous measurements with fast-scan cyclic voltammetry. *J Neurochem* 119: 932-944.
37. Hashemi P, Dankoski EC, Lama R, Wood KM, Takmakov P, Wightman RM (2012) Brain dopamine and serotonin differ in regulation and its consequences. *Proc Natl Acad Sci USA* 109(29): 11510-11515.
38. Xu Y, Venton BJ (2010) Rapid determination of adenosine deaminase kinetics using fast-scan cyclic voltammetry. *Phys Chem* 12(34): 10027-10032.

39. Roberts JG, Hamilton KL, Sombers LA (2011) Comparison of electrode materials for the detection of rapid hydrogen peroxide fluctuations using background-subtracted fast scan cyclic voltammetry. *Analyst* 136(17): 3550-3556.

40. Shippenberg TS, He M, Chefer V (1999) The use of microdialysis in the mouse: conventional versus quantitative techniques. Psychopharmacology (Berl) 147: 33-34.

41. Pradyot N, Lunte SM (2009) Recent trends in microdialysis sampling integrated with conventional and microanalytical systems for monitoring biological events: A review. *Analytica Chimica Acta* 651:1–14.

42. Lacher NA, Garrison KE, Martin RS, Lunte SM (2001) Microchip capillary electrophoresis/electrochemistry. *Electrophoresis* 22: 2526-2536.

43. Gabler J, Willer A, Wange S (2011) A simple liquid chromatography-tandem mass spectrometry method for measuring metanephrine and normetanephrine in urine. *Clin Chem Lab Med* 49: 1213-1216.

44. Whiting MJ (2009) Simultaneous measurement of urinary metanephrines and catecholamines by liquid chromatography with tandem mass spectrometric detection. *Ann Clin Biochem* 46: 129-136.

45. Zhang G, Zhang Y, Ji C, McDonald T, Walton J, Groeber EA, Steenwyk RC, Lin Z (2012) Ultra sensitive measurement of endogenous epinephrine and norepinephrine in human plasma by semi-automated SPE-LC-MS/MS. *J Chromatogr B* 895: 186-190.

46. Mecker LC, Martin RS (2008) Integration of microdialysis sampling and microchip electrophoresis with electrochemical detection. *Anal Chem* 80(23): 9257-9264.

47. Castaño-Alvarez M, Fernández-Abedul MT, Costa-García A, Agirregabiria M, Fernández LJ, Ruano-López JM, Barredo-Presa B (2009) Fabrication of SU-8 based microchip electrophoresis with integrated electrochemical detection for neurotransmitters. *Talanta* 80: 24-30.

48. Fernández-la-Villa A, Pozo-Ayuso DF, Castaño-Alvarez M (2010) New analytical portable instrument for microchip electrophoresis with electrochemical detection. *Electrophoresis* 31: 2641-2649.

49. Johnson AS, Selimovic A, Martin RS (2011) Integration of microchip electrophoresis with electrochemical detection using an epoxy-based molding method to embed multiple electrode materials. *Electrophoresis* 32: 3121-3128.

50. Wang M, Slaney T, Mabrouk O, Kennedy RT. (2010) Collection of nanoliter microdialysate fractions in plugs for off-line in vivo chemical monitoring with up to 2 s temporal resolution. *J of Neuroscience Methods*: 39-48.

51. Wang M, Hershey ND, Mabrouk OS, Kennedy RT (2011) Collection, storage, and electrophoretic analysis of nanoliter microdialysis samples collected from awake animals in vivo. *Anal Bioanal Chem* 400: 2013-2023.

52. Wu RG, Yang CS, Cheing CC, Tseng FG (2011) Nanocapillary electrophoretic electrochemical chip: towards analysis of biochemicals released by single cells. *Interface Focus* 1: 744-753.

53. Fang H, Vickrey TL, Venton BJ (2011) Analysis of biogenic amines in a single Drosophila larva brain by capillary electrophoresis with fast-scan cyclic voltammetry detection. *Anal Chem* 83: 2258-2264.

54. Paxinos G, Franklin KBJ (2001) The Mouse Brain in Stereotaxic Coordinates, 2nd ed. Academic Press, San Diego.

55. Burton NC, Guilarte TR (2008) Manganese neurotoxicity: lessons learned from longitudinal studies in nonhuman primates. *Environmental Health Perspectives* 117: 325-332.

56. Gwiazda R, Lucchini R, Smith D (2007) Adequacy and consistency of animal studies to evaluate the neurotoxicity of chronic low-level manganese exposure in humans. *J Toxicology and Environmental Health, Part A* 70: 594-605.

57. Couper, J. (1837) On the effects of black oxide of manganese when inhaled into the lungs. *Br Ann Med Pharmacol Vital Stat Gen Sci* 1:41-42.

58. Mergler D, Baldwin M. 1997. Early manifestations of manganese neurotoxicity in humans: An update. Environmental Research 73: 92-100.

59. Guilarte TR (2010) Manganese and Parkinson's disease: A critical review and new findings. *Environmental Health Perspectives* 118(8): 1071-1080.

60. Dodd CA, Ward DL, Klein BG. 2005. Basal ganglia accumulation and motor assessment following manganese chloride exposure in the C57BL/6 mouse. *International Journal of Toxicology* 24: 389-397

61. Racette BA, McGee-Minnich L, Moerlein SM, Mink JW, Videen TO, Perlmutter JS (2001) Welding-related parkinsonism: clinical features, treatment, and pathophysiology. *Neurology* 56: 8-13.

62. Pal PK, Samii A, Calne DB (1999) Manganese neurotoxicity: a review of clinical features, imaging and pathology. *Neurotoxicology* 20: 227-238.

63. Cotzias GC, Miller ST, Papavasiliou PS, Tang LC (1976) Interactions between manganese and brain dopamine. *Med Clin North Am* 60: 729-738.

64. Nam J, Kim K (2008) Abnormal motor function and the expression of striatal dopamine D2 receptors in manganese-treated mice. *Biol Pharm Bull* 31: 1894-1897.

65. Aschner JL, Aschner M (2005) Nutritional aspects of manganese homeostasis. *Mol Aspects Med* 26: 353-362.

66. Bowler RM, Nakagawa S, Drezgic M, Roels HA, Park RM, Diamond E (2007) Sequelae of fume exposure in confined space welding: a neurological and neuropsychological case series. *Neurotoxicology* 28: 298-311.

67. Bader M, Dietz MC, Ihrig A, Triebig G (1999) Biomonitoring of manganese in blood, urine and axillary hair following low-dose exposure during the manufacture of dry cell batteries. *In Arch Occup Environ Health* 72: 521-527.

68. Montes S, Riojas-Rodriquez H, Sabido-Pedraza E, Rios C (2008) Biomarkers of manganese exposure in a population living close to a mine and mineral processing plant in Mexico. *Environ Res* 106: 89-95.

69. Rodriquez-Agudelo Y, Riojas-Rodriquez H, Rios C, Rosas I, Sabido PE, Miranda J (2006) Motor alterations associated with exposure to manganese in the environment in Mexico. *Sci Total Environ* 368: 542-556.

70. Zheng G, Xu X, Li B, Wu K, Yekeen TA, Huo X (2013) Association between lung function in school children and exposure to three transition metals from an e-waste recycling area. *J Expo Sci Environ Epidemiol* 23(1): 67-72.

71. Aschner M, Erikson KM, Herrero Hernández E, Tjalkens R (2009) Manganese and its role in Parkinson's disease: from transport to neuropathology. *Neuromolecular Med 11(4)*: 252-66.

72. Crossgrove JS, Yokel RA (2005) Manganese distribution across the blood-brain barrier. IV. Evidence for brain-influx through store operated calcium channels. *Neurotoxicology* 26: 297-307.

73. Aschner M, Gannon M (1994) Manganese (Mn) transport across the rat blood-brain barrier: saturable and transferring-dependent transport mechanisms. *Brain Res Bull* 33:345-349.

74. Itoh K, Sakata M, Watanabe M, Aikawa Y, Fujii H (2008) The entry of manganese ions into the brain is accelerated by the activation of N-methyl-D-aspartate receptors. *Neuroscience* 154: 732-740.

75. Au C, Benedetto A, Aschner M (2008) Manganese transport in eukaryotes: the role of DMT1. *Neurotoxicology* 29: 569-576.

76. Fitsanakis VA, Zhang N, Anderson JG, Erikson KM, Avison MJ, Gore JC, Aschner M (2008) Measuring brain manganese and iron accumulation in rats following 14 weeks of low-dose manganese treatment using atomic absorption spectroscopy and magnetic resonance imaging. *Toxicol Sci* 103(1): 116-24.

77. Kim Y, Park JK, Choi Y, Yoo CI, Lee CR, Lee H, Lee JH, Kim SR, Jeong TH, Yoon CS, Park JH (2005) Blood manganese concentration is elevated in iron deficiency anemia patients, whereas globus pallidus signal intensity is minimally affected. *Neurotoxicology* 26(1): 107-111.

78. Roth JA, Garrick MD (2003) Iron interactions and other biological reactions mediating the physiological and toxic actions of manganese. *Biochemical Pharmacology* 66:1-13.

79. Hauser RA, Zesiewicz TA, Rosemurgy AS, Martinez C, Olanow CW (1994) Manganese intoxication and chronic liver failure. *Ann Neurol* 36: 871-875.

80. da Silva CJ, da Rocha AJ, Jeronymo S, Mendes MF, Milani FT, Maia AC, Jr., Braga FT, Sens YA, Miorin LA (2007) A preliminary study revealing a new association in patients undergoing maintenance hemodialysis: manganism symptoms and T1 hyperintense changes in the basal ganglia. *AJNR Am J Neuroradiol* 28: 1474-1479.

81. Ohtake T, Negishi K, Okamoto K, Oka M, Maesato K, Moriya H, Kobayashi S. Manganese-induced parkinsonism in a patient undergoing maintenance hemodialysis. Am J Kidney Dis, 2005; 46: 749-53.

82. Ostiguy C, Asselin P, Malo S; Nadeau D, DeWals P (2005) Management of occupational manganism: consensus of an experts' panel studies and research projects/report R-417, Montréal, IRSST, 57 pages.

83. Maina, F, Khalid, M**,** Apawu, A, Mathews, TA (2012) Presynaptic dopamine dynamics in striatal brain slices with fast-scan cyclic voltammetry. *J Vis Exp*: 59.

84. Kawagoe KT, Zimmerman JB, Wightman RM (1993) Principles of voltammetry and microelectrode surface states. *J Neurosci Meth* 48: 225-240.

85. Kissinger PT, Hart JB, Adams RN (1973) Voltammetry in brain tissue – a new neurophysiological measurement. *Brain Res* 55(1): 209-213.

86. Lack AK, Diaz MR, Chappell A, DuBois DW, McCool BA (2007) Chronic ethanol and withdrawal differentially modulate pre- and postsynaptic function at glutamatergic synapses in rat basolateral amygdala. J Neuropyhysiol 98: 3185-96.

87. John CE, Jones SR (2007) Voltammetric characterization of the effect of monoamine uptake inhibitors and release on dopamine and serotonin uptake in mouse caudate-putamen and substantia nigra slices. *Neuropharmacology 52*: 1596-1605.

88. Khalid M, Aoun RA, Mathews TA (2011) Altered striatal dopamine release following a sub-acute exposure to manganese. *J. Neurosci. Methods* 202(2): 182-191.

89. Mergler D, Huel G, Bowler R, Iregren A, Belanger S, Baldwin M (1994) Nervous system dysfunction among workers with long-term exposure to manganese. *Environ Res* 64: 151-180.

90. Josephs KA, Ahlskog JE, Klos KJ, Kumar N, Fealey RD, Trenerry MR (2005) Neurologic manifestations in welders with pallidal MRI T1 hyperintensity. *Neurology* 64: 2033-2039.

91. Klos KJ, Chandler M, Kumar N, Ahiskog JE, Josephs KA (2006) Neuropsychological profiles of manganese neurotoxicity. *Eur J Neurol* 13: 1139-1141.

92. Dietz MC, Ihrig A, Wrazidlo W, Bader M, Jansen O, Triebig G (2001) Results of magnetic resonance imaging in long-term manganese dioxide-exposed workers. *Environ Res* 85: 37-40.

93. Calne DB, Chu NS, Huang CC, Lu CS, Olanow W (1994) Manganism and idiopathic parkinsonism: similarities and differences. *Neurology* 44: 1583-1586.

94. Perl DP, Olanow CW (2007) The neuropathology of manganese-induced Parkinsonism. *J Neuropathol Exp Neurol* 66: 675-682.

95. Hornykiewicz O (1998) Biochemical aspects of Parkinson's disease. *Neurology* 51: S2-9.

96. Olanow CW (2004) Manganese-induced parkinsonism and Parkinson's disease. *Ann N Y Acad Sci* 1012: 209-223.

97. Olanow CW, Good PF, Shinotoh H, Hewitt KA, Vingerhoets F, Snow BJ, Beal MF, Calne DB, Perl DP (1996) Manganese intoxication in the rhesus monkey: a clinical, imaging, pathologic, and biochemical study. *Neurology* 46: 492-498.

98. Kim Y (2006) Neuroimaging in manganism. *Neurotoxicology* 27: 369-372.

99. Guilarte TR, Chen MK, McGlothan JL, Verina T, Wong DF, Zhou Y, Alexander M, Rohde CA, Syversen T, Decamp E, Koser AJ, Fritz S, Gonczi H, Anderson DW, Schneider JS (2006) Nigrostriatal dopamine system dysfunction and subtle motor deficits in manganese-exposed non-human primates. *Exp Neurol* 202: 381-390.

100. Guilarte TR, Burton NC, McGlothan JL, Verina T, Zhou Y, Alexander M, Pham L, Griswold M, Wong DF, Syversen T, Schneider JS (2008) Impairment of nigrostriatal dopamine neurotransmission by manganese is mediated by pre-synaptic mechanism(s): implications to manganese-induced parkinsonism. *J Neurochem* 107: 1236-1247.

101. McDougall SA, Reichel CM, Farley CM, Flesher MM, Der-Ghazarian T, Cortez AM, Wacan JJ, Martinez CE, Varela FA, Butt AE, Crawford CA (2008) Postnatal manganese exposure alters dopamine transporter function in adult rats: Potential impact on nonassociative and associative processes. *Neuroscience* 154: 848-60.

102. Newland MC (1999) Animal models of manganese's neurotoxicity. Neurotoxicology 20: 415-432.

103. Serra PA, Esposito G, Enrico P, Mura MA, Migheli R, Delogu MR, Miele M, Desole MS, Grella G, Miele E (2000) Manganese increases L-DOPA auto-oxidation in the striatum of the freely moving rat: potential implications to L-DOPA long-term therapy of Parkinson's disease. *Br J Pharmacol* 130: 937-45.

104. Vidal L, Alfonso M, Campos F, Faro LR, Cervantes RC, Duran R (2005) Effects of manganese on extracellular levels of dopamine in rat striatum: an analysis *in vivo* by brain microdialysis. *Neurochem Res* 30: 1147-1154.

105. Chen MK, Lee JS, McGlothan JL, Furukawa E, Adams RJ, Alexander M, Wong DF, Guilarte TR (2006) Acute manganese administration alters dopamine transporter levels in the non-human primate striatum. *Neurotoxicology* 27: 229-36.

106. Kim Y, Kim JM, Kim JW, Yoo CI, Lee CR, Lee JH, Kim HK, Yang SO, Chung HK, Lee DS, Jeon B (2002) Dopamine transporter density is decreased in parkinsonian patients with a history of manganese exposure: What does it mean? *Movement Disord* 17: 568-75.

107. Kessler KR, Wunderlich G, Hefter H, Seitz RJ (2003) Secondary progressive chronic manganism associated with markedly decreased striatal D2 receptor density. *Mov Disord* 18: 217-218.

108. McDougall SA, Der-Ghazarian T, Britt CE, Varela FA, Crawford CA (2011) Postnatal manganese exposure alters the expression of D2L and D2S receptor isoforms: Relationship to PKA activity and Akt levels. *Synapse* 65: 583-591.

109. Erikson KM, Pinero DJ, Connor JR, Beard JL (1997) Regional brain iron, ferritin and transferrin concentrations during iron deficiency and iron repletion in developing rats. *J Nutr* 127: 2030-2038.

110. Jaganathan J, Aggarwal I (1993) Graphite-furnace atomic-absorption spectrometric determination of iron, cobalt, nickel, and copper at parts-per-billion level in high-purity lanthanum fluoride. *Appl Spectrosc* 47: 1169-1170.

111. Liu HM, Tsai SJJ, Cheng FC, Chung SY (2000) Determination of trace manganese in the brain of mice subjected to manganese deposition by graphite furnace atomic absorption spectrometry. *Anal Chim Acta* 405: 197-203.

112. Szapacs ME, Mathews TA, Tessarollo L, Ernest Lyons W, Mamounas LA, Andrews AM. Exploring the relationship between serotonin and brain-derived neurotrophic factor: analysis of BDNF protein and extraneuronal 5-HT in mice with reduced serotonin transporter or BDNF expression. *J Neurosci Methods* 140: 81-92.

113. Papaioannou VE, Fox JG (1993) Efficacy of tribromoethanol anesthesia in mice. *Lab Anim Sci* 43: 189-192.

114. Cosford RJ, Vinson AP, Kukoyi S, Justice JB, Jr (1996) Quantitative microdialysis of serotonin and norepinephrine: pharmacological influences on in vivo extraction fraction. J Neurosci Methods 68: 39-47.

115. Justice JB, Jr (1993) Quantitative microdialysis of neurotransmitters. J Neurosci Methods 48: 263-276.

116. Lonnroth P, Jansson PA, Smith U (1987) A microdialysis method allowing characterization of intercellular water space in humans. *Am J Physiol* 253: E228-E31.

117. Mathews TA, Fedele DE, Coppelli FM, Avila AM, Murphy DL, Andrews AM (2004) Gene dose-dependent alterations in extraneuronal serotonin but not dopamine in mice with reduced serotonin transporter expression. *J Neurosci Methods* 140: 169-181.

118. Acworth I, Cunningham ML (1999) The measurement of monoamine neurotransmitters in microdialysis perfusates using HPLC-ECD. *Methods Mol Med* 22: 219-36.

119. Trillat AC, Malagie I, Scearce K, Pons D, Anmella MC, Jacquot C, Hen R, Gardier AM (1997) Regulation of serotonin release in the frontal cortex and ventral hippocampus of homozygous mice lacking 5-HT1B receptors: in vivo microdialysis studies. *J Neurochem* 69: 2019-2025.

120. Jones SR, Garris PA, Kilts CD, Wightman RM (1995) Comparison of dopamine uptake in the basolateral amygdaloid nucleus, caudate-putamen, and nucleus accumbens of the rat. *J Neurochem* 64: 2581-2589.

121. Heien ML, Phillips PE, Stuber GD, Seipel AT, Wightman RM (2003) Overoxidation of carbon-fiber microelectrodes enhances dopamine adsorption and increases sensitivity. *Analyst* 128: 1413-1419.

122. Menacherry S, Hubert W, Justice JB, Jr (1992) In vivo calibration of microdialysis probes for exogenous compounds. *Anal Chem* 64: 577-583.

123. Parsons LH, Smith AD, Justice JB, Jr (1991) The in vivo microdialysis recovery of dopamine is altered independently of basal level by 6-hydroxydopamine lesions to the nucleus accumbens. *J Neurosci Methods* 40: 139-47.

124. Kennedy RT, Jones SR, Wightman RM (1992) Dynamic observation of dopamine autoreceptor effects in rat striatal slices. *J Neurochem* 59: 449-455.

125. Maina FK, Mathews TA (2010) Functional Fast Scan Cyclic Voltammetry Assay to Characterize Dopamine D2 and D3 Autoreceptors in the Mouse Striatum. *ACS Chemical Neuroscience* 1: 450-462.

126. Mottola DM, Kilts JD, Lewis MM, Connery HS, Walker QD, Jones SR, Booth RG, Hyslop DK, Piercey M, Wightman RM, Lawler CP, Nichols DE, Mailman RB (2002) Functional selectivity

of dopamine receptor agonists. I. Selective activation of postsynaptic dopamine D2 receptors linked to adenylate cyclase. *J Pharmacol Exp Ther* 301: 1166-1178.

127. Aschner M, Erikson KM, Dorman DC (2005) Manganese dosimetry: species differences and implications for neurotoxicity. *Crit Rev Toxicol* 35: 1-32.
128. Parsons LH, Justice JB, Jr (1992) Extracellular concentration and in vivo recovery of dopamine in the nucleus accumbens using microdialysis. *J Neurochem* 58: 212-218.
129. Parsons LH, Justice JB, Jr (1993) Perfusate serotonin increases extracellular dopamine in the nucleus accumbens as measured by in vivo microdialysis. *Brain Res* 606: 195-199.
130. Parsons LH, Justice JB, Jr (1994) Quantitative approaches to in vivo brain microdialysis. *Crit Rev Neurobiol* 8: 189-220.
131. Parsons LH, Koob GF, Weiss F (1996) Extracellular serotonin is decreased in the nucleus accumbens during withdrawal from cocaine self-administration. *Behav Brain Res* 73: 225-228.
132. Jones SR, Gainetdinov RR, Jaber M, Giros B, Wightman RM, Caron MG (1998) Profound neuronal plasticity in response to inactivation of the dopamine transporter. *Proc Natl Acad Sci U S A* 95: 4029-4034.
133. Bungay PM, Newton-Vinson P, Isele W, Garris PA, Justice JB (2003) Microdialysis of dopamine interpreted with quantitative model incorporating probe implantation trauma. *J Neurochem* 86: 932-946.
134. Tang A, Bungay PM, Gonzales RA (2003) Characterization of probe and tissue factors that influence interpretation of quantitative microdialysis experiments for dopamine. *J Neurosci Methods* 126: 1-11.

135. Robinson DL, Venton BJ, Heien ML, Wightman RM (2003) Detecting subsecond dopamine release with fast-scan cyclic voltammetry in vivo. *Clin Chem* 49: 1763-1773.

136. Anderson JG, Cooney PT, Erikson KM (2007) Inhibition of DAT function attenuates manganese accumulation in the globus pallidus. *Environ Toxicol Pharmacol* 23: 179-184.

137. Erikson KM, John CE, Jones SR, Aschner M (2005) Manganese accumulation in striatum of mice exposed to toxic doses is dependent upon a functional dopamine transporter. *Environ Toxicol Phar* 20: 390-394.

138. Ingersoll RT, Montgomery EB, Jr (1999) Aposhian HV. Central nervous system toxicity of manganese. II: Cocaine or reserpine inhibit manganese concentration in the rat brain. *Neurotoxicology* 20: 467-476.

139. Jones SR, Gainetdinov RR, Hu XT, Cooper DC, Wightman RM, White FJ, Caron MG (1999) Loss of autoreceptor functions in mice lacking the dopamine transporter. *Nat Neurosci* 2: 649-655.

140. Kern CH, Stanwood GD, Smith DR (2010) Preweaning manganese exposure causes hyperactivity, disinhibition, and spatial learning and memory deficits associated with altered dopamine receptor and transporter levels. *Synapse* 64: 363-678

141. Kern CH, Smith DR (2011) Preweaning Mn exposure leads to prolonged astrocyte activation and lasting effects on the dopaminergic system in adult male rats. *Synapse* 65: 532-544.

142. Peneder TM, Scholze P, Berger ML, Reither H, Heinze G, Bertl J, Bauer J, Richfield EK, Hornykiewicz O, Pifl C (2011) Chronic exposure to manganese decreases striatal dopamine turnover in human alpha-synuclein transgenic mice. *Neuroscience* 180: 280-292.

143. Prabhakaran K, Chapman GD, Gunasekar PG (2011) alpha-Synuclein overexpression enhances manganese-induced neurotoxicity through the NF-kappaB-mediated pathway. *Toxicol Mech Methods* 6:435-443.

144. Larsen KE, Schmitz Y, Troyer MD, Mosharov E, Dietrich P, Quazi AZ, Savalle M, Nemani V, Chaudhry FA, Edwards RH, Stefanis L, Sulzer D (2006) Alpha-synuclein overexpression in PC12 and chromaffin cells impairs catecholamine release by interfering with a late step in exocytosis. *J Neurosci* 26: 11915-11922.

145. Maroteaux L, Campanelli JT, Scheller RH (1988) Synuclein: a neuron-specific protein localized to the nucleus and presynaptic nerve terminal. *J Neurosci* 8: 2804-2815.

146. Nemani VM, Lu W, Berge V, Nakamura K, Onoa B, Lee MK, Chaudhry FA, Nicoll RA, Edwards RH (2010) Increased expression of alpha-synuclein reduces neurotransmitter release by inhibiting synaptic vesicle reclustering after endocytosis. *Neuron* 65: 66-79.

147. Donaldson J, LaBella FS, Gesser D (1981) Enhanced autoxidation of dopamine as a possible basis of manganese neurotoxicity. *Neurotoxicology* 2: 53-64.

148. Lloyd RV (1995) Mechanism of the manganese-catalyzed autoxidation of dopamine. *Chemical Research in Toxicology* 8: 111-116.

149. Shen XM, Dryhurst G (1998) Iron- and manganese-catalyzed autoxidation of dopamine in the presence of L-cysteine: possible insights into iron- and manganese-mediated dopaminergic neurotoxicity. *Chem Res Toxicol* 11: 824-837.

150. Graumann R, Paris I, Martinez-Alvarado P, Rumanque P, Perez-Pastene C, Cardenas SP, Marin P, Diaz-Grez F, Caviedes R, Caviedes P, Segura-Aguilar J (2002) Oxidation of dopamine to aminochrome as a mechanism for neurodegeneration of dopaminergic systems in

Parkinson's disease. Possible neuroprotective role of DT-diaphorase. *Polish Journal of Pharmacology* 54: 573-579.

151. Chen BT, Avshalumov MV, Rice ME (2001) H_2O_2 Is a Novel, Endogenous Modulator of Synaptic Dopamine Release. *Journal of Neurophysiology* 85: 2468-76.

152. Golub MS, Hogrefe CE, Germann SL, Tran TT, Beard JL, Crinella FM, Lonnerdal B (2005) Neurobehavioral evaluation of rhesus monkey infants fed cow's milk formula, soy formula, or soy formula with added manganese. *Neurotoxicol Teratol* 27(4): 615-627.

153. Dorman DC, Struve MF, Vitarella D, Byerly FL, Goetz J, Miller R (2000) Neurotoxicity of manganese chloride in neonatal and adult CD rats following subchronic (21-day) high-dose oral exposure. *J Appl Toxicol* 20(3): 179-187.

154. Reichel CM, Wacan JJ, Farley CM, Stanley BJ, Crawford CA, McDougall SA (2006) Postnatal manganese exposure attenuates cocaine-induced locomotor activity and reduces dopamine transporters in adult male rats. *Neurotoxicol Teratol* 28(3): 323-332.

155. Cordova FM, Aguiar AS Jr, Peres TV, Lopes MW, Goncalves FM, Remor AP, Lopes SC, Pilati C, Latini AS, Prediger RD, Erikson KM, Aschner M, Leal RB (2012). In vivo manganese exposure modulates Erk, Akt, and Darpp-32 in the striatum of developing rats, and impairs their motor function. *PLoS One* 7(3).

156. Yang Y, An J, Wang Y, Luo W, Wang W, Mei X, Wu S, Chen J (2011) Intrastriatal manganese chloride exposure causes acute locomotor impairment as well as partial activation of substantia nigra GABAergic neurons. *Environ Toxicol Pharmacol* 31(1): 171-178.

157. Leung TK, Lai JC, Tricklebank M, Davison AN, Lim L (1982) Chronic manganese treatment of rats alters synaptosomal uptake of dopamine and the behavioral response to amphetamine administration. *J Neurochem* 39(5): 1496-1499.

158. Solanto MV (1998) Neuropsychopharmacological mechanisms of stimulant drug action in attention-deficit hyperactivity disorder: a review and integration. *Behav Brain Res* 94:127–152.

159. Solanto MV (2002) Dopamine dysfunction in AD/HD: integrating clinical and basic neuroscience research. *Behav Brain Res* 130: 65–71.

160. Tanaka K, Yamamoto A, Kawaguchi C, Shimada T, Baba A (2006) Psychostimulant-induced attenuation of hyperactivity and prepulse inhibition deficits in Adcyap1-deficient mice. *J Neurosci* 26(19): 5091–5097.

161. Ordoñez-Librado JL, Gutierrez-Valdez AL, Colin-Barenque L, Anaya-Martinez V, Diaz-Bech P, Avila-Costa MR (2008) Inhalation of divalent and trivalent manganese mixture induces a Parkinson's disease model: immunocytochemical and behavioral evidences. *Neuroscience* 155: 7-16.

162. Ordoñez-Librado JL, Anaya-Martínez V, Gutierrez-Valdez AL, Colín-Barenque L, Montiel-Flores E, Avila-Costa MR (2010) Manganese inhalation as a Parkinson disease model. *Parkinsons Dis*.

163. Garcia-Hernandez F, Pacheco-Cano MT, Drucker-Colin R (1993) Reduction of motor impairment by adrenal medulla transplants in aged rats. *Physiol. Behav* 54: 589-598.

164. Denker A, Rizzoli S (2010) Synaptic vesicle pools: an update. *Frontiers in Synaptic Neuroscience* 2:1-12.

165. Gandhi SP, Stevens CF (2003) Three modes of synaptic vesicular recycling revealed by single-vesicle imaging. *Nature* 423: 607-613.

166. Aravanis AM, Pyle JL, Tsien RW (2003) Single synaptic vesicles fusing transiently and successively without loss of identity. *Nature* 423, 643–647.

167. Harata NC, Choi S, Pyle JL, Aravanis AM, Tsien RW (2006) Frequency-dependent kinetics and prevalence of kiss-and-run and reuse at hippocampal synapses studied with novel quenching methods. *Neuron* 49, 243–256.

168. Zhang Q, Li Y, Tsien RW (2009) The dynamic control of kiss-and-run and vesicular reuse probed with single nanoparticles. *Science* 323, 1448–1453.

169. Chen X, Barg S, Almers W (2008) Release of the styryl dyes from single synaptic vesicles in hippocampal neurons. *J Neurosci* 28, 1894–1903.

170. Granseth B, Odermatt B, Royle SJ, Lagnado L (2006) Clathrin-mediated endocytosis is the dominant mechanism of vesicle retrieval at hippocampal synapses. *Neuron* 51, 773–786.

171. Willig KI, Rizzoli SO, Westphal V, Jahn R, Hell SW (2006) STED microscopy reveals that synaptotagmin remains clustered after synaptic vesicle exocytosis. *Nature* 440, 935–939.

172. Clayton EL, Evans GJ, Cousin MA (2008) Bulk synaptic vesicle endocytosis is rapidly triggered during strong stimulation. *J Neurosci* 28, 6627–6632.

173. Wu W, Wu LG (2007) Rapid bulk endocytosis and its kinetics of fission pore closure at a central synapse. *Proc Natl Acad Sci U.S.A.* 104, 10234–10239.

174. Andersson F, Jakobsson J, Low P, Shupliakov, O, Brodin L (2008) Perturbation of syndapin/PACSIN impairs synaptic vesicle recycling evoked by intense stimulation. *J. Neurosci* 28, 3925–3933.

175. Heuser JE, Reese TS (1973). Evidence for recycling of synaptic vesicle membrane during transmitter release at the frog neuromuscular junction. *J Cell Biol* 57, 315–344.

176. Wucherpfennig T, Wilsch-Brauninger M, and Gonzalez-Gaitan M (2003) Role of Drosophila Rab5 during endosomal trafficking at the synapse and evoked neurotransmitter release. *J Cell Biol* 161, 609–624.

177. Rizzoli SO, Bethani I, Zwilling D, Wenzel D, Siddiqui T J, Brandhorst D, and Jahn R (2006) Evidence for early endosome-like fusion of recently endocytosed synaptic vesicles. *Traffic* 7, 1163–1176.

178. Stanwood GD, Leitch DB, Savchenko V, Wu J, Fitsanakis VA, Anderson DJ, Stankowski JN, Aschner M, McLaughlin B (2009) Manganese exposure is cytotoxic and alters dopaminergic and GABAergic neurons within the basal ganglia. *J Neurochem* 110(1): 378–389.

179. Rizzoli SO, Betz WJ (2005) Synaptic Vesicle Pools. *Nature Reviews* 6: 57-68.

180. Westphal V, Rizzoli SO, Lauterbach MA, Kamin D, Jahn R, Hell SW (2008) Video-rate far-field optical nanoscopy dissects synaptic vesicle movement. *Science* 320: 246–249.

181. Shtrahman M, Yeung C, Nauen DW, Bi GQ, Wu XL (2005). Probing vesicle dynamics in single hippocampal synapses. *Biophys J* 89: 3615–3627.

182. Gaffield MA, Betz WJ (2007) Synaptic vesicle mobility in mouse motor nerve terminals with and without synapsin. *J Neurosci* 27: 13691–13700.

183. Gaffield MA, Rizzoli SO, Betz WJ (2006) Mobility of synaptic vesicles in different pools in resting and stimulated frog motor nerve terminals. *Neuron* 51: 317–325.

184. Kamin D, Lauterback MA, Westphal V, Keller J, Schönle A, Hell SW, Rizzoli SO (2010) High- and low-mobility stages in the synaptic vesicle cycle. *Biophys J* 99: 675–684.

185. Darcy KJ, Staras K, Collinson LM, Goda Y (2006) Constitutive sharing of recycling synaptic vesicles between presynaptic boutons. *Nat Neurosci* 9: 315–321.

186. Fernandez-Alfonso T, Kwan R, Ryan TA (2006) Synaptic vesicles interchange their membrane proteins with a large surface reservoir during recycling. *Neuron* 51: 179–186.

187. Venton BJ, Seipel AT, Phillips PEM, Wetsel WC, Gitler D, Greengard P, Augustine GJ, Wightman RM(2006) Cocaine increases dopamine release by mobilization of a synapsin-dependent reserve pool. *The Journal of Neuroscience* 26(12)*:* 3206-3209.

188. Ortiz AN, Kurth BJ, Osterhaus GL, Johnson MA (2010) Dysregulation of intracellular dopamine stores revealed in the R6/2 mouse striatum. Journal of Neurochemistry 112: 755-761.

189. Chiueh CC, Moore KE (1975) D-amphetamine-induced release of “newly synthesized” and “stored” dopamine from the caudate nucleus in vivo. *J Pharmacol Exp Ther* 192: 642-653.

190. Carmona A, Deves G, Roudeau S, Cloetens P, Bohic S, Ortega R (2010) Manganese accumulates within Golgi apparatus in dopaminergic cells as revealed by synchrotron X-ray fluorescence nano-imaging. *ACS Chemical Neurosciences* 1(3): 194-203.

191. Roth J, Ponzoni S, Aschner M (2013) Manganese homeostasis and transport. *Met Ions Life Sci* 12: 169-201.

192. Sadiq S, Ghazala Z, Chowdhury A, Busselberg D (2012) Metal toxicity at the synapse: presynaptic, postsynaptic, and long-term effects. *Journal of Toxicology* : 42 pages.

193. Swandulla D, Armstrong CM (1989) Calcium channel block by cadmium in chicken sensory neurons,” *Proceedings of the National Academy of Sciences of the United States of America* 86(5): 736–1740.

194. Busselberg D, PlattB , Michael D, Carpenter DO, Haas HL (1994) Mammalian voltage-activated calcium channel currents are blocked by Pb2+, Zn2+, and Al3+. *Journal of Neurophysiology* 71(4): 1491-1497.

195. Julka D, Gill KD (1996) Altered calcium homeostasis: a possible mechanism of aluminum-induced neurotoxicity. D. *Biochimica et Biophysica Acta* 1315(1): 47-54

196. Busselberg D, Evans ML, Rahmann H, Carpenter DO (1991) Lead and zinc block a voltage-activated calcium channel of Aplysia neurons. *Journal of Neurophysiology* 65(4): 786-795.

197. Evans ML, Busselberg D, Carpenter DO (1991)Pb2+ blocks calcium currents of cultured dorsal root ganglion cells. *Neuroscience Letters* 129(1): 103-106.

198. Busselberg D, Evans ML, Haas HL, Carpenter DO (1993) Blockade of mammalian and invertebrate calcium channels by lead. *NeuroToxicology* 14(2-3): 249-258.

199. Audesirk G, Audesirk T (1993) The effects of inorganic lead on voltage-sensitive calcium channels differ among cell types and among channel subtypes. *NeuroToxicology* 14 (2-3): 259-266.

200. Ravindran A, Schild L, Moczydlowski E (1991) Divalent cation selectivity for external block of voltage-dependent Na+ channels prolonged by batrachotoxin. Zn2+ induces discrete substates in crdiac Na+ channels. *Journal of General Physiology*, 97(1): 89-115.

201. Mayer ML, Sugiyama K (1988) A modulatory action of divalent cations on transient outward current in cultured rat sensory neurons. *Journal of Physiology* 396: 417-433.

ABSTRACT

STRIATAL DOPAMINE DYNAMICS UPON MANGANESE ACCUMULATION

by

MADIHA KHALID

August 2013

Advisor: Dr. Tiffany Mathews

Major: Chemistry (Analytical)

Degree: Doctor of Philosophy

Although manganese (Mn) is fundamental for many biological processes, exposure to excess amounts leads to a neurological disorder termed manganism. Due to its symptomatic similarity to Parkinson's disease, as well its preferential accumulation in dopamine rich brain regions, alterations in the dopamine system are implicated in the onset of manganism. In my research, Mn overexposure is mimicked via subcutaneous administration of manganese chloride to C57BL/6 mice over the course of seven days using a protocol that has been shown to result in accumulation of Mn in the basal ganglia. The subsequent short and long term effects of this treatment on striatal dopamine function were evaluated 1, 7, and 21 days after treatment cessation. This work used a variety of complementary analytical methods to take a multifaceted approach in studying the Mn-treated animals. The first study used fast scan cyclic voltammetry, microdialysis, and tissue content analysis to characterize the dopamine system after the sub-acute treatment protocol. Behavioral tests were subsequently used to elucidate any phenotypic differences in the treated mice as compared to controls. Finally, pharmacological studies were

conducted to test the hypothesis of intraneuronal dysfunction to explain the changes observed in the first study.

Overall, these findings revealed that the dopamine system in the striatum has lower extracellular levels of dopamine after Mn accumulation due to a functional defect in the release mechanism that is apparent within a week of treatment. Interestingly, most behavioral changes appear to manifest within 24 hours of treatment, when no dopamine change is observed, indicating the involvement of other neurotransmitter systems in the onset of motor deficits following Mn exposure. Finally, by methodically evaluating the quantity and functionality of dopamine vesicles at the axon terminal, we were able to provide evidence against the theory that dopamine release following Mn accumulation is due to an inability of the reserve pool of dopamine to mobilize to the terminal for release.

AUTOBIOGRAPHICAL STATEMENT

Education

- **Wayne State University, Detroit, MI** August 2013
  Doctor of Philosophy (PhD), Chemistry (Analytical)
  Dissertation: Striatal Dopamine Dynamics upon Manganese Accumulation
  (Advisor: Dr. Tiffany A. Mathews)

- **University of Michigan – Dearborn, MI** May 2008
  Bachelor of Science (BS), Chemistry (minors: Statistics & Psychology)

Employment

- **Wayne State University, Detroit, MI**
  Graduate Research Assistant to Dr. Tiffany A. Mathews August 2008 – May 2013
  Graduate Teaching Assistant August 2008 – May 2012

- **University of Michigan – Dearborn, MI** January 2007 – August 2008
  Undergraduate Research Assistant to Dr. Krisanu Bandyopadhyay

Honors and Awards

- David F. Boltz Award in Analytical Chemistry 2013
- Thomas C. Rumble University Graduate Fellowship 2012 – 2013
- Summer 2012 Dissertation Fellowship 2012
- Honor Citation for Excellence in Teaching Service in Chemistry 2011, 2012
- Graduate Student Professional Travel Award 2011
- Undergraduate Research Fellowship 2008
- Distinguished Graduate 2008
- Distinguished Research Award 2008
- William J. Branstrom Prize 2004

Publications

- Maina, F.,* **Khalid, M.,*** Apawu, A.,* and Mathews, T.A., "Presynaptic Dopamine Dynamics in Striatal Brain Slices with Fast-Scan Cyclic Voltammetry" *J Vis Exp*, **59**, pii: 3464. doi: 10.3791/3464 (2012). *indicates co-first authors.
- **Khalid, M.,** Aoun, R.A., Mathews, T.A., "Altered Striatal Dopamine Release Following a Sub-acute Exposure to Manganese," *J. Neurosci. Methods,* **202**(2), 182-191 (2011).
- **Khalid, M.**, Wasio, N., Chase, T., Bandyopadhyay, K., "*In Situ* Generation of Two-Dimensional Au-Pt Core-Shell Nanoparticle Assemblies" *Nanoscale Res. Lett.*, **5**, 61-67 (2010).
- **Khalid, M.**, Pala, I., Wasio, N., Bandyopadhyay, K., "Functionalized Surface As Template For *In Situ* Generation of Two-Dimensional Metal Nanoparticle Assembly" *Colloids and Surfaces A: Physicochem. Eng. Aspects*, **348**, 263-269 (2009).